

Enhancing the Energy Efficiency of Radio Base Stations

Hauke Andreas Holtkamp



THE UNIVERSITY
of EDINBURGH

Thesis submitted in fulfilment of
the requirements for the degree of
Doctor of Philosophy
to the
University of Edinburgh — 2013

Declaration

I declare that this thesis has been composed solely by myself and that it has not been submitted, either in whole or in part, in any previous application for a degree. Except where otherwise acknowledged, the work presented is entirely my own.

Hauke Andreas Holtkamp
September 2018

Abstract

This thesis is concerned with the energy efficiency of cellular networks. It studies the dominant power consumer in future cellular networks, the Long Term Evolution (**LTE**) radio Base Station (**BS**), and proposes mechanisms that enhance the **BS** energy efficiency by reducing its power consumption under target rate constraints. These mechanisms trade spare capacity for power saving.

First, the thesis describes how much power individual components of a **BS** consume and what parameters affect this consumption based on third party experimental data. These individual models are joined into a component power model for an entire **BS**. The component model is an essential step in analysis but is too complex for many applications. It is therefore abstracted into a much simpler parameterized model to reduce its complexity. The parameterized model is further simplified into an affine model which can be applied in power minimization.

Second, Power Control (**PC**) and Discontinuous Transmission (**DTX**) are identified as promising power-saving Radio Resource Management (**RRM**) mechanisms and applied to multi-user downlink transmission. **PC** reduces the power consumption of the Power Amplifier (**PA**) and is found to be most effective at high traffic loads. **DTX** mostly reduces the power consumption of the Baseband (**BB**) unit while interrupting transmission and is better applied in low traffic loads. Joint optimization of these two techniques is found to enable additional power-saving at medium traffic loads and to be a convex problem which can be solved efficiently. The convex problem is extended to provide a comprehensive power-saving Orthogonal Frequency Division Multiple Access (**OFDMA**) frame resource scheduler. The proposed scheduler is shown to reduce power consumption by 25-40% in computer simulations, depending on the traffic load.

Finally, the thesis investigates the influence of interference on power consumption in a network of multiple power-saving **BSs**. It discusses three popular alternative distributed uncoordinated methods which align **DTX** mode between neighboring **BSs**. To address drawbacks of these three, a fourth memory-based **DTX** alignment method is proposed. It decreases power consumption by up to 40% and retransmission probability by around 20%, depending on the traffic load.

Lay Summary

This thesis is about reducing the power consumption of mobile phone networks. Base Stations, the antennas on rooftops everywhere, currently require a large amount of electricity which is expensive. This thesis studies base stations and proposes mechanisms which reduce their power consumption while providing an unchanged connection quality. This is achieved by reducing the base station power when only few people use their mobile phones.

First, the thesis describes how much power the individual electronic elements of a BS consume and what parameters this consumption depends on. These individual models are joined into a component power model for an entire base station. With this power model, one can study a base station in theory without having an expensive laboratory. The component model is very complex and is therefore further simplified into a so-called parameterized model.

Second, two techniques are studied which reduce the power consumption of base stations when it is transmitting data to mobile phones. One is Power Control (PC), which reduces the power at the antenna when it is not needed, because users are standing near the base stations. The other is Discontinuous Transmission (DTX). DTX turns off the base station for a very short time, which is not noticeable for mobile phones. Using the parameterized power model, PC is found to work very well when many people use their phones, for example, at daytime. DTX is more effective, when few people use their phones, for instance at nighttime. It is found that we can mathematically combine both techniques to save even more power. Using a mathematical technique called convex optimisation, this can be done extremely fast. Using this technique, the power consumption could be reduced by 25-40% in computer simulations, depending on how many people use their phones at one time.

Finally, the thesis investigates how much power an entire network consumes when all base stations are transmitting. When all base stations transmit at the same time, the network becomes noisy. It is better for base stations to take turns. The thesis discusses three popular alternative methods which try to organize when the different base stations in the network transmit. To address disadvantages of these three, a fourth method is proposed which provides a trade-off between user satisfaction and power-saving. A small decrease in network quality could reduce power consumption by 20%, depending on how many people use their phone at one time.

Acknowledgements

This document could not have been produced without help. I owe deep gratitude to my academic supervisor, Professor Harald Haas of the University of Edinburgh, for believing in me and providing me with guidance and support. This work is in its current shape only through his teachings, insistence and attention to detail. Furthermore, I am grateful to the thesis examiners, Dr James R. Hopgood of the University of Edinburgh, and Dr Emad Alsusa of the University of Manchester.

Extended thanks goes to DOCOMO Euro-Labs GmbH in Munich. There, Dr. Gunther Auer was the best industry supervisor any PhD student could wish for. He pulled me back on track when I drifted. Guido Dietl helped me through extended technical discussions. The entire DOCOMO team over the years were my friends, sharpened my technical understanding and provided support when it was needed. Thanks, Emmanuel, Iwamura-san, Marwa, Matthias, Patrick, Petra, Samer, Serkan, Shinji, Toshi, and Zubin.

At the University of Edinburgh, Bogomil, Harald, Nikola, and Stefan have helped me to get through the university jungle and lead the way to a PhD. Go Jacobs/IUB alumni!

My friends have provided me with the indispensable social support. Most of all I am thankful to my parents without whom I would not be where I am today.

Contents

Abstract	v
Lay Summary	vii
Contents	xi
List of Tables	xv
List of Figures	xvii
List of Acronyms	xix
1 Introduction	1
1.1 Overview	1
1.2 Thesis Context	1
1.3 Thesis Contributions	3
1.4 Thesis Structure	3
1.5 The EARTH Project	4
2 Motivation and Background	7
2.1 Overview	7
2.2 Energy Efficient Base Stations	7
2.3 Quantifying Energy Efficiency	10
2.4 Green Radio in Literature	11
2.5 Technical Background	14
2.5.1 LTE	14
2.5.2 Multi-carrier Technology	15
2.5.3 Multiple Antenna Technology	19
2.5.4 Convex Optimization	21
2.5.5 Network Simulation	22
2.6 Summary	26

3	Power Saving on the Device Level	27
3.1	Overview	27
3.2	Challenges in Power Modeling	28
3.3	Existing Power Models	28
3.4	The Component Power Model	29
3.4.1	Remarks	29
3.4.2	The Components of a BS	30
3.4.3	BS Power Consumption	40
3.5	The Parameterized Power Model	43
3.6	The Affine Power Model	46
3.7	Summary	48
4	Power Saving on the Cell Level (Single-cell)	51
4.1	Overview	51
4.2	Power-saving RRM in Literature	52
4.3	PC and TDMA	53
4.4	Power and Resource Allocation Including Sleep (PRAIS)	58
4.5	Resource allocation using Antenna adaptation, Power control and Sleep modes (RAPS)	63
4.5.1	Problem Formulation	65
4.5.2	Step 1: Antenna Adaptation (AA), DTX and Resource Allocation	67
4.5.3	Step 2: Subcarrier and Power Allocation	69
4.5.4	Results	72
4.6	Summary	79
5	Power Saving on the Network Level (Multi-cell)	81
5.1	Overview	81
5.2	Channel Allocation in Literature	81
5.3	System Model and Problem Formulation	83
5.4	DTX Alignment Strategies	84
5.4.1	Sequential Alignment	84
5.4.2	Random Alignment	85
5.4.3	P-persistent Ranking	85
5.4.4	Distributed DTX Alignment with Memory	86
5.5	Results	87
5.6	Summary	92
6	Conclusions, Limitations and Future Work	95
6.1	Summary and Conclusions	95
6.2	Limitations and Future Work	97
	Appendices	99

A Appendix	99
A.1 Proof of Convexity for Problem (4.12)	99
A.2 Proof of Convexity for Problem (4.15)	99
A.3 Margin-adaptive Resource Allocation	100
B List of Publications	103
B.1 Published	103
B.2 Accepted	104
B.3 Submitted	104
B.4 Project Reports	104
B.5 Contributions	104
C Attached Publications	105
Literature References	107

List of Tables

3.1	Model parameters assumed for figures of Chapter 3	30
3.2	Reference power consumption values of RF transceiver blocks . . .	34
3.3	Complexity of BB operations	35
3.4	Parameter breakdown	46
3.5	Summary of affine power model parameters	48
3.6	Comparison of required input parameters for different power models	49
4.1	Simulation parameters	57
4.2	Power model parameters used in Section 4.4	62
4.3	System parameters	74
5.1	Simulation parameters	88

List of Figures

1.1	Mobile traffic forecast 2012-2017	2
2.1	The carbon footprint for an average subscriber in 2007	8
2.2	European daily traffic pattern	9
2.3	Adoption of LTE technology	15
2.4	Mobile subscriptions by technology, 2009-2018	16
2.5	An illustration of TDM	17
2.6	An illustration of FDM	17
2.7	Resource allocation in a combined OFDMA/TDMA system	18
2.8	Example of multi-user diversity	19
2.9	Comparison of Multiple-Input Multiple-Output (MIMO) capacities	20
2.10	Geometric interpretation of a simple convex problem	22
2.11	A network in the network simulator	24
2.12	Sample simulation flowchart	25
3.1	The components of the modelled BS	30
3.2	The power-added efficiency over the maximum output power	32
3.3	P_{PA} as a function of bandwidth used	33
3.4	P_{RF} as a function of bandwidth used	34
3.5	P_{BB} as a function of bandwidth used	36
3.6	DC conversion loss function	37
3.7	P_{DC} as a function of bandwidth used	38
3.8	AC conversion loss function	38
3.9	P_{AC} as a function of bandwidth used	39
3.10	P_{COOL} as a function of bandwidth used	40
3.11	P_{supply} as a function of bandwidth used	41
3.12	P_{supply} per component in percent	42
3.13	Load-dependent power model for an LTE BS	45
3.14	Comparison of the parameterized with the complex model	47
4.1	Illustration of two possible power/time trade-offs	54
4.2	Comparison of the effect of load dependence	57
4.3	Illustration of PRAIS for two links	58
4.4	Supply power consumption for a target spectral efficiency	60
4.5	Fundamental limits for power consumption in BSs	64

4.6	OFDM frame structure	65
4.7	Illustration of margin-adaptive power allocation over three steps	72
4.8	Outline of the RAPS algorithm.	73
4.9	Performance comparison in step 1	75
4.10	Outage probability in step 1 and the BA benchmark	76
4.11	Average number of DTX time slots over increasing target link rates	77
4.12	Supply power consumption for different RRM schemes overall	77
4.13	Supply power consumption for different RRM schemes in step 2	78
4.14	Energy efficiency as a function of sum rate	79
5.1	Illustration of DTX alignment in a network	82
5.2	Illustration of sequential alignment	85
5.3	BS power consumption over different cell sum rates	89
5.4	BS power consumption over OFDMA frames at 1 Mbps per mobile	90
5.5	BS power consumption over OFDMA frames at 2 Mbps per mobile	91
5.6	Retransmission probability over targeted rate.	92

List of Acronyms

3GPP	3rd Generation Partnership Project
AA	Antenna Adaptation
AC	Alternating Current
ADC	Analog-to-Digital Converter
BA	Bandwidth Adaptation
BB	Baseband
BS	Base Station
CDM	Code Division Multiplexing
CSI	Channel State Information
DAC	Digital-to-Analog Converter
DC	Direct Current
DTX	Discontinuous Transmission
EARTH	Energy Aware Radio and neTwork tecHnologies
FDM	Frequency Division Multiplexing
FPGA	Field-Programmable Gate Array
GOPS	Giga Operations Per Second
GSM	Global System for Mobile communications
HetNet	Heterogeneous Network
ICT	Information and Communication Technologies
IQ	In-phase/Quadrature
LNA	Low-Noise Amplifier

LTE	Long Term Evolution
M2M	Machine-to-Machine
MIMO	Multiple-Input Multiple-Output
OFDM	Orthogonal Frequency Division Multiplexing
OFDMA	Orthogonal Frequency Division Multiple Access
PA	Power Amplifier
PC	Power Control
PRAIS	Power and Resource Allocation Including Sleep
QoS	Quality of Service
RAPS	Resource allocation using Antenna adaptation, Power control and Sleep modes
RF	Radio Frequency
RCG	Rate Craving Greedy
RRH	Remote Radio Head
RRM	Radio Resource Management
SIMO	Single-Input Multiple-Output
SINR	Signal-to-Interference-and-Noise-Ratio
SISO	Single-Input Single-Output
SNR	Signal-to-Noise-Ratio
SotA	State-Of-The-Art
TDM	Time Division Multiplexing
TDMA	Time Division Multiple Access
UE	User Equipment
UMTS	Universal Mobile Telecommunications System
VCO	Voltage-Controlled Oscillator

Chapter 1

Introduction

1.1 Overview

In the first section of this chapter, it is argued why energy efficiency in wireless networks is an important research topic and what goals this thesis sets out to achieve. The second section introduces the contributions of this thesis towards achieving these goals. The third section outlines the thesis structure. In the last section, the Energy Aware Radio and neTwork tecHnologies (**EARTH**) project is briefly introduced which provided laboratory results for the contents of Chapter 3.

1.2 Thesis Context

Since the emergence of mobile communications, both the number and the density of mobile devices have constantly increased [Bi *et al.*, 2001]. They are predicted to rise further, fueled by innovations such as Machine-to-Machine (**M2M**) communication and the ‘Internet of Things’ [Wu *et al.*, 2011, Brazell *et al.*, 2005]. It is predicted that a trillion devices will be connected to the Internet by the end of 2013 [Wireless Week, 2010], with a growing share of these on mobile networks. Fig. 1.1 shows a forecast of the resulting mobile traffic until 2017. To serve this growing traffic load, the capacity, size and density of the infrastructure network are continually upgraded by network operators.

While for the past 20 years network capacity, reliability and deployment were the main concerns during these upgrades, new factors like rising energy prices, increasing consumer attention to the emission of CO₂, the deployment of Base Stations (**BSs**) in remote off-grid locations, and disaster recovery have come into play. To respond to these new factors, the energy efficiency of the current and future mobile networks needs to be enhanced. Delivery of bits through the cellular network has to become cheaper. CO₂ emissions have to be reduced. **BSs** in remote locations must become self-sustaining. And maintaining connectivity after disasters is critical as the dependence of people and services on mobile communication in a disaster aftermath grows.

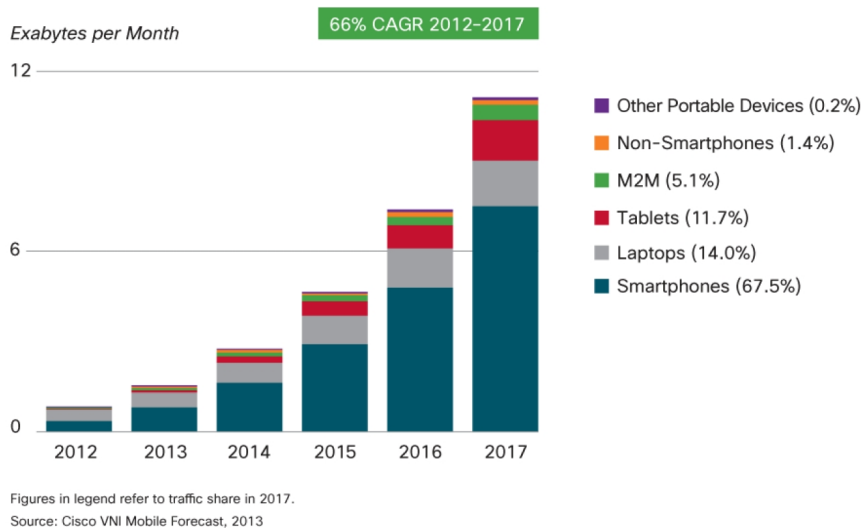


Figure 1.1: Mobile traffic forecast 2012-2017 with a Compound Annual Growth Rate of 66% [Cisco, 2013, p. 7].

Lowering the power consumption of the BSs in cellular networks addresses all of these problems. It reduces the network operational cost and the required CO₂ emission. Installing grid-independent BSs becomes more feasible when less power is needed for their operation. Furthermore, connectivity can be provided for a longer period of time in case of disastrous power interruptions.

However, the causes of power consumption in BSs have not been studied in depth. Whether and by how much this power consumption can be lowered through operational modifications is an open problem. The answer to this problem affects the design of future transmission schemes and hardware. Once the most effective mechanisms for reducing power consumption are understood, they can be used to operate BSs with lower power consumption and, thus, with higher efficiency. Radio resource schedulers need to be developed which enhance the efficiency of operation in both individual BSs and a network of BSs.

As such, this thesis sets out to achieve the following goals:

- Identify how the power consumption of a BS is comprised in terms of hardware components. Evaluate what operating parameters have the strongest effect on the BS power consumption. Model this consumption in equations such that it can be reused and modified.
- Identify promising operational techniques to reduce a BS's power consumption without affecting the Quality of Service (QoS). Generate resource schedulers which employ such techniques.
- Understand how power consumption can be reduced in a network of multiple BSs. Provide solutions to address power consumption on the network level.

1.3 Thesis Contributions

This thesis contributes towards the enhancement of energy efficiency in wireless networks by reducing the power consumption of radio BS through Radio Resource Management (RRM) without affecting the QoS. In particular, it provides the following contributions:

- First, the power consumption of State-Of-The-Art (SotA) Long Term Evolution (LTE) BSs is studied and presented in detail. The number of antennas, the transmission power and the lowered consumption through Discontinuous Transmission (DTX) are derived as the most relevant operating parameters. A general, practical power model for cellular BSs is constructed.
- Second, the attainable power savings of power control, DTX and Antenna Adaptation (AA) are quantified. The three techniques are jointly applied to a new energy efficient and spectrum efficient Orthogonal Frequency Division Multiple Access (OFDMA) scheduler.
- Third, the alignment of DTX time slots between neighbouring BSs is identified as a multi-cell power-saving mechanism. Three alternative alignment schemes are studied with regard to their power consumption. The findings lead to a novel time slot alignment scheme which is shown to overcome the limitations of the other techniques.

1.4 Thesis Structure

Chapter 2 first addresses the issue why this work is concerned with the supply power consumption of cellular BSs in particular. Next, it provides an overview of Green Radio research alongside a review of relevant literature. Finally, a technical background for Chapters 3, 4, and 5 is provided about the topics LTE, multi-carrier technology, multi-antenna transmission, convex optimization, and computer simulation techniques.

Chapter 3 begins with an analysis of the power consumption of a SotA BS in order to identify opportunities for power saving. Each subcomponent is individually inspected and described with regard to its power consumption. A comprehensive BS power model is established as the sum of each subcomponent's power consumption. Relevant and promising saving mechanisms are identified. A parameterized power model is proposed which encompasses these saving mechanisms and abstracts architectural details in favor of simplicity. Finally, an affine power model is derived, which is used through the remainder of this thesis. The affine mapping this model provides between transmission power and supply power is advantageous for its application in optimization.

Chapter 4 applies the knowledge on BS power consumption from Chapter 3 by proposing power-saving RRM mechanisms. On the basis of the affine power

model, Power Control (**PC**) and **DTX** are studied. The potential of their joint optimization is identified. The power savings achieved by this method over the **SotA** are quantified in simulation. The joint optimization of **PC**, **DTX** and **AA** is applied in a comprehensive scheduler for power-saving in **OFDMA** downlink transmission within a cell.

Chapter 5 adds the consideration of intercell interference. When multiple **BSs** are considered, the use of sleep modes in each **BS** results in significant fluctuations of interference. Constructive alignment of interference is proposed to exploit this effect and can be employed for a decrease of power consumption. To address multi-cell power saving resource allocation, *distributed DTX with memory* is proposed and compared to alternative alignment mechanisms. Network simulations are used to estimate achievable savings.

Finally, conclusions of the above research, a discussion of limitations and an outlook for future research is provided in Chapter 6.

Regarding the format of this document: There are two non-overlapping bibliographies at the end of this document. One contains publications by the author of this thesis. References to these publications are made with alphabetic indices, such as '[a]' or '[b]'. References to other literature are written with numeric indices such as '[1]' or '[22]'.

1.5 The *EARTH* Project

The research presented in Chapters 3 and 4 of this thesis has received funding and experimental data from the Energy Aware Radio and neTwork tecHnologies (*EARTH*) project. Initiated by the European Union's Framework Programme (FP) 7, the *EARTH* project aligned cooperation between 15 industry and academic institutions towards the common goal of driving up energy efficiency in current and future cellular networks. The project lasted from January 2010 to June 2012. It was founded to work on

- deployment strategies,
- network architectures,
- network management,
- adaptation to load variations with time,
- innovative component designs with energy efficient adaptive operating points,
- and new radio and network resource management protocols for multi-cell cooperative networking.

The most prominent outcomes of the project were

- the cellular network life cycle analysis [[Fehske et al., 2010](#)],
- the energy efficiency evaluation framework [[Auer et al., 2011a](#), [EARTH Project Work Package 2, 2010](#)],
- the BS power model [[Desset et al., 2012](#)],
- hardware implementations of Power Amplifiers (PAs) with improved dynamics [[Gonzalez et al., 2011](#)] and a sleep mode enabled small cell [[EARTH Project Work Package 4, 2012](#)],
- and numerous individual techniques which reduce the power consumption of cellular networks such as the ones presented in Chapter 4 [[EARTH Project Work Package 3, 2012](#)].

All project deliverables are available on the project website for reference [[01b, a](#)].

Chapter 2

Motivation and Background

2.1 Overview

This chapter first outlines the motivation why reducing the power consumption of cellular Base Stations (BSs) constitutes a large step towards energy efficient wireless networks and how this reduction can be achieved. Second, it discusses the difficulties of quantifying energy efficiency and provides an overview of Green Radio research topics in literature. Finally, technical concepts which are applied in Chapters 4 and 5 are briefly introduced for the unfamiliar reader.

The work in Section 2.2 has been previously published by the author of this thesis in [Auer *et al.*, 2010]. The technical background in Section 2.5 is sourced from literature as referenced.

2.2 Energy Efficient Base Stations

Life cycle analyses of mobile networks and their equipment have shown that the access infrastructure (BSs, data centers, controllers) generates significantly more CO₂ than the connected mobile devices [Fehske *et al.*, 2010]. They also reveal that mobile devices cause the majority of CO₂ emissions during manufacturing due to their battery-optimized operation and short life times. In contrast, BSs tend to be less power optimized with longer life times leading to the majority of CO₂ emitted during operation. This is illustrated in Fig. 2.1 by the detailed carbon footprint of the average mobile network subscriber in 2007, the most recent data available. It shows that only 20% of the CO₂ emissions over the life of a mobile device were caused during operation. On the contrary, 82% of BS emissions are owed to operation, either as diesel or electricity consumption.

While the power consumption of mobile devices has always been a topic of research and development due to the constraints imposed by battery operation, BSs were usually installed in urban locations with good connections to the power grid providing little incentive for efforts in energy efficiency. However, as briefly

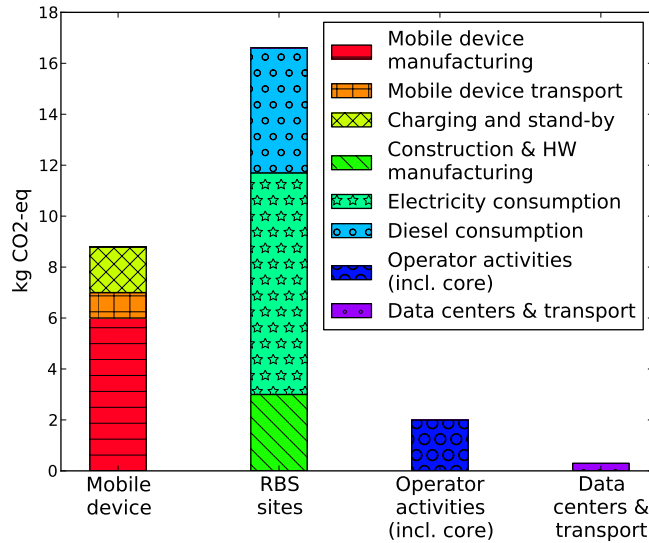


Figure 2.1: The carbon footprint (CO₂-equivalent emissions, see Section 2.3) for an average subscriber in 2007 [Malmudin *et al.*, 2010], with a focus on radio base stations (RBS).

mentioned in Chapter 1, the energy efficiency of cellular BSs is receiving more attention due to several factors [Louhi & Scheck, 2008]:

- Rising energy prices [Alekkett *et al.*, 2010] combined with decreasing profit margins [Fettweis & Zimmermann, 2008] require operators to optimize their operational expenses by decreasing power bills.
- In countries with incomplete or unreliable power grids, BSs are operated with grid-independent power sources like diesel generators or renewable energy sources [Fettweis & Zimmermann, 2008]. The costly deliveries of diesel and size of renewable energy sources like wind engines or solar panels make low consumption of the BS desirable [Nema *et al.*, 2010].
- In the face of global warming, customers have developed an understanding and sensibility for power consumption. Companies aim to apply *green* labels to their products [Han *et al.*, 2011a, Sugiyama, 2012].
- Disasters like the 2011 Tohoku earthquake and tsunami have shown that the installed battery backups were insufficient for long power grid interruptions [NTT DOCOMO Technical Journal Editorial Office, 2012]. After the disaster, BSs (and, thus, most communication) were unavailable for days until repair units had reconnected them to the power grid. Efforts in disaster recovery include low-power emergency modes and a generally lower power consumption to enable BSs to operate longer on battery power [Ran, 2011].

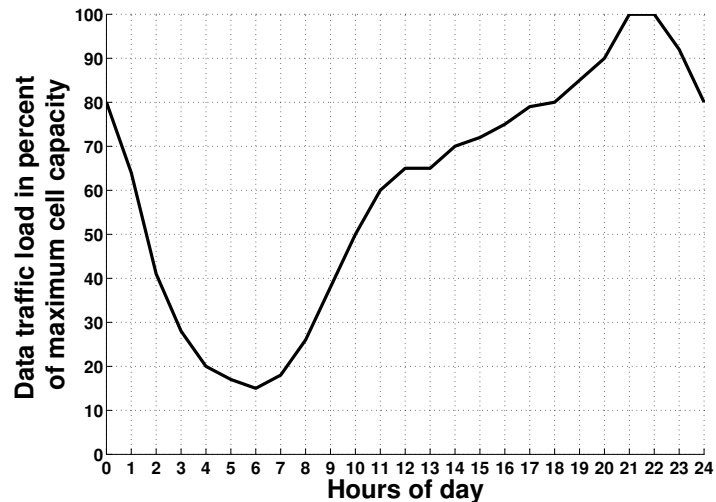


Figure 2.2: European average wireless daily traffic in 2010 [Auer *et al.*, 2011b].

For these reasons, reducing the operating power consumption of Long Term Evolution (LTE) BSs is the goal of the work presented in this thesis. Recent analyses provided information on how this goal could be achieved. In particular, it was found that while the cell traffic load fluctuates significantly, BSs are mostly unable to adapt to these fluctuations.

BSs have been designed and deployed to provide peak capacities to minimize outages. However, in practical scenarios, traffic is rarely at its peak. While BSs may be designed for crowded midday downtown situations, there are strong variations over time and location with regard to the density of mobile traffic. For example, see the typical mobile traffic in Europe over the course of a day in Fig. 2.2. It varies over a range of more than 80% and has an average of only 60% load [Auer *et al.*, 2011b]. Yet, although load varies so strongly, the power consumption of cellular BSs was found to vary as little as 2% over the course of a day [Arnold *et al.*, 2010]. BS power consumption is thus not yet sufficiently adaptive to the traffic demand. Hence, the times of day when the traffic load is below peak provide room for exploitation. During such times, the capacity of a BS can be reduced to achieve lower power consumption without affecting the user satisfaction or Quality of Service (QoS). How this could be achieved is the contribution of this thesis.

Note here an important differentiation between Green Radio technology proposals being either in design or in operation. Design proposals are made to affect the architecture or hardware of a BS, such as changing the type of Power Amplifier (PA). Design changes may take a long time to reach the market due to specification, approval or manufacturing. In contrast, operation proposals, like turning a BS off when it is unused, can reach the market much faster. They may be applicable to existing hardware and can be applied via software upgrades.

Although design and operation changes can be made independently, they affect each other. For example, a change in design—like the introduction of a secondary low power wake-up controller—may enable new types of operation like a cognitive wake-up functionality. In turn, the popular application of a certain type of operation, like sleep modes, may have consequences for future design decisions by providing incentive for producing sleep-mode-enabled hardware. In this thesis, this intertwining of design and operation is taken into account by first identifying the structure and potential of the hardware and then exploiting this potential in operational improvements to the BS.

2.3 Quantifying Energy Efficiency

Enhancing the energy efficiency of communication networks has led to a field of research popularly labelled *Green Radio*, which this thesis is part of. This field encompasses all efforts taken to increase the ratio of network quality over energy spent or CO₂ emitted. Making ‘radios greener’ can be achieved by either increasing network quality at unchanged energy expenditure, by providing equal quality at a lower cost, or both. Here, typical network quality indicators to be improved are capacity, fairness, latency, reliability, and range. Cost is often measured in CO₂ emission, energy consumption, or power consumption. Note that energy consumption is equal to the product of the average power consumption and a certain duration. In other words, power is energy normalized over time.

When discussing Green Radio research and results, it is important to be aware of some intricacies and necessary differentiations. Energy efficiency is not easily compared when considering different network quality indicators. For example, at equal energy consumption, an increase in capacity may come at the cost of increased latency, which cannot be easily weighted against each other. Alternatively, a decrease in power consumption through reduced network quality may trigger users to change their behavior which negates the initial savings. These problems are present in many fields of research and have led to discussions about QoS, which tries to assess the alternative a user may be more satisfied with [Andrews *et al.*, 2001]. But since an industry standard for the QoS does not yet exist, the common ground is to measure capacity as the most basic metric while stating the considered scenario assumptions such as geographic location, transmission duration, latency, *etc.* [EARTH Project Work Package 2, 2010].

Just as there are several ways to measure network quality, there are several alternatives to measuring the cost incurred. The simplest is to only consider *transmission power* at the antenna of a wireless transmitter. This number is usually well-known as it is regulated and targeted in hardware design. A more comprehensive approach is to consider total power spent by a transmitter which includes the heat generated while producing or processing a wireless signal. This number can usually be measured at the mains supply or deduced from battery durations. It is called the *supply power*. But even the supply power required by

a device during operation may not display the full picture. Aside from operation, a wireless device requires production before and disposal after. These steps can consume significant energy, particularly in electronic devices. They are composed of resource acquisition and mining, transportation, design, facility construction, production, and recycling. When widening the inspection of power or energy consumption to this global level, the consideration of watts or joules is insufficient. Rather, the global cost of the steps is measured in terms of CO₂ emission. Comparing CO₂ emissions instead of power consumptions allows taking into account that the CO₂ emitted by generating a watt of power varies depending on many factors. For instance, a BS operated in a remote location on imported diesel may cause much higher CO₂ emissions than a solar-powered BS on an urban rooftop. As energy generation usually does not lead to the emission of pure CO₂, but rather a mixture of global warming affecting gases, the effects of these actions are typically normalized to CO₂-equivalent (or CO₂-eq). For example, the Information and Communication Technologies (ICT) industry is estimated to have caused about 1.5% of global CO₂-eq emissions in 2007 [Malmudin *et al.*, 2010]. From 2007 to 2020, the CO₂-eq emission caused by mobile networks is predicted to grow from 0.2% to 0.4% [Fehske *et al.*, 2010]. Thus, a doubling of the energy efficiency of mobile communications would allow keeping CO₂-eq emissions on the 2007 level which is a common research and development target [Blume *et al.*, 2010].

As described above, both measuring network quality as well as measuring cost are very intricate. Therefore, the metric of watts of supply power per bit alongside clear network definitions has been chosen as the reference for this thesis. When applying techniques described here to larger scenarios, the additional definitions provide the information necessary for converting watts to CO₂-eq over a regional expanse and duration of operation.

2.4 Green Radio in Literature

Historically, the early works on energy efficiency for wireless networks have been triggered by a desire to extend battery lives in cellular, ad hoc or sensor networks, for example see [Ye *et al.*, 2002, Cui *et al.*, 2004, Cui *et al.*, 2005, Bhatia & Kodialam, 2004]. By the early 2000s, growing environmental concerns had led to extensive life cycle analyses of cellular networks [Malmudin *et al.*, 2001, Weidman & Lundberg, 2000]. These analyses collected all steps in a devices' life, quantified them with regard to energy expenditure and CO₂ emissions and joined them with the number of units sold and installed. The resulting statistics revealed that the power consumption of mobile network infrastructure was significant and that the CO₂ emissions of the ICT industry were as high as those of international air traffic [Fehske *et al.*, 2010, Fettweis & Zimmermann, 2008]. Through these findings, interest grew with regard to the energy efficiency of transmitters which are powered by the mains grid.

As a consequence, in 2008, the collaborative *Green Radio* project was initiated in the UK which coined the term [Mobile VCE, a]. The efforts were extended in 2009 by the European Energy Aware Radio and neTwork tecHnologies (EARTH) project [Gruber *et al.*, 2009]. Both projects encouraged specifically the enhancement of the energy efficiency of cellular access networks by improving their architecture and operation. The works proposed since then can be distinguished by the network aspects they consider.

For one, there are works which address the hardware of the radio access network. A general overview of such hardware improvements is provided in [Ferling *et al.*, 2010]. Specifically, the improvement of transceiver units is considered in [Gonzalez *et al.*, 2011, Bories *et al.*, 2011]. New PA architectures are proposed in [Hammi *et al.*, 2010]. The EARTH project has summarized proposed hardware improvements to LTE BSs in [EARTH Project Work Package 4, 2012].

Another group of works is the field of Heterogeneous Networks (HetNets). These works are concerned with the power consumption of future networks which are predicted to consist of a very large number of low power small BSs, such as micro, pico, or femto, in addition to macro BSs. The study in [Klessig *et al.*, 2011] finds the optimal density of small cells to match a traffic requirement from an energy perspective. In [Richter *et al.*, 2009], the area power consumption metric is proposed to enable comparison between different HetNets. Badic *et al.* [Badic *et al.*, 2009] formalize the trade-off that is present between capacity and power consumption in HetNets. In [Khirallah & Thompson, 2012], it is suggested that the overlap between macro and small cells in HetNets should be used in combination with sleep modes when the capacity increase provided by small cells is not needed. The authors in [Hoydis *et al.*, 2011] argue that due to the complexity of HetNets, they should be self-organizing and self-adapting to the traffic situation.

As a third topic, several kinds of sleep modes are proposed. Long sleep modes with duration of minutes or hours are very effective in reducing power consumption, but require a wake-up mechanism and reduce coverage. Short sleep modes in the order of microseconds to seconds, which are also called dozing, micro sleep or Discontinuous Transmission (DTX), do not pose these problems but promise smaller reductions of the power consumption. As a consequence, long sleep modes are proposed for situations in which coverage can be maintained through other means. For example, when network densities are sufficient such that neighbouring BSs can take over the coverage of sleeping BSs [Oh & Krishnamachari, 2010, Ashraf *et al.*, 2011]. Short sleep modes can be applied independent of coverage. The authors in [Frenger *et al.*, 2011] propose to use DTX when a cell is completely empty, posing a simple but very inflexible mechanism. In [Saker *et al.*, 2010] it is assumed that a BS consists of multiple independent transmitters, some of which can be deactivated according to traffic requirements, thus increasing the adaptivity to load. With regard to an entire network of sleep capable cells, Abdallah *et al.* [Abdallah *et al.*, 2012] study the

alignment of sleep modes between neighbouring cells and conclude that sleep modes should be synchronized and orthogonal for maximum efficiency.

Related to sleep modes is the field of cell breathing, cell shrinking or cell zooming through the adjustment of the transmission power [Han & Ansari, 2012, Abgrall *et al.*, 2010, Niu *et al.*, 2010]. By introducing flexibility with regard to the transmission power of a BS, a network can flexibly adjust to coverage requirements by increasing or decreasing cell sizes. For example, an increase of a cell's size may be needed when neighbouring cells enter sleep mode.

An extension of sleep modes is the topic of adapting multi-antenna transmission. Rather than using all installed antennas, a BS could deliberately reduce its Multiple-Input Multiple-Output (MIMO) degree to deactivate some antennas when high capacities are not required [Hedayati *et al.*, 2012, Skillermark & Frenger, 2012, Kim *et al.*, 2009, Xu *et al.*, 2011]. These approaches are labeled MIMO adaptation, antenna adaptation or MIMO muting. An alternative approach to exploit multiple antennas for energy efficiency is proposed by Wu *et al.* [Wu *et al.*, 2012b] and Stavridis *et al.* [Stavridis *et al.*, 2012], who, through—spatial modulation—use all antennas, but never at the same time.

Resource scheduling is a diverse group of works in which different approaches are proposed. Relaxing the delay requirement can be exploited for opportunistic power saving [Gupta & Strinati, 2011, Chong & Jorswieck, 2012]. Spreading signals over a larger bandwidth allows reducing the transmission power [Ambrosy *et al.*, 2012, Videv & Haas, 2011]. Approaches such as game theory promise gains by providing trading mechanisms for a self-organized allocation of resources for enhanced energy efficiency [Meshkati *et al.*, 2007].

In order to exploit the typically deployed overlapping radio access network generations, it is proposed in [EARTH Project Work Package 3, 2012] to combine a deactivation of one network technology, *e.g.* Global System for Mobile communications (GSM), with the fall-back to another such as LTE. However, this generates issues with backward compatibility and QoS.

To exploit spare backhaul capacity, it is suggested in [Scalia *et al.*, 2011] to use coordinated multi-point transmission between multiple BSs while deactivating parts of each BS. However, the benefits strongly depend on the additional power consumption caused by the backhaul link. When combined with sleep modes, it was found in [Han *et al.*, 2011b] that this approach only reduces power consumption in the presence of high data rate users.

In [Hevizi & Gódor, 2011] it is proposed to switch sectorized macro BSs to omni-directional operation when the capacity requirements are low. While this promises to save two thirds of the power consumption in typical three-sector setups, it also requires the installation of additional omni-directional antennas at BS sites.

The most far-reaching proposals for energy efficient cellular networks break with the cellular assumptions presumed in GSM, Universal Mobile Telecommunications System (UMTS) or LTE. By separating data and control planes from one

another, future networks could have large, long-range ‘umbrella’ control transmitters which take care of discovery and coverage. These would overarch small data plane BSs which are only activated when they are needed. Such a network setup would provide a very high capacity at a very high degree of load flexibility. These proposals are referred to in literature as ‘ghost’ or ‘phantom’ cell concepts [Strinati *et al.*, 2011, Ternon *et al.*, 2013], since the small data plane BS are ‘invisible’ to the User Equipment (UE).

For good surveys on Green Radio topics, the reader is referred to [Han *et al.*, 2011a, Auer *et al.*, 2011b, Wang *et al.*, 2012, Ephremides, 2002, Capozzi *et al.*, 2012].

Note that detailed literature backgrounds are again provided for each individual chapter in Chapters 3, 4 and 5.

In this wide field of research, this thesis can be placed in the group of works dealing with resource scheduling.

2.5 Technical Background

The following sections outline some fundamental concepts which reappear in Chapters 3, 4, and 5 of this thesis, namely, LTE, multi-carrier technology, multiple antenna transmission, convex optimization, and the usage of simulations to model complex cellular systems.

2.5.1 LTE

LTE [Dahlman *et al.*, 2011] is a wireless access standard superseding the GSM and UMTS for increased network capacities. It is predicted to be adopted in 93 countries by the end of 2013 [GSA Secretariat, 2013]. See Fig. 2.3 for an illustration on the world map. To this extent, the number of LTE subscriptions is rising steadily as it replaces older network technologies, as shown in Fig. 2.4. LTE is being continually standardized and developed by the 3rd Generation Partnership Project (3GPP). It is designed to achieve the following set of goals [Sesia *et al.*, 2009]:

- faster connection establishment and shorter latency;
- higher user spectral efficiencies of more than 5 bps/Hz on the downlink using link bandwidths of up to 20 MHz;
- uniformity of service provision independent of mobile position in a cell;
- improved cost per bit;
- flexibility in spectrum usage to accommodate to national band allocations;
- simplified network architecture;

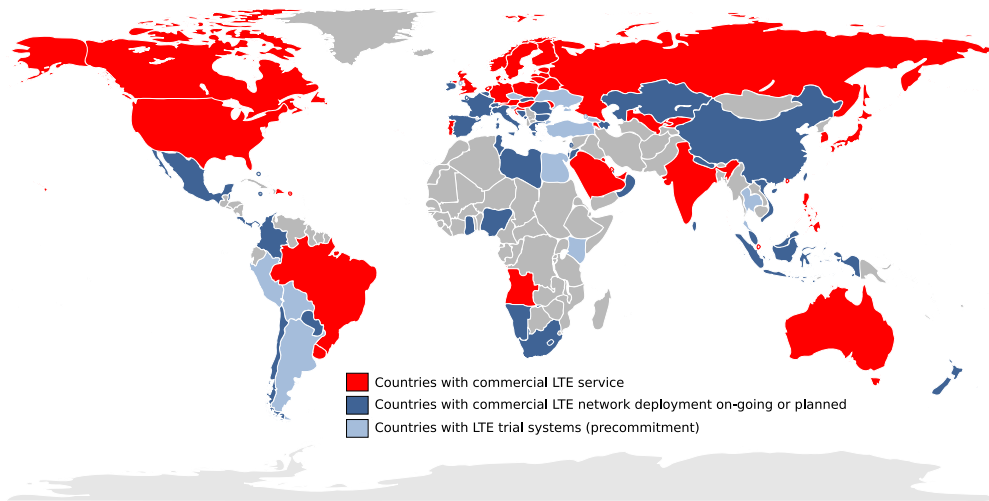


Figure 2.3: Adoption of LTE technology as of May 8, 2012 [GSA Secretariat, 2013].

- seamless switching between different radio access technologies;
- reasonable power consumption for the mobile terminal.

As LTE is a wireless technology on a shared medium, it is required to handle resource sharing and interference. These two important challenges are addressed in Chapters 4 and 5, respectively. Note that while LTE also consists of non-radio aspects such as the System Architecture Evolution (SAE), this thesis is only concerned with its BS and radio access aspects.

2.5.2 Multi-carrier Technology

The wireless medium is inherently shared. Wireless transmissions occur simultaneously in resources such as the frequency spectrum, time, and location. Therefore, transmissions can negatively affect one another through interference. The technique of dividing a resource into chunks to avoid overlap between multiple transmissions is called *multiplexing*. Time is typically shared via Time Division Multiplexing (TDM), frequency via Frequency Division Multiplexing (FDM), and location via installing BSs a significant distance apart from one another. Multiplexing allows providing multiple independent links carrying independent information streams on the wireless medium. These streams can be allocated to different users or scheduled to the same user for increased sum data rates, thus increasing the scheduling flexibility. In TDM, the shared resource is the time domain in which only one link can be active at any point in time and all links are spread over the entire available bandwidth. This concept is illustrated in Fig. 2.5 for four users. In FDM, the shared resource is the frequency domain. Here, links only take up a portion of the available frequency spectrum. See Fig. 2.6 for an illustration of FDM with multiple carriers and four users. Both of these technologies have been applied commercially in wireless technologies for decades. For

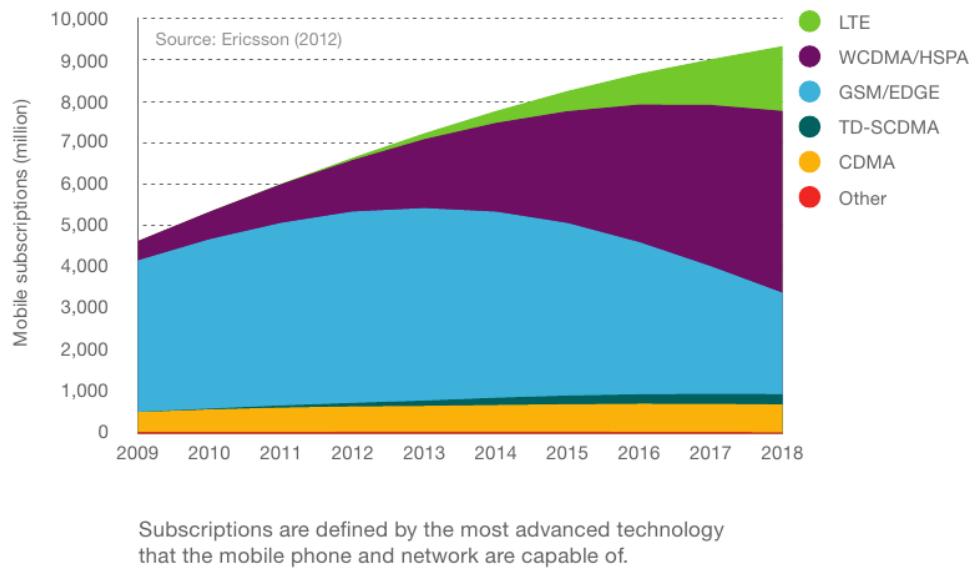


Figure 2.4: Mobile subscriptions by technology, 2009–2018 [Ericsson AB, 2012, p. 7].

example, **TDM** is the access scheme of choice in the **GSM** standard [Glover & Grant, 1998], whereas **FDM** has been employed in cordless phones [Garg, 2010]. A third popular multiple access scheme, Code Division Multiplexing (**CDM**)—*e.g.* used in the **UMTS** [Pike, 1998]—is not discussed here as it is not related to this thesis.

Orthogonal Frequency Division Multiplexing (**OFDM**) extends **FDM** to provide a very flexible high capacity multiple access scheme. Similar in notion to **FDM**, **OFDM** subdivides the bandwidth available for signal transmission into a multitude of narrowband subcarriers. The channels affecting these subcarriers are sufficiently narrow in the frequency domain to be considered flat-fading [Dahlman *et al.*, 2011] which is important for link adaptation. Unlike in **FDM** where frequency bands are non-overlapping, **OFDM** subcarriers are packed tightly and do overlap. Yet, through selection of the right pulse shape, the signals on each subcarrier remain orthogonal and can be transmitted in parallel with little to no mutual interference.

In addition to this fine separation in frequency, in **OFDM**, the transmission duration is divided into short slots to create an **OFDM block** with flat-fading characteristics in which one modulation symbol is transmitted (Multiple antenna technology allows the transmission of multiple symbols, as described in the following section). The modulation symbols can be from any modulation alphabet such as Quadrature Phase Shift Keying (QPSK), 16-Quadrature Amplitude Modulation (QAM), or 64-QAM. In **LTE**, such an **OFDM block** is labeled a *resource element*. The available bandwidth and a duration called *frame* are divided into a number of resource elements. Multiple resource elements are combined to constitute *resource blocks*. When **OFDM** is used to grant multiple

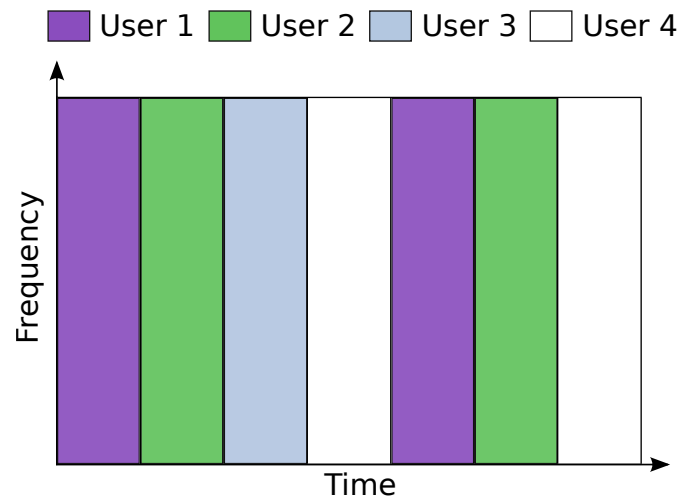


Figure 2.5: An illustration of **TDM**. Different users are assigned non-overlapping shares of the transmission time spanning a wide bandwidth.

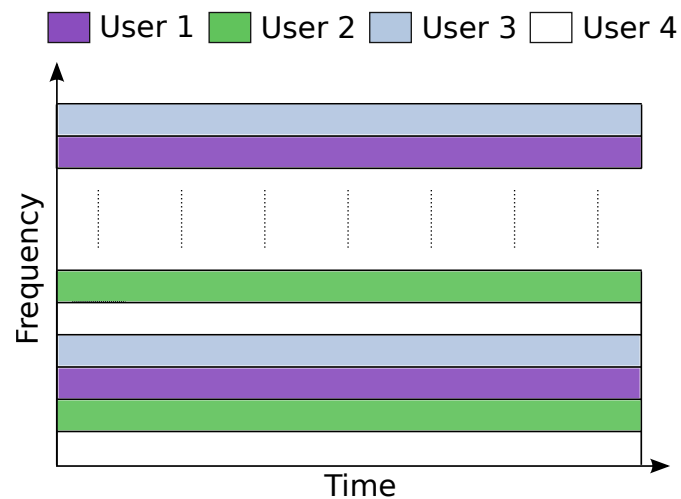


Figure 2.6: An illustration of **FDM**. Different users are assigned non-overlapping shares of the transmission bandwidth over a significant duration.

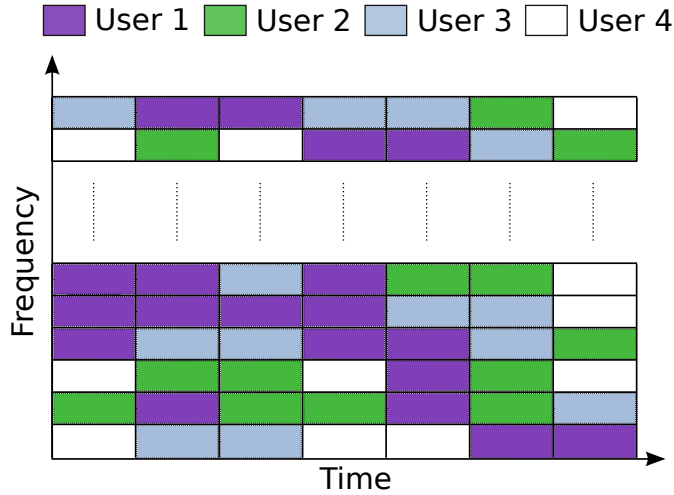


Figure 2.7: Example of resource allocation in a combined **OFDMA/TDMA** system constituting an **OFDMA** frame [Sesia *et al.*, 2009].

users access to the shared transmission medium, it is called Orthogonal Frequency Division Multiple Access (**OFDMA**). An illustration of a resulting **OFDMA** frame consisting of a set of resource blocks scheduled to different users is shown in Fig. 2.7. For a typical **LTE** system with a subcarrier spacing $\Delta_w = 15$ kHz, a system bandwidth $W = 10$ MHz, 12 subcarriers per resource block and a 10% guard band, the number of available resource blocks over the frequency domain is

$$N = \frac{0.9W}{12\Delta_w} = 50. \quad (2.1)$$

Although a resource block consists of multiple subcarriers constituting resource elements, it is the smallest unit which can be individually scheduled, according to the **LTE** standard [3GPP, 2010b]. For this thesis, it is thus assumed that a resource block consists of one subcarrier and stretches over the duration of one time slot. A frame is comprised of T time slots. For example, with $N = 50$ and $T = 10$, there are

$$NT = 500 \quad (2.2)$$

resource blocks available for scheduling in an **OFDMA** frame.

The option to schedule each resource block to any user in the system enables exploitation of an effect called *multi-user diversity*. As the channels on each resource block between each user and the **BS** is different, resource blocks can be scheduled such that only good channels are used. Statistically, over a certain bandwidth, number of time slots, and number of users, it is very probable that a good channel exists. This high probability results in an increase of the transmission data rate compared to a system which does not exploit this effect. An example of scheduling frequency by multiuser diversity is illustrated in Fig. 2.8.

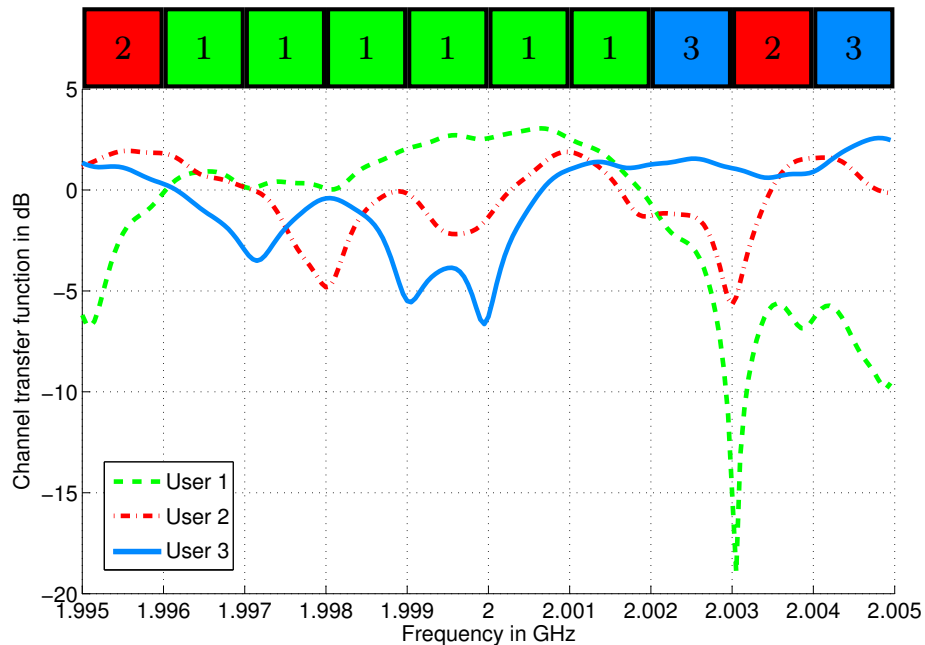


Figure 2.8: Example of multi-user diversity scheduling. For each frequency chunk the user with the best channel is selected.

Opportunistic scheduling between multiple users in a system is an important technique employed in Chapter 4.

2.5.3 Multiple Antenna Technology

The transmission and reception of wireless signals with multiple antennas is a standard technique in modern communication systems [Kühn, 2006]. Exploiting multi-path scattering, MIMO techniques deliver significant performance enhancements in terms of data transmission rate and interference reduction. The term *multi-path* refers to the arrival of transmitted signals at an intended receiver through differing angles, time delays and/or frequency shifts due to the scattering of electromagnetic waves in the environment, *i.e.* over multiple paths. Consequently, the received signal power fluctuates through the random superposition of the arriving multi-path signals. This random fluctuation allows the recognition and separation of the paths signals take between the multiple transmit antennas and multiple receive antennas, allowing to benefit from two important effects. First, like with multi-user diversity described in the previous section, having multiple signal paths reduces the probability of a deep fade. Hence, the reliability of the transmission is increased. The benefit of this effect is called the spatial diversity gain. Second, under suitable conditions such as rich scattering in the environment, separate data streams can be transmitted on the multiple paths. Thus, at the same time, on the same frequency spectrum, and in the same place, multiple data streams can be transmitted, increasing the data rate compared to

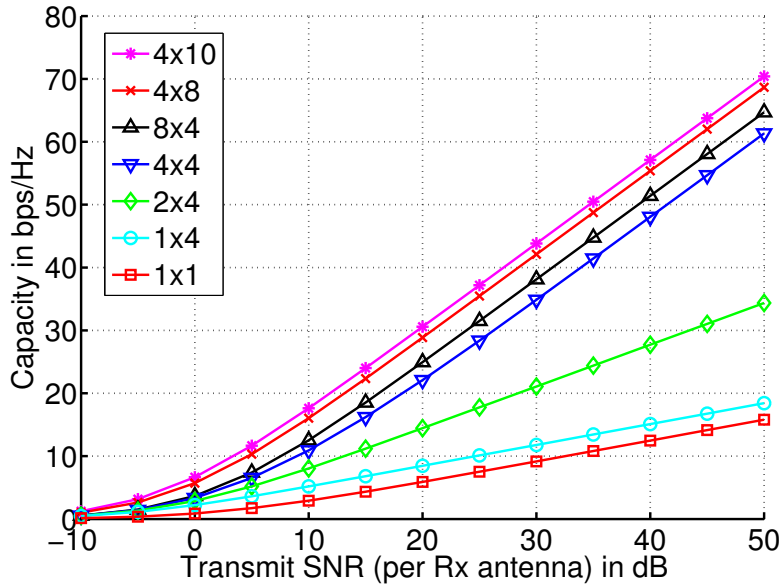


Figure 2.9: Power-fair **MIMO** capacities at perfect **CSI** at the receiver and statistical **CSI** at the transmitter.

a system with fewer antennas [Biglieri *et al.*, 2007]. The benefit of this effect is called the spatial multiplexing gain.

Under the assumption of statistical Channel State Information (**CSI**) at the transmitter, full **CSI** at the receiver and equal power allocated to each antenna, the ergodic **MIMO** link capacity is given by

$$C = \mathbb{E}_{\mathbf{H}} \left[\log_2 \det \left(\mathbf{I}_{M_R} + \frac{P_{T_x}}{D} \mathbf{H} \mathbf{H}^H \right) \right], \quad (2.3a)$$

$$= \sum_{i=1}^{\min(D, M_R)} \log_2 \left(1 + \frac{P_{T_x}}{D} \epsilon_i \right) \quad (2.3b)$$

with the expected value operator $\mathbb{E}_{\mathbf{H}}(\cdot)$, transmit power P_{T_x} , channel state matrix \mathbf{H} , the number of transmit and receive antennas D and M_R , respectively, identity matrix of size M_R , \mathbf{I}_{M_R} , and ϵ_i as the i -th singular value of $\mathbf{H} \mathbf{H}^H$ [Goldsmith *et al.*, 2003]. The gains in capacity through the use of multiple antennas can be charted by generating a number of Rayleigh distributed channel coefficients \mathbf{H} and plotting the achieved capacities. Figure 2.9 shows an illustration of achievable capacities, revealing two important characteristics of the **MIMO** capacity. First, it can be seen that capacity grows linearly with Signal-to-Noise-Ratio (**SNR**) at high **SNRs**. Second, the capacity grows linearly with $\min(D, M_R)$. Thus, more antennas yield a higher capacity. In this thesis, up to four receive and transmit antennas are considered due to limitations detailed in Section 4.5.2.

While raising the number of antennas increases the capacity, it also increases the complexity of transmitters and receivers. As will be shown in Chapter 3,

this increase in complexity is accompanied by a larger power consumption. It is studied in Chapter 4 how to trade off power consumption with capacity for energy efficiency by changing the MIMO mode through Antenna Adaptation (AA).

2.5.4 Convex Optimization

An important topic employed in Chapter 4 is convex optimization which is briefly introduced here.

A general optimization problem is often written as

$$\begin{aligned} & \text{minimize} && f_0(\mathbf{x}) \\ & \text{subject to} && f_i(\mathbf{x}) \leq b_i, \quad i = 1, \dots, m \\ & && h_i(\mathbf{x}) = 0, \quad i = 1, \dots, p. \end{aligned} \tag{2.4}$$

The problem consists of the optimization variable $\mathbf{x} = (x_1, \dots, x_n)$, the objective function $f_0 : \mathbb{R}^n \mapsto \mathbb{R}$, the inequality constraint functions $f_i : \mathbb{R}^n \mapsto \mathbb{R}$, $i = 1, \dots, m$ and equality constraint functions $h_i : \mathbb{R}^n \mapsto \mathbb{R}$, $i = 1, \dots, p$, and the constraints b_1, \dots, b_m . \mathbf{x}^* is the solution of the problem (2.4) if for any \mathbf{z} , $f_1(\mathbf{z}) \leq b_1, \dots, f_m(\mathbf{z}) \leq b_m$ and $h_1(\mathbf{z}) = 0, \dots, h_p(\mathbf{z}) = 0$, it holds that $f_0(\mathbf{z}) \geq f_0(\mathbf{x}^*)$ [Boyd & Vandenberghe, 2004].

This form of optimization problems is convex, if the functions f_0, \dots, f_m satisfy

$$f_j(\alpha \mathbf{x} + \beta \mathbf{y}) \leq \alpha f_j(\mathbf{x}) + \beta f_j(\mathbf{y}) \tag{2.5}$$

for all $\mathbf{x}, \mathbf{y} \in \mathbb{R}^n$, all $\alpha, \beta \in \mathbb{R}$ with $\alpha + \beta = 1$, $\alpha \geq 0$, $\beta \geq 0$, and $j = 0, \dots, m$. In other words, it is convex if the objective function as well as all constraints are convex. Furthermore, any equality constraints h_i have to be affine as any

$$h(\mathbf{x}) = 0 \tag{2.6}$$

can be represented as

$$h(\mathbf{x}) \leq 0, \tag{2.7a}$$

$$-h(\mathbf{x}) \geq 0. \tag{2.7b}$$

If $h(\mathbf{x})$ were convex, $-h(\mathbf{x})$ would be concave. The only way for both (2.7a) and (2.7b) to be convex is when $h(\mathbf{x})$ is affine.

The important property of convex optimization problems is that they can be solved by interior point methods and that the local optimum is always also the global solution [Palomar & Eldar, 2010]. Furthermore, convex optimization problems can often be solved very efficiently enabling their application even in real-time systems such as resource schedulers. A one-dimensional convex optimization problem without constraints can be graphically illustrated. An example is shown in Fig. 2.10 for some $t = f_0(x)$.

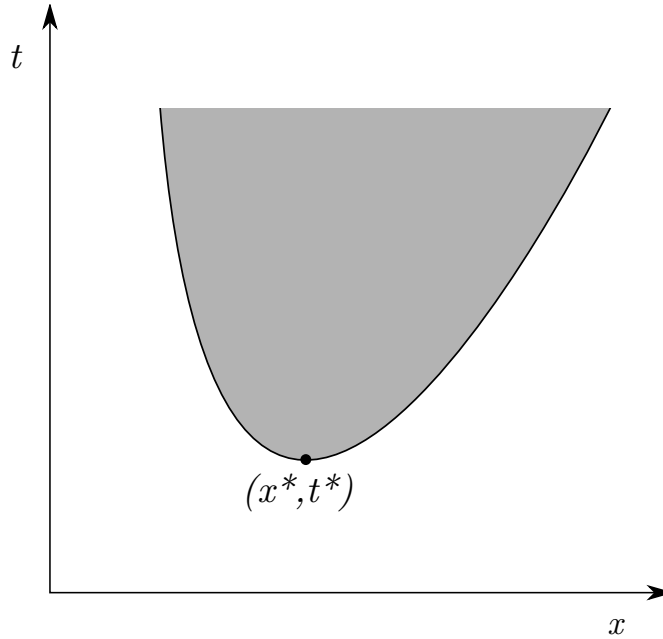


Figure 2.10: Geometric interpretation of a simple convex problem [Boyd & Vandenberghe, 2004].

A simple example of a two-dimensional convex optimization problem is

$$\begin{aligned}
 &\text{minimize} && f_0(\mathbf{z}) = z_1^2 + z_2 + 1 \\
 &\text{subject to} && f_1(\mathbf{z}) = -1 - z_1 \leq 0 \\
 &&& h_1(\mathbf{z}) = z_2 - 1 = 0.
 \end{aligned} \tag{2.8}$$

The second gradient of $f_0(\mathbf{z})$ is

$$\nabla^2 f_0(\mathbf{z}) = \begin{pmatrix} 2 & 0 \\ 0 & 0 \end{pmatrix}. \tag{2.9}$$

The objective function and its inequality constraints are convex as $\nabla^2 f_0(\mathbf{z})$ is greater or equal to zero on all entries. The equality constraint is affine. The sample problem is thus a convex optimization problem. By inspection of (2.8), it can be found that the solution is

$$\mathbf{z}^* = (0, 1). \tag{2.10}$$

Either proving convexity of a problem or transforming a problem into a convex problem are ways to efficiently solve optimization problems.

2.5.5 Network Simulation

For many problems in communications research, analytical solutions have not yet been found. To still be able to evaluate such problems, researchers resort to repeated independent trial executions of a given problem. The statistical outcomes

of these trials provide insight into the problems and potential solutions. These trials are often performed as computer simulations—rather than in hardware—to avoid costly and time consuming prototyping. Such computer simulations allow to model specific problems, vary their nature and generally experiment on them. They can also be used to test solutions and assess whether inventions deliver the anticipated results. As they prove to be such a versatile tool, they are used also in this thesis to assess the proposed solutions, when analytical solutions cannot be found.

More specifically, cellular networks are simulated which are as large as the computational constraints allow. For example, see Fig. 2.11 for the layout of a typical network simulation consisting of UEs and BSs distributed over an area.

The network simulator which produced the results shown in this thesis was developed from the ground up by the author and contains the following elements:

- A configuration interface via configuration files,
- Network generation consisting of:
 - Geometric modules for the distribution of physical entities onto hexagonally arranged three-cell BS sites,
 - Path loss and shadowing modules for the association of UEs to BSs as defined by the 3GPP [3GPP, 2010a],
 - OFDM MIMO Signal-to-Interference-and-Noise-Ratio (SINR) calculation,
- A frequency-selective fading model calibrated according to the Wireless world INitiative NEw Radio (WINNER) air interface configuration [IST-4-027756 WINNER II, 2006],
- Margin-adaptive resource allocation,
- Several modules for the algorithms described in Chapters 4 and 5,
- Interior point convex optimization via the Interior Point OPTimizer (IPOPT) [Wächter & Laird, a],
- Data collection, analysis and plotting tools,
- A unit test suite,
- Detailed event logging,
- Parallelization via the high-throughput parallelization system HTCondor [Condor Team, 2013].

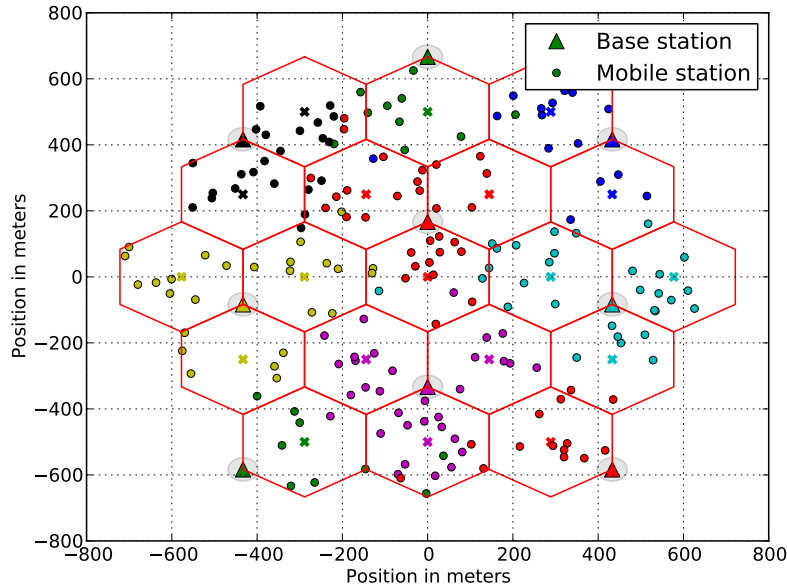


Figure 2.11: A sample network generated by the network simulator.

In addition to the list of simulator elements, it is also important to note what is not modelled. For example, capacity is calculated based on **SINR** by the Shannon limit. Bit errors, retransmission, error correction or protocols are not included; neither are pilots, channel sounding or **LTE** signaling and, thus, imperfect **CSI**. **UE** mobility is modelled as a fast-fading component rather than a change in position on the network map.

A typical simulation consists of a large number of independent trials executed in Monte Carlo fashion, *i.e.* in parallel, thus yielding statistical outcomes over all trials. A flowchart of the most important steps involved in a simulation run is provided in Fig. 2.12. To ensure sufficient consideration of interference, data is only collected from cells which are surrounded by at least two layers (tiers) of cells causing interference.

The simulators which produced the results presented in Chapters 3 and 4 were written as MATLAB [01a, a] scripts. Required packages are the Optimization and Statistics Toolboxes. An optional package is the Parallel Computing Toolbox. The network simulator employed in Chapter 5 was written in python [01, a] using numpy, scipy, matplotlib, virtualenv, IPOPT, ATLAS, LAPACK, MKL and ACML libraries. Depending on the network size, extensive simulation runs can take up to several days on a parallelized system. Unlike the highly optimized convex optimization processes, computation of **SINRs** and data handling are very time consuming, causing long simulation run times.

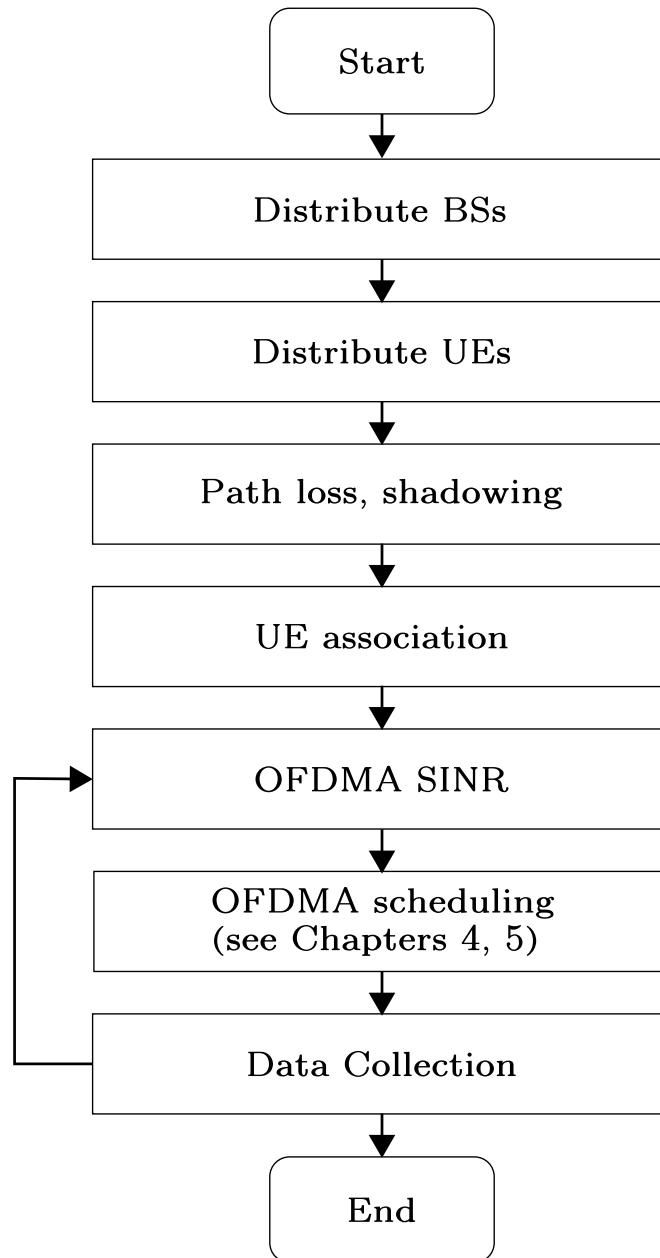


Figure 2.12: Sample simulation flowchart.

2.6 Summary

This chapter served to provide the motivation for **BS** power saving, establish the literature context, and briefly introduce key technical concepts. To begin with, it was explained that cellular **BSs** contribute significantly to the power consumption and CO₂ emission of mobile networks and that they do so during operation. Low load situations, such as night time, were identified as opportunities for reducing **BS** power consumption. The necessity of observing **BS** design along with **BS** operation for power saving was emphasized which is reflected in the structure of this thesis. Next, the Green Radio literature was discussed. In the last part of this chapter, key technical concepts were introduced which reappear in the following chapters. **LTE**, multicarrier and multiple antenna technology, and convex optimization are all important topics applied in this thesis. Furthermore, the computer simulation of cellular networks was described in detail as it was used for producing numerical results where analytical solutions could not be found.

Chapter 3

Power Saving on the Device Level

3.1 Overview

Power models describe how much power a device consumes in different configurations or scenarios. Depending on their depth, power models may also reveal architectural details and allow comparisons between different scenarios or assist the exploration of configurations which are not available for measurement in laboratories.

In energy efficiency research, power models are the basis of any power consumption analysis. Solid models are required to produce reliable results, since the model assumptions significantly affect the energy efficiency solutions proposed. For example, if a model were to falsely describe heat dissipation as a major contributor to power consumption, research efforts with regard to the reduction of heat dissipation might be ineffectively spent. Therefore, it is immensely important to have reliable power models such as the ones presented in this chapter.

In this chapter, three levels of detail of a power model for Long Term Evolution (LTE) Base Stations (BSs) are derived. The reason is that higher levels of detail allow ensuring the reliability of the model, manipulating specific aspects and parameters and recognizing the underlying architecture. In contrast, lower levels of detail abstract the model specifics in favor of applicability. The goal of this chapter is to allow the reader to first follow the construction of the component model and later the simplification towards the affine model.

The remainder of this chapter is structured as follows. Section 3.2 summarizes the challenges encountered when modeling BS power consumption. Existing power models are discussed in Section 3.3. Section 3.4 describes the *component power model* in detail. This model reveals the sources of power consumption within cellular BSs. In Section 3.5, the complex component model is parameterized into a *parameterized power model* such that only those parameters which are often manipulated for power saving remain, greatly reducing the model complexity. In Section 3.6, an *affine power model* approximation is defined. The affine

mapping contained in this model allows integrating it into analytical problems in Chapters 4 and 5. Section 3.7 summarizes the chapter and compares the three models with regard to their complexity.

The component model was developed in collaboration with the Energy Aware Radio and neTwork tecHnologies (EARTH) project. Hardware manufacturers have provided the experimental data on individual components. The author of this thesis has contributed to this power model by capturing it in MATLAB source code and aligning its concurrent development between EARTH partners. The model has been published and applied in parts in [EARTH Project Work Package 2, 2010, Auer *et al.*, 2011a, Auer *et al.*, 2011b, Desset *et al.*, 2012]. The detailed description of the model in this chapter is an original contribution. The parameterized model has been submitted for publication in [Holtkamp *et al.*, 2013b].

3.2 Challenges in Power Modeling

Generic modeling of BS power consumption is not a trivial task for multiple reasons. First, in order to protect their industrial designs, equipment vendors and manufacturers are hesitant to reveal the architecture of their products. They go so far as to contractually prohibit the opening of device casings for customers. Consequently, it is difficult to understand the contributing components to power consumption within cellular BSs. Second, vendors and manufacturers have differing designs, such that a power model may either only be valid for a single brand of devices or that multiple models would have to be developed. Third, architectures and technologies continually evolve, weakening the long-term applicability of power models. As such, a particular model may only be valid for a certain generation of BSs.

All of these problems have been addressed in the component power model as follows: By the combined effort of experts from multiple manufacturers, general common architectures were agreed upon without revealing competitive technical differences. These common architectures also helped bridge the design differences present between competing manufacturers. Finally, to ensure the lasting applicability of the model, foreseen technical advances were included in the model. As LTE is the prominent cellular network technology of the coming decade (see Section 2.5), the component power model describes an LTE BS.

The data sets provided in this chapter were all obtained through measurements within the EARTH project.

3.3 Existing Power Models

In the literature, three distinct power models for wireless transmitters are proposed and applied.

While in need of a power model for the comparison of the power efficiency of Multiple-Input Multiple-Output (MIMO) with Single-Input Single-Output (SISO) transmission, Cui *et al.* [Cui *et al.*, 2004] derived a first technology-independent model for the total power consumption of a generic radio transceiver. It was established that power consumption can be divided into the power consumption of the Power Amplifier (PA) and the power consumption of all other circuit blocks. The power consumption of the PA was described to vary with transmission settings like the number of antennas, the energy per bit, the bit rate, and the channel gain, while the consumption of circuit blocks was assumed a constant. Note that this power model is not a power model for cellular BSs, but for a generic wireless transceiver. Yet, it represents the first steps towards modeling the power consumption of wireless devices.

Arnold *et al.* [Arnold *et al.*, 2010] derive the power consumption of cellular BSs by considering that a typical BS consists of multiple sectors, has multiple PAs, a cooling unit, and a power supply loss. The remaining components' consumption is considered a constant. This model is accurate in its assumptions. But it only has data available for Global System for Mobile communications (GSM) and Universal Mobile Telecommunications System (UMTS) BSs. For LTE, the model is based on predictions and differs significantly from the values presented in this chapter.

Deruyck *et al.* [Deruyck *et al.*, 2012] used extensive experimental measurements to determine the power consumption of several types of State-Of-The-Art (SotA) BSs, like the macro cell, micro cell and femto cell. The power consumption of a BS is assumed to be a constant, independent of the traffic load. Thus, this model is not suitable for the exploration of BS operating power consumption as is required in Chapters 4 and 5.

The model described in the following has partly been published as an element of an EARTH project deliverable [EARTH Project Work Package 2, 2010]. It has been published in abbreviated form in [Auer *et al.*, 2011a, Auer *et al.*, 2011b, Desset *et al.*, 2012].

3.4 The Component Power Model

Before the description of the model, it is necessary to make some introductory remarks.

3.4.1 Remarks

First, this model describes the supply power consumption of a LTE cellular BS and is derived as the sum of the consumption of its subcomponents. The consumption of each subcomponent is derived from experimental measurements. The prediction of the dependence on operating parameters is derived from their architecture.

Parameter	Value
Feeder loss, σ_{feed}	0.5
Number of radio chains, D	2
Transmitted power, P_{Tx}	40 W
Number of BS sectors, M_{sec}	3
System bandwidth, W	10 MHz

Table 3.1: Model parameters used in figures of this chapter.

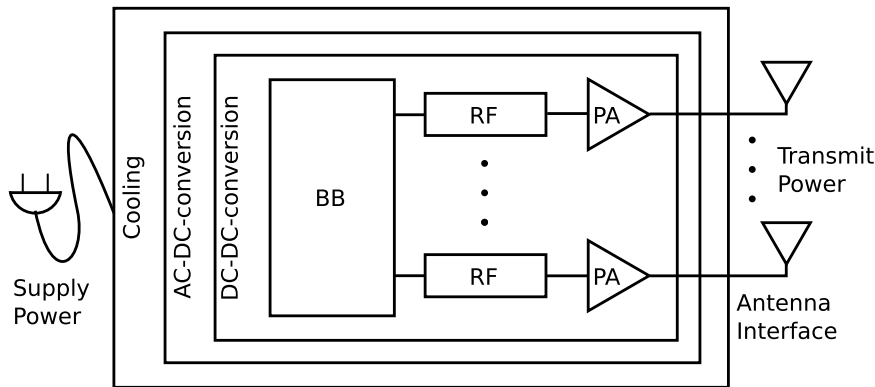


Figure 3.1: The components of the modelled BS.

Second, the model is an instantaneous model. It does not model effects which occur over time, such as power up or power down. Rather it models instantaneous power consumption at a certain configuration. When estimating power consumption over a time duration consisting of different configurations, a weighted averaging of the instantaneous values needs to be performed.

Third, this model encompasses the architecture of an **LTE BS** entering the market in the year 2012. For figures in this chapter, the system parameters in Table 3.1 are used. It represents the architecture found in most BSs which is foreseen to remain unchanged for the coming five to ten years. Note that this chapter is not concerned with how the hardware could be improved. Such hardware improvements were published in [EARTH Project Work Package 4, 2012].

3.4.2 The Components of a BS

The modelled **LTE** macro **BS** consists of a transceiver with multiple antennas. The transceiver comprises one or more lossy antenna interfaces, PAs and Radio Frequency (RF) transceiver sections as well as one Baseband (BB) interface including both a receiver section for uplink and transmitter section for downlink, one Direct Current (DC)-DC power supply regulation, one active cooling system and one mains Alternating Current (AC)-DC power supply for connection to the electrical power grid. Fig. 3.1 shows an illustration.

In practice, a **BS** may be serving multiple cells by sectorization. In that case, there may be overlap between the components and the sectors. For example, a single cooling cabinet may be used to house the electronics for all sectors. However, for purposes of modeling, it is assumed that a **BS** only serves a single cell. Thus, the power consumption of a **BS** for multiple cells can be found as the sum of the individuals.

In currently prevailing architecture as portrayed in Fig. 3.1, the **BS** contains one or multiple so-called *radio chains* each consisting of one **RF** transceiver, one **PA** and one antenna. Thus, the number of radio chains, antennas, **PA**s, and **RF** transceivers is identical and terminology can be used interchangeably.

In the following, the power consumption of each individual component is inspected to generate the component power model for the entire **BS**. Components are treated from right to left as depicted in Fig. 3.1.

Antenna Interface

This passive component is listed here for completeness, although it has no power consumption characteristics. For macro **BS** with long feeder cables between the **PA** and the antenna, a feeder loss has to be compensated for, which typically reduces the signal power by around 3 dB. For the model, this feeder loss is included in the modeling of the **PA**.

PA

The **PA** amplifies the signal before it is transmitted by the antenna. Due to low achievable efficiencies, **PA**s contribute significantly to the overall power consumption if high powers are targeted at the antenna, as described in Section 2.2.

Note that when comparing transmission powers in this study, it is referred to as the sum measured at the inputs of all antenna interfaces. Thus, feeder cable losses are included and **BS**s with differing numbers of antennas can be compared fairly with regard to their transmission power.

Due to its non-linearity, the **PA** modeling involves measurement results of the power-added efficiency. The power-added efficiency of the **PA** is looked up during modeling via the function $l_{\text{PA}}(\cdot)$. The efficiency function is shown in Fig. 3.2. The efficiency of the **PA** can reach up to 54% at very high transmission powers. However, these high efficiencies can rarely be achieved in operation due to the strong transmission power fluctuation of Orthogonal Frequency Division Multiple Access (**OFDMA**) signals and power control. At low transmission powers, **PA**s have very low efficiencies. This effect cancels the power saving of power control to some degree.

At constant power spectral density, the power output of each **PA**, P_{out} in W, is a function of the transmission power, P_{Tx} in W, the number of antennas, D , the share of the maximum bandwidth used for transmission, $f \in [0, 1]$, and an

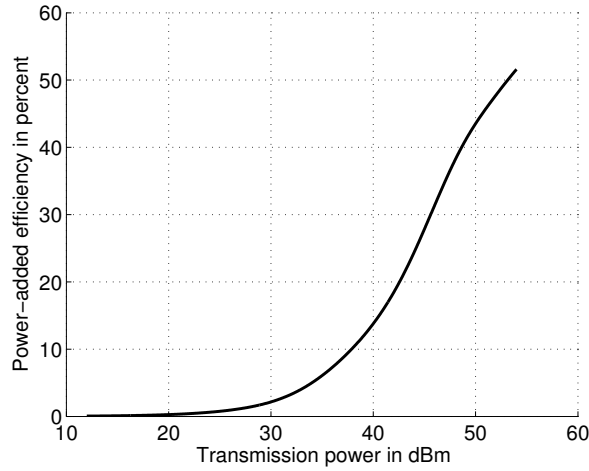


Figure 3.2: The power-added efficiency, $l_{\text{PA}}(\cdot)$, over the maximum output power as measured within the **EARTH** project.

adjustment for feeder losses, $\sigma_{\text{feed}} \in [0, 1]$ is given as

$$P_{\text{out}} = \frac{P_{\text{Tx}} f (1 - \sigma_{\text{feed}})}{D}. \quad (3.1)$$

The power consumption of the **PAs** in W is then determined by the efficiency and the number of **PAs**, such that

$$P_{\text{PA}} = D \frac{P_{\text{out}}}{l_{\text{PA}}(P_{\text{out}})}. \quad (3.2)$$

The power consumption in sleep mode, $P_{\text{PA,S}}$ in W , scales with the number of **PAs**. The power consumption of one **PA** in sleep mode, $P'_{\text{PA,S}}$, was found by experimental measurement, such that

$$P_{\text{PA,S}} = D P'_{\text{PA,S}}, \quad (3.3)$$

with $P'_{\text{PA,S}} = 27.75 \text{ W}$.

The power consumption of the **PA** over f is shown in Fig. 3.3. The effect of the reduced **PA** efficiency at lower transmission powers results in an almost linear relationship of bandwidth/transmission power to power consumption. At a maximum of 250 W, the **PAs** can consume a significant amount of power. However, this can be mitigated by reducing the transmission bandwidth. Also, as an analog component, a **PA** can be switched to a sleep mode with low power consumption quickly which has just above 50 W power consumption.

RF Transceiver

The **RF** transceiver provides the signal conversion between the digital and analog domain as well as frequency conversion between the **BB** and **RF** frequencies.

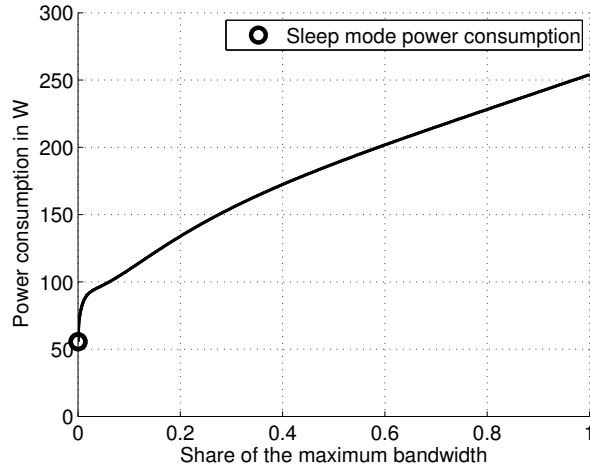


Figure 3.3: P_{PA} as a function of bandwidth used.

It consists of a large number of elements such as In-phase/Quadrature (IQ)-Modulators, voltage-controlled oscillators, mixers, Digital-to-Analog Converters (DACs) and Analog-to-Digital Converters (ADCs), low-noise and variable gain amplifiers and clocks. Power consumption of each of these elements is independent of external factors in measurement. The values and the resulting sum consumption are shown in Table 3.2. Thus, the power consumption of the RF transceiver is modelled as a constant. As one RF transceiver is installed in each antenna chain, RF power consumption scales with the number of antenna chains.

The power consumption of all RF transceivers, P_{RF} in W, is modelled as a linear function of an individual transceiver, P'_{RF} , with

$$P_{RF} = DP'_{RF}, \quad (3.4)$$

where P'_{RF} in W is comprised of reference values for commercially available components as shown in Table 3.2. A technology scaling factor, a_{TECH} , is included to account for different generations of RF transceivers.

The RF transceiver as present in currently manufactured BSs is incapable of sleep mode operation. Therefore, its power consumption in sleep mode is equal to its power consumption when active.,

$$P_{RF,S} = P_{RF}. \quad (3.5)$$

The power consumption of the RF transceiver is shown as a function of f in Fig. 3.4. Since it is constant, it can only be manipulated through the number of RF transceivers in operation. Sleep mode operation is not yet foreseen for RF transceivers.

Block element	Power consumption in mW
IQ Modulator, DL	1000
Variable attenuator, DL	10
Buffer, DL	300
Voltage-Controlled Oscillator (VCO), DL	340
Feedback mixer, DL	1000
Clock Generation, DL	990
DAC , DL	1370
ADC , DL	730
Low-Noise Amplifier (LNA) 1, UL	300
Variable Attenuator, UL	10
LNA 2, UL	1000
Dual mixer, UL	1000
Variable Gain Amplifier, UL	650
Clock generation, UL	990
ADC 1, UL	1190
Sum P''_{RF}	10880
Technology scaling a_{TECH}	1.19
$P'_{\text{RF}} = a_{\text{TECH}} P''_{\text{RF}}$	12940

Table 3.2: Reference power consumption values of **RF** transceiver blocks, where UL and DL refer to blocks which are part of the uplink or downlink operation, respectively.

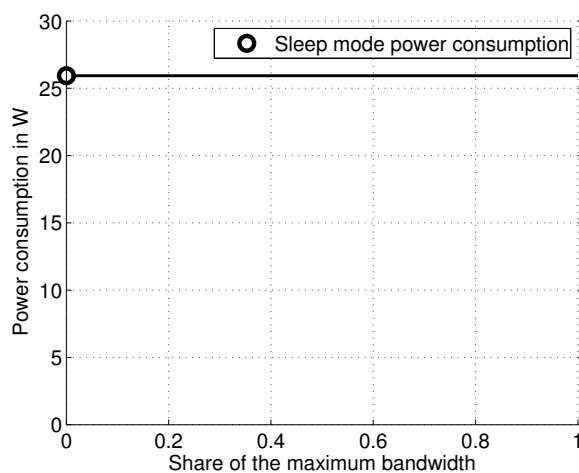


Figure 3.4: P_{RF} as a function of bandwidth used.

Type of processing, i	GOPS	$P_{i,\text{BB}}^{\text{ref}}$ in W	y_i^D	y_i^f	z_s
Time Domain Processing	360	9.0	1	0	0
Frequency Domain Processing	60	1.5	2	1	0
Forward Error Correction	60	1.5	1	0	1
Central Processing Unit	400	10.0	1	0	1
Common Public Radio Interface	300	7.5	1	0	1
Leakage	118	3.0	1	0	1

Table 3.3: Complexity of **BB** operations and their scaling with the number of transmit antennas and the transmission bandwidth.

BB Unit

The **BB** unit generates and processes the digital signal before it is passed to the **RF** transceiver. The **BB** unit of macro **BS**s is typically a stand-alone system-on-chip based on flexible Field-Programmable Gate Array (**FPGA**) architecture. Since this component is a digital processor, it is best modelled by its operations, namely by Giga Operations Per Second (**GOPS**). As the power cost of **GOPS** can be estimated at 40 **GOPS**/W and a set of different functions of the **BB** unit, I_{BB} , can be associated with the number of **GOPS** required, the power consumption can be modelled. Unlike in other **BS** components, the **BB** unit scales non-linearly with D and f . For example, the frequency domain processing complexity grows exponentially with the number of antennas. The exact scaling exponents along with the reference complexities for the modeling of **BB** operations are shown in Table 3.3.

These reference values and scaling exponents are used to find the **BB** unit power consumption in W, with

$$P_{\text{BB}} = \sum_{i \in I_{\text{BB}}} P_{i,\text{BB}}^{\text{ref}} D^{y_i^D} f^{y_i^f}, \quad (3.6)$$

where $P_{i,\text{BB}}^{\text{ref}}$ in W is the power consumption per sub-component, y_i^D is the scaling exponent for the number of radio chains, and y_i^f is the scaling exponent for the share of bandwidth used, each as provided in Table 3.3.

The sleep mode power consumption of the **BB** units, $P_{\text{BB,S}}$ in W, is lower than when in active mode, as time domain and frequency domain processing can be disabled as indicated by the sleep mode switch, z_s . Like the active power consumption, sleep mode power consumption is found by the combination of reference values and scaling exponents,

$$P_{\text{BB,S}} = \sum_{i \in I_{\text{BB}}} P_{i,\text{BB}}^{\text{ref}} D^{y_i^D} f^{y_i^f} z_s. \quad (3.7)$$

When drawn over the transmission bandwidth, see Fig. 3.5, the power consumption of the **BB** unit is found to be only lightly affected by load, *i.e.* the

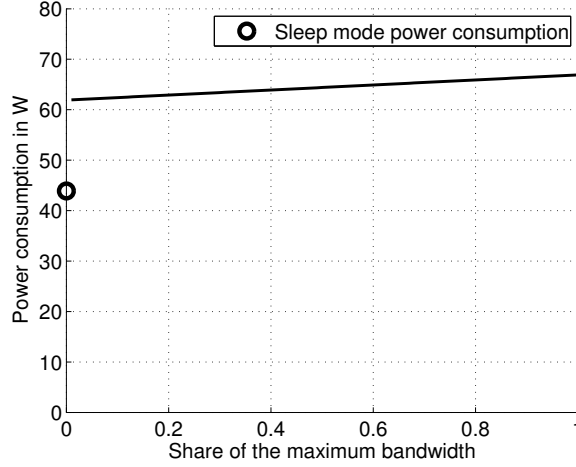


Figure 3.5: P_{BB} as a function of bandwidth used.

bandwidth used. However, sleep modes are available for the **BB** which can reduce its power consumption by more than 30%. **MIMO** operation has a significant effect on the **BB** power consumption, as it is modelled with a quadratic scaling factor due to the added computational complexity of **MIMO** processing.

DC-DC-Conversion

To supply the required **DC** voltages for the various components mentioned above, a **BS** is equipped with several **DC-DC**-converters. As the architectures of these converters may vary across vendors, the conversion is modelled as a single component. Laboratory measurements have been taken from one representative **DC-DC**-converter during the **EARTH** project as a function of the required load. Conversion has an efficiency of less than one, which can also be represented as a loss. With the **DC-DC**-converter built for a maximum power output of $P_{\text{DC,out,max}}$ in W, the loss is larger the further the actual required power by the **PA**, **RF** transceiver and **BB** unit is from $P_{\text{DC,out,max}}$. See Fig. 3.6 for the measured losses function, $l_{\text{DC}}(\zeta_{\text{DC}})$, of the ratio of maximum power output to actual power output, ζ_{DC} , with

$$\zeta_{\text{DC}} = \frac{P_{\text{DC,out,max}}}{P_{\text{PA}} + P_{\text{RF}} + P_{\text{BB}}}. \quad (3.8)$$

The power consumption caused by **DC-DC**-conversion in W is then found as

$$P_{\text{DC}} = l_{\text{DC}}(\zeta_{\text{DC}}) (P_{\text{PA}} + P_{\text{RF}} + P_{\text{BB}}). \quad (3.9)$$

SoTA **DC-DC**-converters are assumed to possess no capability for sleep modes and, thus, remain activated during **BS** sleep mode, with power consumption during sleep mode, $P_{\text{DC,s}}$ in W,

$$P_{\text{DC,s}} = P_{\text{DC}}. \quad (3.10)$$

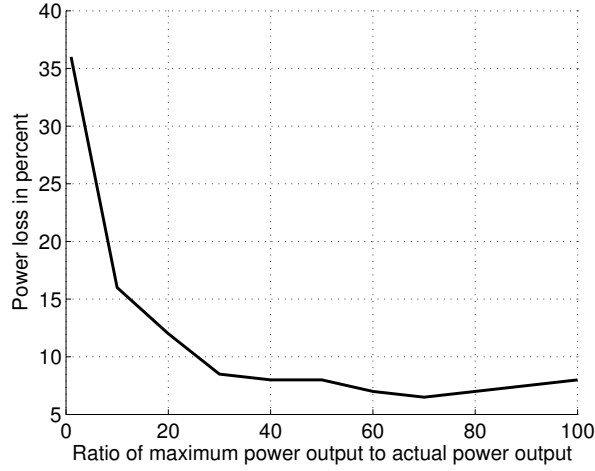


Figure 3.6: DC conversion loss function $l_{DC}(\zeta_{DC})$ as measured within the EARTH project.

The power consumption of the DC-DC-converter is shown as a function of f in Fig. 3.7. It is directly dependent on the components the DC-DC-converter powers and varies by less than 20% over all bandwidths. The reduced power consumption in sleep mode is only a passive effect and not an active switching process.

Mains Supply/AC-DC-Conversion

Power from the AC mains grid is converted to DC by the mains power supply unit. This unit is measured and modelled in the same fashion as DC-DC-conversion with conversion loss. See Fig. 3.8 for the measured losses as a function of the ratio of maximum power output to actual power output, ζ_{AC} , with

$$\zeta_{AC} = \frac{P_{AC,out,max}}{P_{PA} + P_{RF} + P_{BB} + P_{DC}}. \quad (3.11)$$

The power consumption caused by AC-DC-conversion is then found as

$$P_{AC} = l_{AC}(\zeta_{AC}) (P_{PA} + P_{RF} + P_{BB} + P_{DC}). \quad (3.12)$$

SotA AC-DC-converters are assumed to possess no special adaptation to sleep modes and, thus, remain activated during BS sleep mode, with power consumption during sleep mode, $P_{AC,S}$ in W,

$$P_{AC,S} = P_{AC}. \quad (3.13)$$

The power consumption of the AC-DC-converter is shown as a function of f in Fig. 3.9. Although the converter has non-linear efficiencies, these seem to compensate for the non-linearities of the components it powers. As a result, the power consumption curve is close to a straight line.

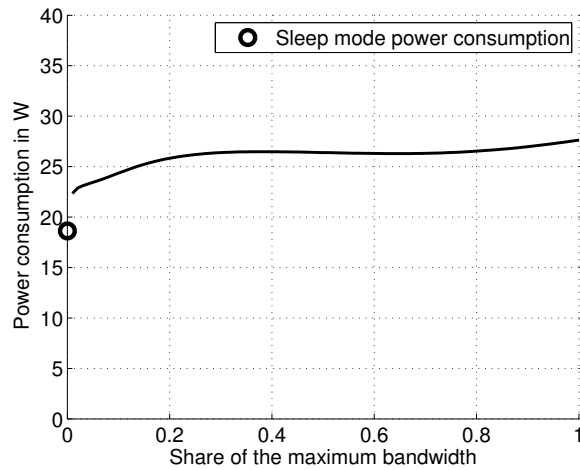


Figure 3.7: DC-DC-converter power consumption as a function of bandwidth used.

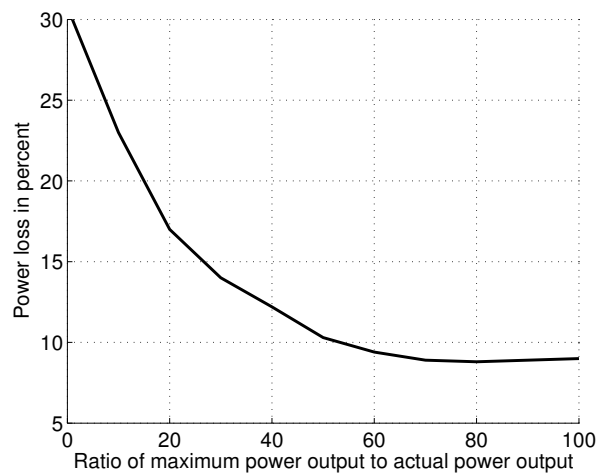


Figure 3.8: AC conversion loss function $l_{AC}(\zeta_{AC})$ as measured within the EARTH project.

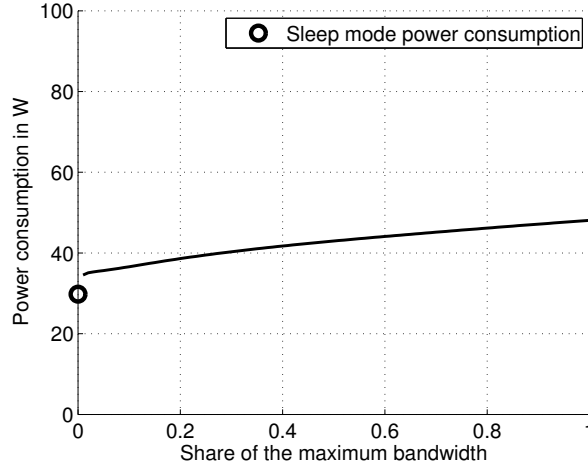


Figure 3.9: AC-DC-converter power consumption as a function of bandwidth used.

Cooling

Macro BSs are typically housed in a cooled cabinet. This cooling is a very difficult effect to model. Cooling requirements vary greatly between different geographic locations, positioning in or on buildings and the size of the storage cabinet. Different vendors recommend different operating temperatures for their devices and these recommendations may not be followed by the network operators. Furthermore, cooling is generally a very slow process compared to the orders of timing in a BS. Thus, considering cooling at its instantaneous power consumption may be misleading. As there is no simple solution to this problem, cooling is modelled as a fixed power loss.

The heat dissipation of all other components needs to be compensated for by active cooling. This heat dissipation can be assumed to be proportional to the power consumed. Thus, cooling power consumption is modelled to be proportional to the consumption of all other components. With cooling loss, $\xi_{\text{COOL}} = 0.12$, the power consumption of the cooling unit in W is

$$P_{\text{COOL}} = \xi_{\text{COOL}} (P_{\text{PA}} + P_{\text{RF}} + P_{\text{BB}} + P_{\text{DC}} + P_{\text{AC}}). \quad (3.14)$$

In this model, there are no further assumptions with regard to cooling during sleep mode. The power consumption of the cooling unit during sleep mode, $P_{\text{COOL,S}}$ in W, is therefore identical, with

$$P_{\text{COOL,S}} = P_{\text{COOL}}. \quad (3.15)$$

The power consumption of the cooling unit as a function of f is shown in Fig. 3.10. As it depends on all other components, it follows their power consumption behavior and is almost affine.

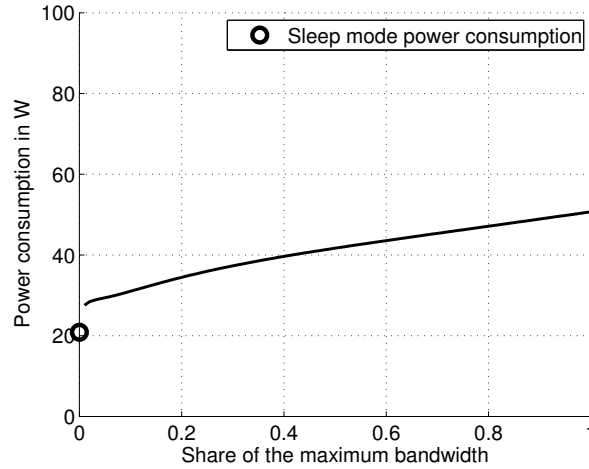


Figure 3.10: Cooling power consumption as a function of bandwidth used.

3.4.3 BS Power Consumption

The power consumption, P_{supply} in W, of an entire LTE BS is found as the sum of its components. With M_{sec} the number of sectors,

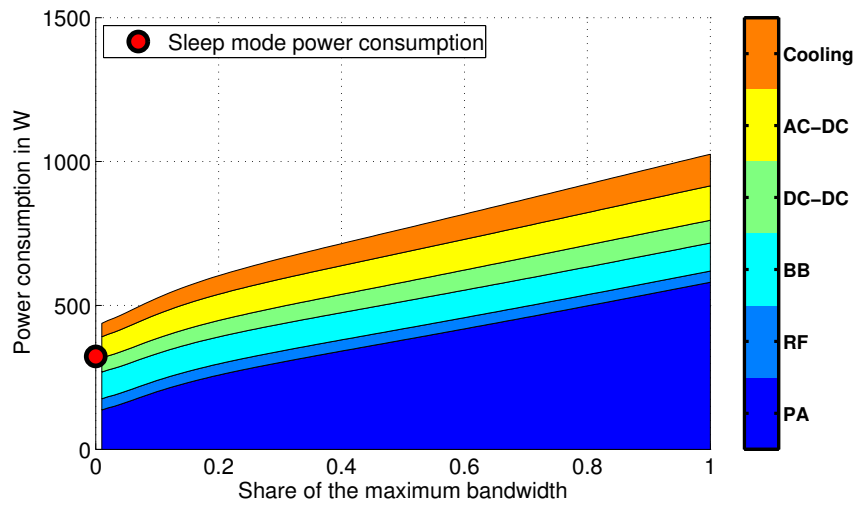
$$P_{\text{supply}} = M_{\text{sec}} (P_{\text{PA}} + P_{\text{RF}} + P_{\text{BB}} + P_{\text{DC}} + P_{\text{AC}} + P_{\text{COOL}}). \quad (3.16)$$

It is illustrated in Fig. 3.11 for $D = \{1, 2\}$. Fig. 3.12 provides a normalized comparison of the shares of power consumption at the two edge points of Fig. 3.11, namely at zero and at full bandwidth.

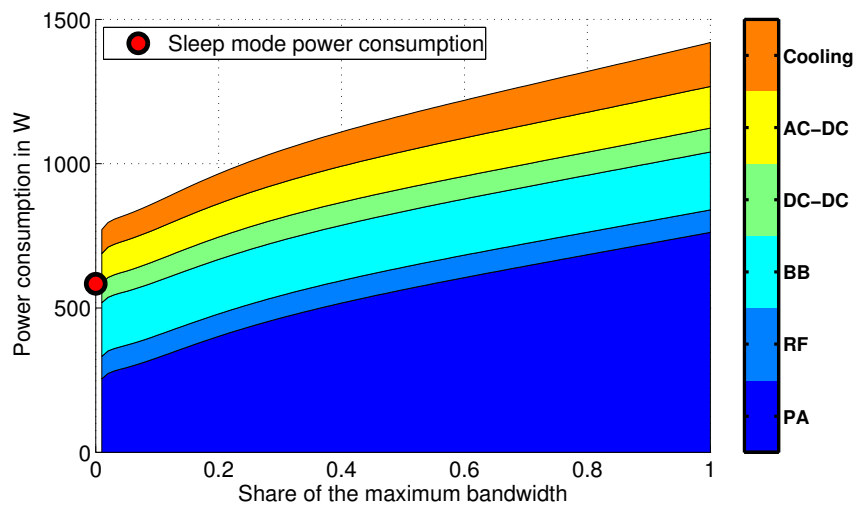
In both cases, for $D = 1$ and $D = 2$, respectively, the largest contributors to power consumption, especially at full bandwidth transmission, are found to be the PAs with 56.6% and 53.7%. At zero bandwidth, with 25.8% and 28.5%, the PAs still consume a larger share of the power than other components, but significantly less than for higher transmission bandwidths. Therefore, reducing the PA power consumption significantly affects the power consumption of the entire device.

With regard to sleep modes, for $D = 1$ and $D = 2$, respectively, they are estimated to lower consumption to 322 W and 583 W compared to an overall consumption of 437 W and 771 W at zero bandwidth, and 1025 W and 1419 W at full bandwidth usage. That corresponds to a reduction of power consumption by 26% and 24% at zero bandwidth and by 69% and 59% at full bandwidth usage. Thus, sleep modes can reduce the supply power consumption significantly, especially in high load operation.

Overall, it is important to recognize that the power consumption of a BS is far from constant and can be varied through operation parameters by as much as 69%. To reduce its power consumption, it should be operated with low power, low bandwidth or in sleep mode. In addition, the slope of the variation is nearly constant over f for both one and dual antenna operation. This allows for a greatly simplified power consumption model.

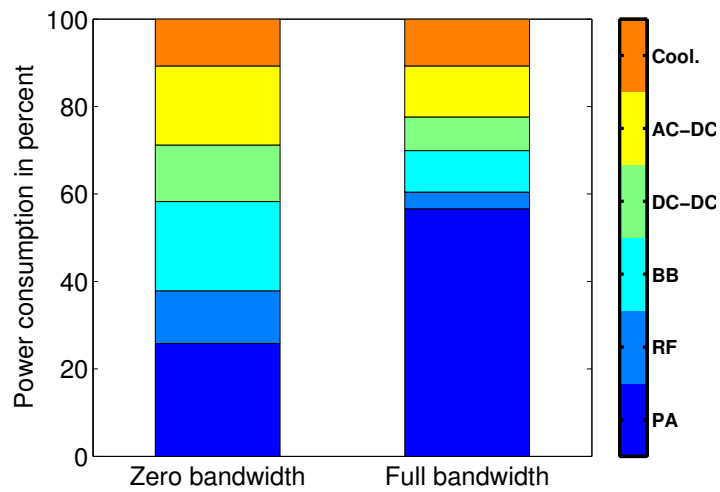


(a) One antenna.

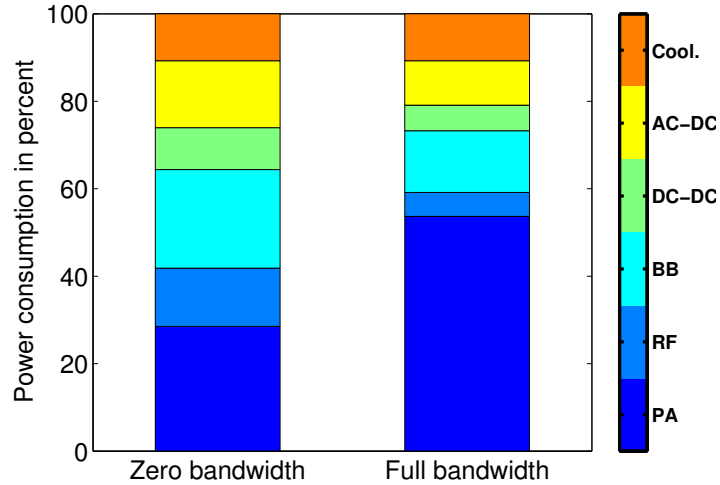


(b) Two antennas.

Figure 3.11: BS power consumption per component as a function of bandwidth used.



(a) One antenna



(b) Two antennas

Figure 3.12: BS power consumption per component at zero and full bandwidth.

The power model described in this section can be generated for other than macro BS types such as micro, pico, femto or Remote Radio Head (RRH) in similar fashion. However, as this thesis is only concerned with the power consumption of macro type BSs, these types are not discussed here.

3.5 The Parameterized Power Model

The power model described above is very useful for purposes of derivation, understanding, calibration and exploration of changes in architecture. The effect of changes to individual components on the power consumption of the entire BS can be studied. However, it is often unnecessary to derive the power consumption of a BS from the component level up. When exploring power saving techniques, only few parameters are varied regularly while many remain constant for an entire study. To address this need, this section proposes a simpler, parameterized power model. It abstracts architectural details for simplicity and only keeps those parameters which are regularly altered. It is based on the identification of power saving techniques.

In the literature, specific power saving techniques are suggested: namely, the effects of the number of antennas on power consumption [Cui *et al.*, 2004], the reduction of transmission power [Holtkamp *et al.*, 2011a, López-Pérez *et al.*, 2011, Miao *et al.*, 2008a], the deactivation of unneeded antennas [Hedayati *et al.*, 2012, Xu *et al.*, 2011], the adaptation of the transmission bandwidth [Ashraf *et al.*, 2011, Ambrosy *et al.*, 2012] and the use of low power consumption sleep modes of varied durations [Frenger *et al.*, 2011, Abdallah *et al.*, 2012, Videv & Haas, 2011, de Domenico, 2012].

The parameterized model encompasses all of these approaches to allow a direct comparison while abstracting parameters which can either be assumed to be constant or have little effect in the studied scenarios, such as GPRS, lookup tables, equipment manufacturing details or leakage powers. To this extent, only the following is covered in the proposed model:

- The different BS types of a heterogeneous network are modelled by applying different parameter sets to the same model equations.
- The number of transmission antennas and radio chains affects consumption during design and operation.
- The same holds true for transmission power, which affects the design indirectly by choice of a suitable power amplifier as well as the operation directly.
- Also, transmission bandwidth and sleep modes are modelled to allow the investigation of their impact on BS power consumption.

For parameterization, the maximum supply power consumption, P_1 in W, is first found establishing how power consumption scales with bandwidth, W , the number of BS radio chains/antennas, D , and the maximum transmission power, P_{\max} . This requires the consideration the main units of a BS as presented earlier: PA, RF small-signal transceiver, BB unit, DC-DC converter, mains supply and active cooling. Summarizing Section 3.4, the dependence of the BS units on W , D and P_{\max} can be approximated as follows:

- Both BB and RF power consumption, $P_{\text{BB}}^{\text{ppm}}$ in W and $P_{\text{RF}}^{\text{ppm}}$ in W, respectively, are assumed to scale nearly linearly with bandwidth, W , and the number of BS antennas, D .
- The PA power consumption, $P_{\text{PA}}^{\text{ppm}}$, depends on the maximum transmission power per antenna, P_{\max}/D , and the PA efficiency, η_{PA} . Also, possible feeder cable losses, σ_{feed} , have to be accounted for, such that

$$P_{\text{PA}}^{\text{ppm}} = \frac{P_{\max}}{D\eta_{\text{PA}}(1-\sigma_{\text{feed}})}. \quad (3.17)$$

- Losses incurred by DC-DC conversion, AC-DC conversion and active cooling scale linearly with the power consumption of other components and may be approximated by the constant loss factors σ_{DC} , σ_{AC} , and σ_{COOL} , respectively.

These assumptions allow calculating the maximum power consumption of a BS sector,

$$P_1 = \frac{\left[D \frac{W}{10 \text{ MHz}} (P_{\text{BB}}^{\text{ppm}} + P_{\text{RF}}^{\text{ppm}}) + P_{\text{PA}}^{\text{ppm}} \right]}{(1-\sigma_{\text{DC}})(1-\sigma_{\text{AC}})(1-\sigma_{\text{COOL}})}. \quad (3.18)$$

An important characteristic of a PA is that operation at lower transmit powers reduces the efficiency of the PA and that, consequently, power consumption is not a linear function of the PA output power. This is resolved by taking into account the ratio of maximum transmission power of a PA from its data sheet, $P_{\text{PA,limit}}$ in W, to the maximum transmission power of the PA during operation, $\frac{P_{\max}}{D}$. In typical PAs, the current transmission power can be adjusted by adapting the DC supply voltage, which impacts the offset power of the PA. The efficiency is assumed to decrease by a factor of θ for each halving of the transmission power. The efficiency is thus maximal when $P_{\max} = P_{\text{PA,limit}}$ in single antenna transmission and is heuristically well-described by

$$\eta_{\text{PA}} = \eta_{\text{PA,max}} \left[1 - \theta \log_2 \left(\frac{P_{\text{PA,limit}}}{P_{\max}/D} \right) \right], \quad (3.19)$$

where $\eta_{\text{PA,max}}$ is the maximum PA efficiency.

The reduction of power consumption in sleep mode is achieved by powering off PAs and reduced computations necessary in the BB engine. For simplicity,

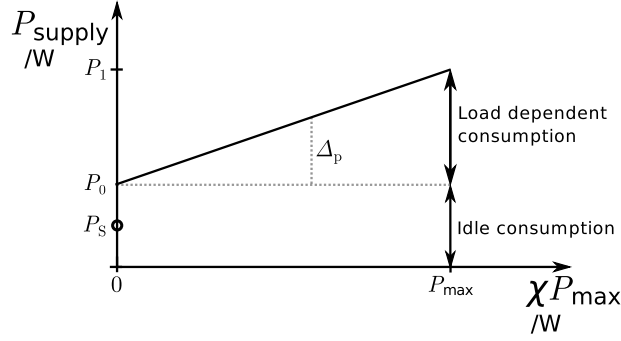


Figure 3.13: Load-dependent power model for an **LTE BS**.

only the dependence on D is modelled as each **PA** is powered off. Thus, P_S , is approximated as

$$P_S = DP_{S,0}, \quad (3.20)$$

where $P_{S,0}$ is a reference value for the single antenna **BS** chosen such that P_S matches the complex model power consumption for two antennas.

It can be approximated from Fig. 3.11 to treat the supply power consumption as an affine function of the bandwidth and, thus,—given constant power spectral density—of the transmission power. In other words, the consumption can be represented by a static (load-independent) share, P_0 in W , with an added load-dependent share that increases linearly by a power gradient, Δ_p , see Figure 3.13. The maximum supply power consumption, P_1 in W , is reached when transmitting at maximum total transmission power, P_{\max} . Furthermore, a **BS** may enter a sleep mode with lowered consumption, P_S , when it is not transmitting. Total power consumption considering the number of sectors, M_{sec} , is then formulated as

$$P_{\text{supply}}(\chi) = \begin{cases} M_{\text{sec}} (P_1 + \Delta_p P_{\max} (\chi - 1)) & \text{if } 0 < \chi \leq 1 \\ M_{\text{sec}} P_S & \text{if } \chi = 0, \end{cases} \quad (3.21)$$

where $P_1 = P_0 + \Delta_p P_{\max}$. The scaling parameter, χ , is the load share, where $\chi = 1$ indicates a fully loaded system, *e.g.* transmitting at full power and full bandwidth, and $\chi = 0$ indicates an idle system.

The parameterized power model is applied to approximate the consumption of the **BS** which was described in the component model. Parameters are chosen where possible according to [Auer *et al.*, 2011b], such as losses, efficiencies and power limits. The remaining parameters are adapted such that a closer match to the component model could be achieved. The resulting parameter breakdown is provided in Table 3.4. The two power models are compared over f for one and two antennas in Figure 3.14. Although two parameters, the bandwidth and the number of **BS** antennas, are varied, the parameterized model can be seen to closely approximate the complex model for all **BS** types. The largest deviation of the parameterized model from the complex model occurs when modeling four

$P_{\text{PA,limit}}$ /W	$\eta_{\text{PA,max}}$	θ	P_{BB} /W	P_{RF} /W	σ_{feed}	σ_{DC}	σ_{COOL}	σ_{AC}	M_{Sec}
80.00	0.36	0.15	29.4	12.9	0.5	0.075	0.1	0.09	3
			P_{max} /W	P_1 /W	Δ_p *10 MHz	$P_{\text{S},0}$ /W			
			40.00	460.4	4.2	324.0			

Table 3.4: Parameter breakdown.

transmit antennas. This is caused by the fact that the parameterized model considers a constant slope, Δ_p , which is independent of D . In contrast, the **PA** efficiency in the complex model decreases with rising D , leading to an increasing slope which can not be matched by a constant slope. This deviation is a trade-off between simplicity and model accuracy.

In addition to providing a solid reference, the model and the parameters can provide a basis for exploration. Individual parameters can be changed to observe the resulting variation in power consumption. With regard to the number of antennas, the parameterized model can only be verified up to four antennas, which is the extent of the complex model. Extending the system bandwidth, for example to 20 MHz, is expected to increase the **BB** and **RF** power consumption. The other parameters such as the transmission power and losses are expected to remain unaffected by different system bandwidths. Adapting the design maximum transmission power, P_{max} , affects the **PA** efficiencies, which decrease with P_{max} .

3.6 The Affine Power Model

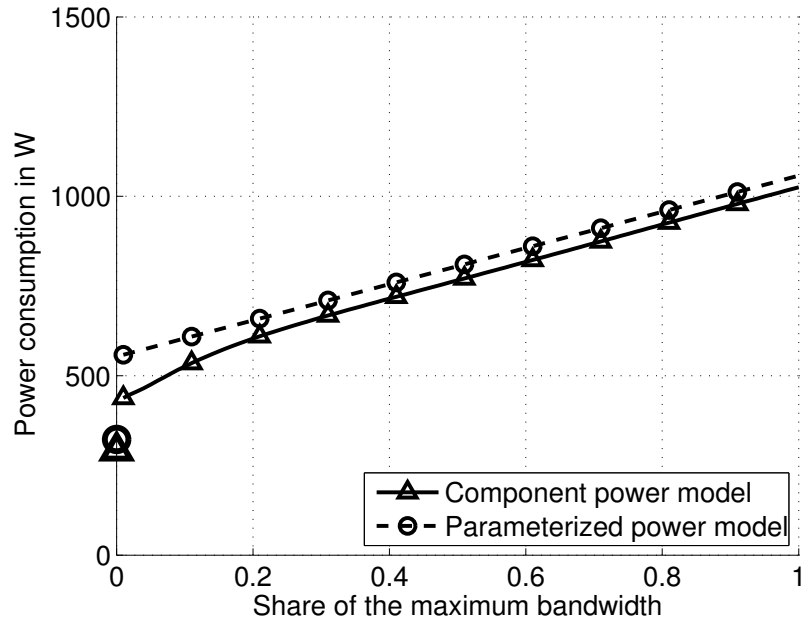
In preparation for the following chapters of this thesis, one more simplification to power modeling is made. When the input parameters for (3.18) and (3.20) are not changed, the power model can be reduced to (3.21) as a function of the load χ . When considering Antenna Adaptation (**AA**), a separation has to be made depending on D . This simplification carries the benefit of turning the power model into an affine function. As will be shown in the next chapter, the treatment of power consumption as an affine function maintains convexity.

Let the general affine model be

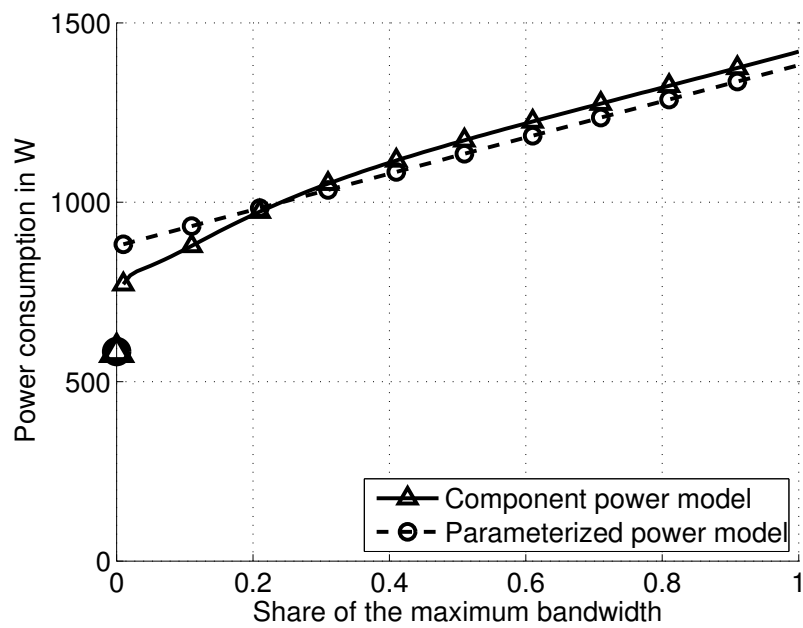
$$P_{\text{supply}}(\chi) = \begin{cases} 3(P_{1,D} + \Delta_p P_{\text{max}}(\chi - 1)) & \text{if } 0 < \chi \leq 1, \\ 3 \cdot P_{\text{S},D} & \text{if } \chi = 0, \end{cases} \quad (3.22)$$

with $P_{1,D} = P_{0,D} + \Delta_p P_{\text{max}}$.

For the remainder of this thesis, power consumption will therefore be modelled according to (3.22). This is a combination of the parameterized affine function and the component model sleep mode value in Fig. 3.14.



(a) One antenna



(b) Two antennas

Figure 3.14: Comparison of the parameterized with the complex model [Desset *et al.*, 2012] power models for the macro BS type with 40 W transmission power.

D	$P_{1,D}$ /W	$P_{0,D}$ /W	$P_{S,D}$ /W	Δ_p
1	354	186	107	4.2
2	460	292	216	4.2

Table 3.5: Summary of affine power model parameters.

For later reference, the affine power model for a single antenna **BS** is explicitly written as

$$P_{\text{supply}}(\chi) = \begin{cases} 3(354 + 4.2P_{\text{max}}(\chi - 1)) & \text{if } 0 < \chi \leq 1, \\ 321 & \text{if } \chi = 0. \end{cases} \quad (3.23)$$

The affine power model for a two-antenna **BS** is

$$P_{\text{supply}}(\chi) = \begin{cases} 3(460 + 4.2P_{\text{max}}(\chi - 1)) & \text{if } 0 < \chi \leq 1, \\ 648 & \text{if } \chi = 0. \end{cases} \quad (3.24)$$

A tabular summary is provided in Table 3.5.

3.7 Summary

In this chapter, three different power models have been derived, namely the component model, the parameterized model, and the affine model. The component model was derived by first defining the architecture of a typical **LTE BS** and then inspecting each component with regard to its power consumption. The **PA** was found to have a power consumption which strongly depends on the transmission power with some capability for sleep mode. The **RF** transceiver in its current implementation has limited adaptability and, therefore, constant power consumption. The **BB** unit's power consumption is determined by the internal computing operations, some of which can be reduced for power saving. The power consumption components such as power conversions and cooling, strongly depends on the power consumption of other components. Altogether, the power consumption of the individual components comprises the component **BS** power model. While very detailed and necessary for derivation, the component model is too elaborate for many uses. To address this complexity, the parameterized power model was derived from it, which only considers typical operating parameters while abstracting architectural and technical details. It was shown to closely approximate the component model for a range of parameters. Instead of using measured data ranges containing many values in the model, all input parameters are generalized to scalars (single values). When employed in an analytical context, a further fixation of input parameters is advisable, yielding the affine model. Overall, the number of input parameters including experimental data was reduced

Parameter	Component model	Parameterized model	Affine model
Feeder loss	S	S	
PA efficiency	V	S	
PA sleep consumption	S		
RF consumption	V	S	
BB consumption	V	S	
Scaling exponent for D	V		
Scaling exponent for f	V		
Sleep switching BB	V		
DC-DC loss	V	S	
Maximum DC-DC output	S		
AC-DC loss	V	S	
Maximum AC-DC output	S		
Cooling efficiency	S	S	
Number of sectors	S	S	
Number of radio chains	S	S	S
Maximum transmission power		S	
PA efficiency decrease		S	
PA limit		S	
Sleep consumption reference		S	S
Power consumption load factor		S	S
Maximum power consumption			S
Number of data range vectors (V)	8	0	0
Number of scalars (S)	7	14	4

Table 3.6: Comparison of required input parameters for different power models.

from 15 parameters (out of which 8 are data ranges) in the component model to 14 scalar parameters in the parameterized model and to four scalar parameters in the affine model. See Table 3.6 on page 49 for the detailed comparison.

Chapter 4

Power Saving on the Cell Level (Single-cell)

4.1 Overview

As introduced in Chapter 2, current cellular systems are capacity optimized with little consideration of the power consumed. In contrast, for power saving, networks need to be efficiency optimized. The difference between a power efficient and a capacity maximizing system is that a power efficient system only consumes the resources that are *needed* while a capacity maximizing system consumes those that are *available*. As described in Section 2.2, cellular systems are rarely fully loaded and at times completely unloaded [Sandvine, 2010]. This implies that not all of the bandwidth, time or transmission power are needed. The power-saving Radio Resource Management (RRM) mechanisms proposed in this chapter address this issue and exploit spare capacity to increase the system efficiency.

In this chapter the previously established power models are applied to study power-saving Base Station (BS) operation. Section 4.2 discusses the State-Of-The-Art (SotA) of power-saving RRM in the literature. It is then identified in Section 4.3 how a transmission consumes power and which parameters should be optimized to minimize consumption on the basis of general communication theory. Trade-offs are identified between Time Division Multiple Access (TDMA) and Power Control (PC). In Section 4.4, the solution to multi-user BS PC is proposed and studied. Once the system is optimized with regard to PC, Discontinuous Transmission (DTX) is added to further drive down power consumption via joint optimization. The general real-valued TDMA solution is derived. In Section 4.5, the convex optimization problem is then extended into a single-cell multi-user Multiple-Input Multiple-Output (MIMO) Orthogonal Frequency Division Multiple Access (OFDMA) power-saving algorithm. The chapter is summarized in Section 4.6.

The material presented in this chapter has previously been published or

submitted for publication in [Holtkamp & Auer, 2011, Holtkamp *et al.*, 2011b, Holtkamp *et al.*, 2011a, Holtkamp *et al.*, 2013a, Wu *et al.*, 2012a].

4.2 Power-saving **RRM** in Literature

In the literature, **PC** is the most prominent power-saving **RRM** mechanism with numerous proposals for a range of different problems, for example the related works in [Sinanović *et al.*, 2007, Wong *et al.*, 1999, Miao *et al.*, 2008b, Kivanc *et al.*, 2003, Al-Shatri & Weber, 2010]. This prominence is due to the fact that, in addition to reducing power consumption, **PC** is also beneficial to link adaptation and interference reduction. Sinanović *et al.* [Sinanović *et al.*, 2007] explore the optimal power points in a network with two interfering links and provide a communication theoretic basis for this work. Wong *et al.* [Wong *et al.*, 1999] minimize transmit power for multi-user Orthogonal Frequency Division Multiplexing (**OFDM**) under rate constraints. Although their work is pioneering, it has the drawbacks that the **PC** algorithm is computationally complex and does not consider a transmit power constraint or a power model. Miao *et al.* [Miao *et al.*, 2008b] presented an early work on efficiency in which they derive the uplink data rate which maximizes the transmitted information per unit energy (bit per joule). Kivanc *et al.* [Kivanc *et al.*, 2003] allocate subcarriers such that transmission powers are reduced. Their algorithm is modified and applied in this chapter. Al-Shatri *et al.* [Al-Shatri & Weber, 2010] approach sum rate maximization by using margin-adaptive power allocation, a method which is also used towards the end of this chapter.

More recently, acknowledging the significance of transmission-power-independent power consumption for energy efficiency, **DTX** and Antenna Adaptation (**AA**) have been identified as promising energy saving **RRM** techniques. The term **DTX** refers to an interruption of transmission which can be used to enter a short sleep mode. This interruption can be short enough to be unnoticeable to a receiver and fit into an **OFDMA** frame. This allows to schedule **DTX** flexibly without affecting the User Equipment (**UE**). Thus, **DTX** carries the benefit of not increasing delay or inhibiting discovery compared to longer sleep modes. **DTX** is first proposed in [Frenger *et al.*, 2011]. To the best of the author's knowledge, there are no prior works which consider **DTX** in combination with other power saving **RRM** mechanism. With regard to **AA**, Cui *et al.* analyze the energy efficiency of **MIMO** transmissions, being the first to consider the supply power consumption in energy efficient operation [Cui *et al.*, 2004]. They show that in terms of energy efficiency, the optimal number of transmit antennas used for **MIMO** transmission is not the highest by default, but rather depends on the Signal-to-Noise-Ratio (**SNR**). Kim *et al.* [Kim *et al.*, 2009] establish **AA** as a **MIMO** resource allocation problem and adapt the number of transmit antennas on a single link. However, solutions provided for **AA** on the link level cannot be directly applied to the **BS**, since for the latter multiple transmissions

are active simultaneously on the same set of antennas. Xu *et al.* [Xu *et al.*, 2011] propose a convex optimization scheme to reduce the number of transmission antennas during transmission. A related approach is applied in this chapter to the optimization of sleep modes. Hedayati *et al.* [Hedayati *et al.*, 2012] propose to perform AA without informing the receiver, thus mimicking deep fades on some antennas. This is predicted to reduce power consumption by up to 50%.

Note that—as mentioned in Chapter 2—there is also a number of works concerned with *long sleep* modes, such as [Oh & Krishnamachari, 2010, Ashraf *et al.*, 2011, Vereecken *et al.*, 2012, Xiang *et al.*, 2011]. In comparison with DTX, such long sleep modes are applied for minutes, hours or days. This increases the achievable power saving, as devices are completely turned off. However, long sleep modes cause problems with coverage and discovery, as two communication devices may be completely unaware of one another. Also, such sleep modes clearly affect the Quality of Service (QoS), unless redundant network elements exist. Thus, they are not considered here. The work presented in this chapter can be combined with long sleep modes as part of future work as the two are not mutually exclusive.

4.3 PC and TDMA

When the number of bits transmitted on a link with fixed bandwidth and optimal modulation and coding is to be increased, there are two options: either to increase the link rate by raising the transmission power or to transmit for a longer time. From a power efficiency perspective, providing a fixed rate is thus a trade-off between transmit power and transmission duration. A higher power for smaller duration can provide the same rate as a lower power with higher transmission duration. Therefore, for power minimization on a single link, transmission should always be as long as possible to allow for the lowest transmit power. However, in a shared multi-user channel with orthogonal access, such as Time Division Multiplexing (TDM), Frequency Division Multiplexing (FDM), or OFDM, all links have to be considered which each have individual rate requirements that have to be fulfilled in a given time. This problem is illustrated in Fig. 4.1 for two links. Which combination of transmission duration and transmission power achieves the lowest overall power consumption is the problem discussed in this section.

Power allocation on the link level

It follows a derivation of the power optimal allocation strategy of transmission power and time for a single link. The Shannon bound [Shannon, 1948]—as one of the most fundamental laws in communications—is employed to map transmission power to achievable rate. It is assumed that in a cellular system a set of mobiles with known channel gains has a set of rate requirements that needs to be fulfilled.

A cell consists of one BS and K links (mobiles). The capacity in bps per link

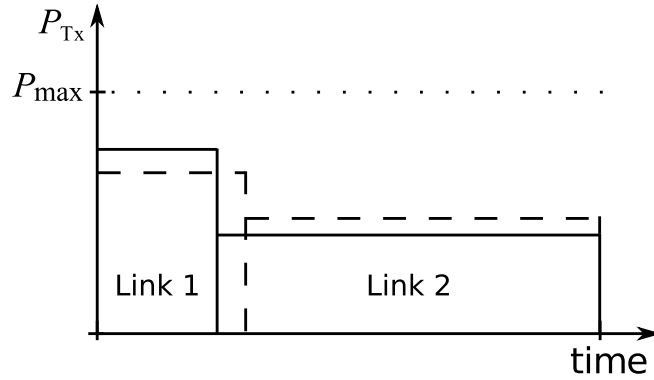


Figure 4.1: Illustration of two possible power/time trade-offs that provide equal rates on both links.

k is upper bounded by the Shannon bound as

$$R_k = W \log_2(1 + \gamma_k), \quad (4.1)$$

where W is the channel bandwidth in Hz and $\gamma_k = \frac{G_k P_k}{P_N}$ is the SNR with G_k the link channel gain, P_k the transmit power on link k in W and P_N thermal noise power in W. The noise power is defined as $P_N = W q_B \vartheta$ with Boltzmann constant q_B and operating temperature ϑ in Kelvin. While capacity and bandwidth are linearly related, capacity and transmit power have a logarithmic relationship. As a consequence it is much more expensive in terms of power to increase the channel capacity than in terms of bandwidth. In other words, if there is a choice between

- a) leaving idle spectrum and transmitting at higher power, and
- b) using all available spectrum and transmitting at the lowest required power,

then the latter will always consume less overall transmit power.

Power allocation on the cell level

Next, an optimization problem is proposed which describes this notion for K users on a shared channel. Since all links in the system share the available resources, the RRM of one link affects all others. Thus, power-optimization can not be performed on the link level only, but has to be approached from the cell level.

Let the normalized transmission time per link be given by

$$\mu_k = \frac{\tau_k}{\tau_{\text{frame}}}, \quad (4.2)$$

where τ_k is the transmission time on link k in seconds, τ_{frame} is the frame duration in seconds. Optimization of normalized time rather than absolute time is chosen

here as it results in average power minimization and is more illustrative than energy minimization (which is only meaningful for a known τ_{frame}).

The average capacity, \bar{R}_k , on link k depends on μ_k and R_k , with

$$\bar{R}_k = \mu_k R_k, \quad (4.3)$$

where \bar{R}_k indicates the average of R_k .

Solving (4.1) for P_k and combining with (4.3), the transmission power on link k in W as a function of the required average rate is found to be

$$P_k(\bar{R}_k) = \frac{P_N}{G_k} \left(2^{\frac{\bar{R}_k}{W\mu_k}} - 1 \right), \quad (4.4)$$

where $0 < P_k(\bar{R}_k) < P_{\max}$ for some P_{\max} .

To account for the fact that all links are served by the BS orthogonally within some time τ_{frame} , the system average transmission power at the BS for all links, \bar{P}_{Tx} , is the sum of individual transmit powers weighted with the transmit duration, with

$$\bar{P}_{\text{Tx}} = \sum_{k=1}^K \mu_k P_{\text{Tx},k}(\bar{R}_k) \quad (4.5a)$$

$$= \sum_{k=1}^K \mu_k \frac{P_N}{G_k} \left(2^{\frac{\bar{R}_k}{W\mu_k}} - 1 \right). \quad (4.5b)$$

The combined duration of all transmissions must be less or equal to τ_{frame} . But since it is most efficient to use the entire available τ_{frame} as derived from (4.1), it holds that

$$\sum_{k=1}^K \mu_k = 1. \quad (4.6)$$

Furthermore, time has positive values and a power constraints must be obeyed with

$$\mu_k > 0 \quad \forall k, \quad (4.7a)$$

$$0 < P_k(\bar{R}_k) < P_{\max} \quad \forall k. \quad (4.7b)$$

The allocation vector $\boldsymbol{\mu}^* = (\mu_1, \dots, \mu_K)$ of transmission durations which minimizes (4.5b) is power optimal.

Evaluation

Next, the affine power model is taken into account, as it is important to consider transmission power in relationship with the consumption of the entire BS. Instead of the transmission power, the supply power consumption is minimized. With the

power model from (3.22), the PC cost function (4.5b) and $\chi P_{\max} = P_k(\bar{R}_k)$, the supply power consumption in W is found to be

$$\begin{aligned} P_{\text{supply}}(\bar{R}_k) &= \sum_{k=1}^K \mu_k (P_0 + \Delta_p P_{\text{Tx},k}(\bar{R}_k)) \\ &= \sum_{k=1}^K \mu_k \left(P_0 + \Delta_p \frac{P_N}{G_k} \left(2^{\frac{\bar{R}_k}{W \mu_k}} - 1 \right) \right). \end{aligned} \quad (4.8)$$

Note that, against intuition, the power model has no effect on the solution of (4.8), *i.e.* μ^* is equal for (4.5b) and (4.8). As the power model affects all links equally, the PC solution is the same for any power model and, thus, any BS. However, although the *solution* is independent of the hardware, the *benefits* of PC do strongly depend on hardware. As a metric for characterizing hardware by the share of load-dependent consumption of the overall consumption, the load dependence of a BS is defined as

$$\eta_{\text{ld}} = \frac{\Delta_p P_{\max}}{P_0 + \Delta_p P_{\max}}. \quad (4.9)$$

Using this load dependence, the benefits of PC can be evaluated. Figure 4.2 shows the supply power in a cell with ten users for a range of load dependence values after the application of the PC strategy in (4.5b). The slope of the power model Δ_p was chosen for a representative set of load dependences with $\eta_{\text{ld}} = \{0.1, 0.3, 0.5, 0.8\}$ for $P_1 = 460$ W and $P_{\max} = 40$ W, from (3.22). Channel gains were calculated based on distance by the 3rd Generation Partnership Project (3GPP) path loss model [3GPP, 2010a] after dropping users uniformly on a disc with 250 m radius around the BS in the center. The problem (4.8) was solved iteratively using the interior-point algorithm contained in the MATLAB Optimization Toolbox. The remainder of the simulation parameters was set as described in Table 4.1.

As shown in Fig. 4.2, the effectiveness of PC strongly depends on the underlying hardware. A higher load dependence factor yields a lower supply power consumption for PC. The effectiveness of PC in future BSs therefore strongly depends on hardware developments.

Although PC is thus shown to provide significant saving potential in BSs with high η_{ld} , like macro BSs, the power consumption of a device employing PC is always lower bound by its idle power consumption, P_0 . Even when transmission is stopped, a device employing only PC still consumes a supply power consumption of P_0 . Thus, to further reduce power consumption, a method is required which allows power consumption to reach lower values than P_0 . This can be achieved by employing sleep modes or—in the case of OFDMA scheduling—DTX.

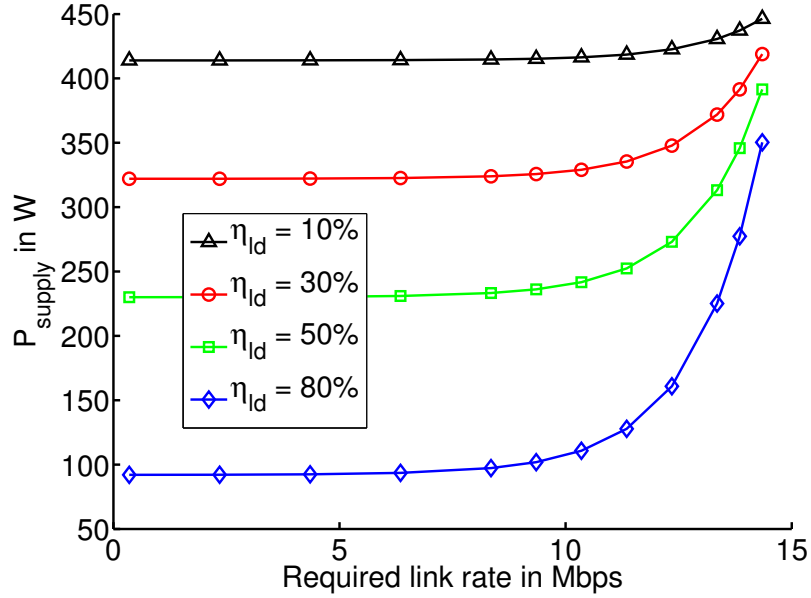


Figure 4.2: Comparison of the effect of load dependence on achievable power savings by PC.

Parameter	Value
Carrier frequency	2 GHz
Cell radius	250 m
Path loss model	3GPP UMa, NLOS, shadowing [3GPP, 2010a]
Shadowing standard deviation	8 dB
Iterations	1,000
Bandwidth W	10 MHz
Maximum transmission power P_{\max}	46 dBm
Operating temperature T	290 K
System/subcarrier bandwidth	10 MHz/200 kHz
Thermal noise power per subcarrier	$4w \times 10^{-21}$ W

Table 4.1: Simulation parameters.

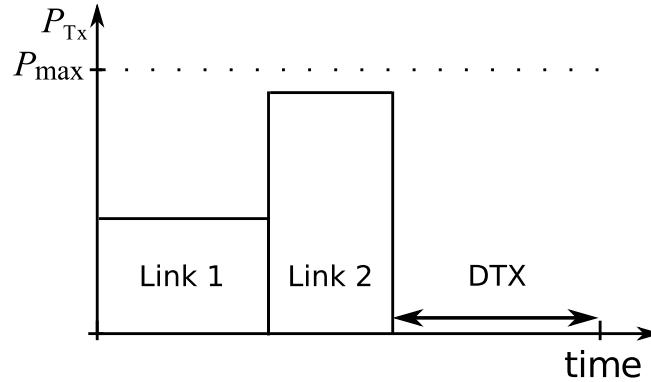


Figure 4.3: Illustration of **PRAIS** for two links: transmit power, resource share and **DTX** are allocated optimally in order to serve the requested rate at minimal supply power consumption.

4.4 Power and Resource Allocation Including Sleep (**PRAIS**)

This section introduces the **PRAIS** scheme, which combines three techniques: **PC**, **TDMA** and **DTX**. See Figure 4.3 for an illustration of **PRAIS** on two links.

The parameterized power model in Section 3.5 derived three general mechanisms which affect the power consumption of **BS**s:

1. The overall power emitted at the antenna(s), P_{Tx} , affinely relates to supply power consumption, see (3.22).
2. If the same **BS** is operated with fewer Radio Frequency (**RF**) chains, it consumes less power, see Fig. 3.14.
3. If the **BS** is put into sleep mode, it consumes less power than in the active (idle) state with zero transmission power, see Fig. 3.14.

These observations lead to the following intuitive saving strategies:

PC : Reduce transmission power.

AA : Reduce the number of **RF** chains.

DTX : Increase the time the **BS** spends in **DTX**.

The first and the last strategy are clearly opposing each other as lower transmission powers lead to lower link rates and thus longer transmission duration (for transmitting a certain number of bits), whereas it would be beneficial for long **DTX** to have short transmissions. The second and third strategy are related, as **AA** can be considered a weak form of **DTX** which still allows transmission on a subset of antenna elements. In this section, **PC** and **DTX** are jointly addressed. **AA** is treated in the following section, Section 4.5.

Joint PC and DTX

When employing **DTX** individually to minimize power consumption, the optimal strategy is to serve all links at the maximum available transmission power until target rates are fulfilled, and then set the **BS** to **DTX**. Alternatively, when employing **PC** with **TDMA** individually for maximum efficiency, the transmission duration is stretched over the available time frame with the lowest power necessary to serve the required rates. When **PC** and **DTX** are combined, there is a trade-off. Between the two extremes of maximum transmit power with longest **DTX** and lowest transmit power with no **DTX**, there are configurations with medium transmit power and medium **DTX** duration that consume less supply power.

This can be illustrated graphically for a single link example, as shown in Fig. 4.4. Plotted is the supply power consumption caused by transmitting a fixed number of bits. Let $\Phi \in [0, 1]$ denote the share of time spent transmitting. Three operation modes are defined:

- **PC**: Only **PC** but no **DTX** is available. To this extent, the transmission power is adjusted depending on the transmission time normalized to the time slot duration, Φ , such that the target rate is achieved. The **BS** consumes idle power P_0 when there is no data transmission. Clearly, the point of lowest power consumption in this case is at $\Phi = 1$ where the supply power consumption approaches P_0 . Lower values of Φ increase the required transmission power, until at $\Phi = 0.18$, $P_{\text{Tx}} = P_{\text{max}}$.
- **DTX**: The **BS** transmits with full power $P_{\text{Tx}} = P_{\text{max}}$. Thus, the supply power is $P_0 + \Delta_p P_{\text{max}}$ when transmitting or P_S when in **DTX** mode, yielding an affine function of Φ . At $\Phi = 1$, a higher rate than the target rate is achieved. Reducing Φ from $\Phi = 1$ decreases the supply power consumption linearly up to the point at which the target rate is met with equality. In this mode of operation, the best strategy is to minimize the time transmitting (small Φ), in order to maximize the time in **DTX**, $(1 - \Phi)$. In Fig. 4.4, the point of lowest power consumption for this mode is at $\Phi = 0.19$ with 154 W.
- Joint application of **PC** and **DTX**: In this mode of operation, the **DTX** time $(1 - \Phi)$ is gradually reduced. The transmission power is adjusted to meet the target rate within Φ . Here, the point of lowest power consumption is at $\Phi = 0.25$ with 135 W.

Inspection of Fig. 4.4 reveals that the joint operation of **PC** and **DTX** always consumes less power than either individual mode of operation with an optimal point at $\Phi = 0.25$. This is the power-saving benefit provided by the joint optimization of **PC** and **DTX**.

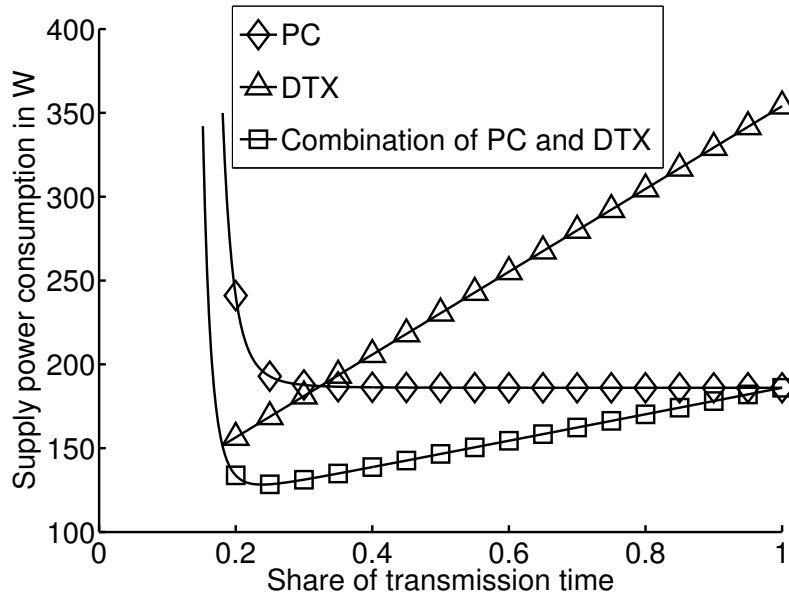


Figure 4.4: Supply power consumption for transmission of a target rate as a function of time spent transmitting, Φ . The combination of **DTX** and **PC** achieves lower power consumption than exclusive operation of either **DTX** or **PC**.

Problem formulation

This section proceeds to derive the power consumption optimization problem for a multi-user single-cell allocation of transmit powers, **DTX** times and transmit durations contained within the **PRAIS** scheme. The normalized time spent transmitting, μ_k , is defined as in (4.2) and the normalized duration spent in **DTX** is

$$\nu = \frac{\tau_S}{\tau_{\text{frame}}}, \quad (4.10)$$

where τ_S is the time spent in **DTX** and

$$\sum_{k=1}^K \mu_k + \nu = 1. \quad (4.11)$$

Combining this with the consumption during **DTX** from (3.22) and (4.5b)

yields the following **PRAIS** optimization problem.

$$\underset{\mu, \nu}{\text{minimize}} \quad P_{\text{supply}}(\bar{R}_k) = \left[\sum_{k=1}^K \mu_k \left(P_0 + \Delta_p \frac{P_N}{G_k} \left(2^{\frac{\bar{R}_k}{W \mu_k}} - 1 \right) \right) \right] + \nu P_S \quad (4.12a)$$

$$\text{subject to} \quad \sum_{k=1}^K \mu_k + \nu = 1, \quad (4.12b)$$

$$\nu \geq 0, \quad (4.12c)$$

$$\mu_k \geq 0 \quad \forall k, \quad (4.12d)$$

$$0 \leq P_k = \frac{P_N}{G_k} \left(2^{\frac{\bar{R}_k}{W \mu_k}} - 1 \right) \leq P_{\text{max}} \quad \forall k. \quad (4.12e)$$

The constraints (4.12b), (4.12c), (4.12d) reflect the facts that normalized time has to be positive and its sum unity. Transmission powers are positive and bounded by a maximum transmit power in (4.12e). The cost function is a non-negative sum of functions that are convex within the constraint domain and is therefore still convex. See Appendix A.1 for a proof. It can be solved efficiently with appropriate software like the MATLAB optimization toolbox. The solution of (4.12) determines the vector $(\mu_1, \dots, \mu_K, \nu)$, which minimizes the overall power consumption under target rates. Note that selecting $P_S \geq P_0$ is equivalent to disabling **DTX**, *i.e.* employing **PC** individually similar to (4.8), whereas fixating $P_{\text{Tx}} = P_{\text{max}}$ is equivalent to disabling **PC**.

The resource allocation problem (4.12) can be solved for any number of users. Without loss of generality, a ten user scenario for numerical evaluation is selected.

Evaluation

For the numerical analysis, the **PRAIS** scheme is evaluated in a Monte Carlo simulation using the parameters shown in Table 4.1. Users are dropped uniformly onto a disk and the associated channel gains G_k are generated by applying the **3GPP** urban macro path-loss model including shadowing with a standard deviation of 8 dB [3GPP, 2010a]. In addition to the individual **DTX** and **PC** allocation schemes and the **PRAIS** scheme, two references that serve as upper limits are presented. First, the maximum transmission power as defined by the Long Term Evolution (**LTE**) standard provides the theoretical reference. Second, the reference against which gains are measured is the power behavior of a **BS** as defined in the power models. This is a Bandwidth Adaptation (**BA**) scheme where each user receives a share of the frequency band as well as the entire considered time slot. This can also be interpreted as ‘**DTX** in the frequency domain’ where $P_S = P_0$.

For power modeling, representative of current and future developments, the affine power model from Chapter 3, a model from the literature and a purely

Model	P_0/W	Δ_P	P_S/W
Affine model in (3.23)	186	4.2	107
Frenger model [Frenger <i>et al.</i> , 2011]	170	3.4	10
Linear model	1	8.8	1

Table 4.2: Single-sector power model parameters used in Section 4.4.

theoretical model are selected; the parameters are normalized for a single sector, single sector and listed in Table 4.2.

For an assessment of the relevance of DTX, an assumption is that DTX will greatly improve, while standby component consumption cannot be reduced substantially in the coming years [Frenger *et al.*, 2011]. This model is labelled the *Frenger model*. This model particularly emphasizes DTX effects.

As a best-case example, the theoretical power model assumes idealized components which scale perfectly with load. Power consumption is set to scale almost linearly with load with near-zero stand-by consumption. This model is not a prediction of technology advances, but provides theoretical limits. Parameters are selected such that the power consumption at full load matches the affine model.

The simulation results are shown in Figure 4.5 where the per-user link rate is plotted against the average supply power consumption under the different schemes. Figures 4.5a, 4.5b, 4.5c reflect the three chosen power models.

It is found in Figure 4.5a that a Single-Input Single-Output (SISO) LTE BS consumes 186 W up to 340 W employing BA, which is considered the operation of the SotA. An important albeit foreseen result is that the consumption curves of BA and PC as well as DTX and PRAIS originate in the same values of P_{supply} at low load. The higher one is P_0 at 186 W and the lower one P_S at 107 W. This is true for all power models and confirms that in an empty cell, power consumption is determined by hardware and resource allocation has no effect.

As shown in Fig. 4.5a, the application of PC only allows keeping the overall consumption constant for a large set of low target rates. In this rate region, transmit powers are very low compared to standby consumption. Only when rates above 10 Mbps are targeted is the transmission power high enough to make a noticeable difference compared to the standby consumption. This is reflected in the rising PC only curve at target rates above 10 Mbps. In contrast, the binary DTX scheme (which transmits either at full power or not at all) has much lower power consumption (up to -45%) than PC only or BA at low rates. However, it rises much quicker than the PC only curve. There is a crossover point at 5.6 Mbps between DTX and PC. The PRAIS scheme, which joins PC and DTX, benefits from both individual schemes and has minimal consumption over all rates. At higher target rates, the PRAIS consumption curve joins the PC only curve. This reflects that it is not feasible to put the BS to sleep at high rates. Employing the

affine power model, the **PRAIS** scheme achieves savings between 42% and 23% over **BA**.

A surprising result is found in Figure 4.5b. Although application of this model has a strong bias towards **DTX** effects, there remains a cross-over point between **DTX** and **PC** after which the use of **PC** can still save 19% of the supply power consumption in addition to **DTX**. In the Frenger model, the **PRAIS** scheme offers between 91% savings at near-zero rates and 23% savings at 15 Mbps.

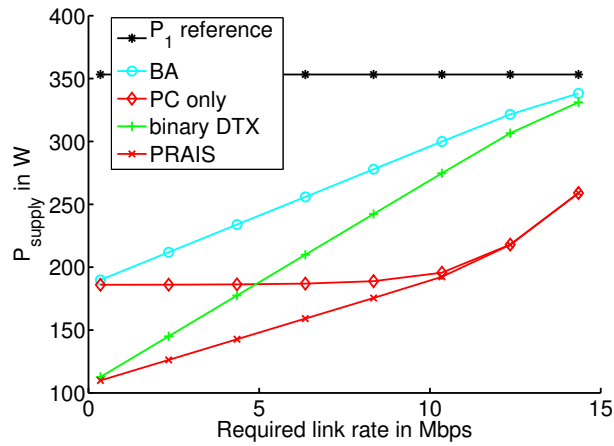
In the future linear model shown in Figure 4.5c, the behavior of **DTX** and **BA**, as well as **PC** and **PRAIS**, are identical, due to the fact that there is no gain of sleep modes over standby consumption. **BA** consumption is significantly lower than for all other power models. All benefits are owed to **PC** which is strongly amplified by the linear model behavior, delivering significant savings over all target rates.

Another finding evident from all figures is that there is no point of ‘full load’ in a cell which causes maximum power consumption. In theory, when a cell is fully loaded—regardless of the resource allocation scheme—the **BS** is expected to consume the maximum supply power, P_1 . However, the chance that the set of target rates matches the given channel conditions to generate a situation of ‘full load’ is extremely low. It is much more probable that either the channels conditions are good enough to have ‘almost full load’ or that the channel conditions are too bad to fulfill the target rates, generating an overload or outage situation. As target rates increase, the probability of the latter increases. To cover only a representative set of target rates, only those data points are plotted which contain less than 10% overload/outage. Due to this outage, the simulated power consumption never reaches the theoretical maximum. Thus, the selection of the resource allocation scheme does in fact matter, even at near-full loads.

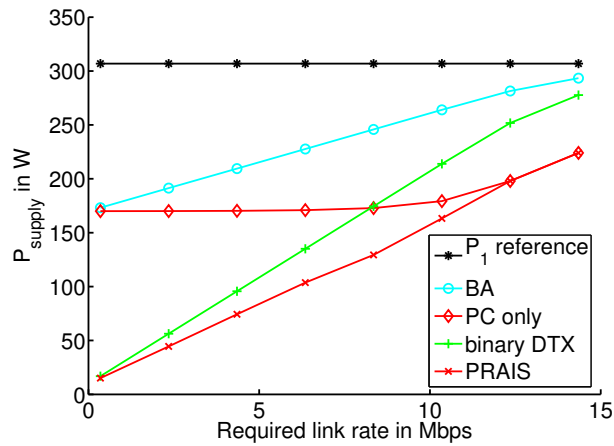
4.5 Resource allocation using Antenna adaptation, Power control and Sleep modes (**RAPS**)

To extend the previous analytical work into a comprehensive, practical mechanism for current cellular systems like **3GPP LTE**, the **RAPS** algorithm is proposed in this section, which reduces the **BS** supply power consumption of multi-user **MIMO-OFDM**. Given the channel states and target rates per user, **RAPS** finds the number of transmit antennas, the number of **DTX** time slots and the resource and power allocation per user. The **RAPS** solution is found in two steps: First, **PC**, **DTX** and resource allocation are joined into a convex optimization problem which can be efficiently solved. Second, subcarrier and power allocation for a frequency-selective time-variant channel pose a combinatorial problem, which is solved by means of a heuristic solution.

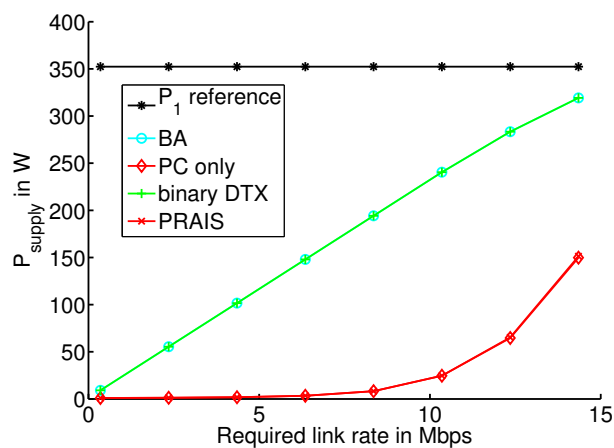
One transmission frame is considered in the downlink of a point-to-multipoint



(a) Supply power consumption under the affine model.



(b) Supply power consumption under the Frenger model.



(c) Supply power consumption under the linear model.

Figure 4.5: Fundamental limits for power consumption in BSs.

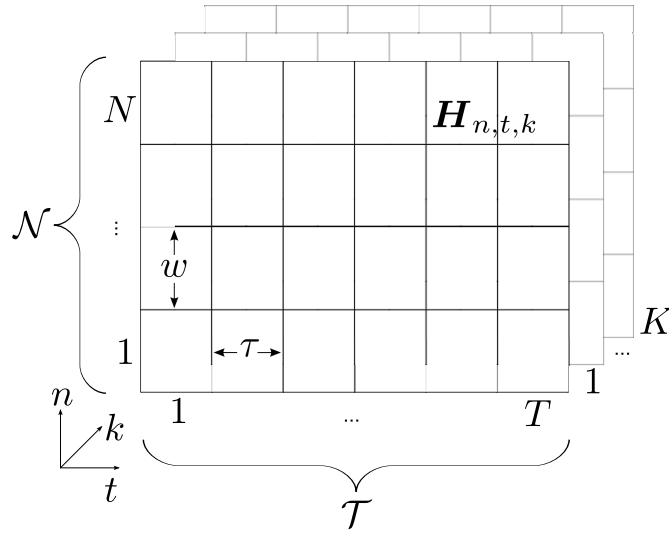


Figure 4.6: OFDM frame structure.

wireless communication system, comprising one serving BS and multiple mobile receivers. The BS transmitter is equipped with D antennas and all antennas share the transmit power budget. Mobile receivers have M_R antennas and system resources are shared via OFDMA between K users on N subcarriers and T time slots. In total, there are NT resource blocks as introduced in Section 2.5.2. A frequency-selective time-variant channel is assumed, with each resource unit characterized by the channel state matrix, $\mathbf{H}_{n,t,k} \in \mathbb{C}^{M_R \times D}$, with subcarrier index $n = 1, \dots, N$, time slot index $t = 1, \dots, T$, user index $k = 1, \dots, K$. The vector of spatial channel eigenvalues per resource unit a and user k is $\mathcal{E}_{a,k}$ and its cardinality is $\min\{D, M_R\}$. The system operates orthogonally such that individual resource units cannot be shared among users. MIMO transmission with a variable number of spatial streams is assumed over the set of resources assigned to each user, \mathcal{U}_k . This frame structure is illustrated in Fig. 4.6.

The PC and DTX trade-off is extended to MIMO-OFDM serving multiple users over frequency-selective channels. The selection of the number of transmit antennas for AA is made once for the entire frame.

For power modeling of single antenna and dual antenna transmission, the affine power models from Chapter 3, (3.23) and (3.24) are employed. It is assumed that the BS is equipped with two antennas out of which one can be deactivated. Since the switch-off process is idealized to be instantaneous, a DTX power consumption of $P_S = 107$ W is assumed for both single and dual antenna transmission.

4.5.1 Problem Formulation

The global problem statement is formulated as follows. Given the channel state matrices $\mathbf{H}_{n,t,k}$ on each channel and the vector of target rates per user $\mathbf{r} = (R_1, \dots, R_K)$, sought are:

- the set of resources allocated to each user \mathcal{U}_k ,
- the power level $P_{a,e}$ per resource block $a = 1, \dots, |\mathcal{U}_k|$ and the spatial channel eigenvalue ϵ_e with $e = 1, \dots, |\mathcal{E}_{a,k}|$,
- and the number of active transmit antennas D ,

such that the supply power consumption is minimized while fulfilling the transmission power constraint, P_{\max} .

Combining (4.1), (4.3) and (2.3a), the sum capacity of user k over one transmission frame of duration τ_{frame} is given by

$$R_k = \frac{w\tau}{\tau_{\text{frame}}} \sum_{a=1}^{|\mathcal{U}_k|} \sum_{e=1}^{|\mathcal{E}_{a,k}|} \log_2 \left(1 + \frac{P_{a,e} \mathcal{E}_{a,k}(e)}{P_N} \right), \quad (4.13)$$

with subcarrier bandwidth w in Hz.

The BS RF transmission power in time slot t is

$$P_{\text{Tx}} = \sum_{a=1}^{|\mathcal{A}_t|} \sum_{e=1}^{|\mathcal{E}_a|} P_{a,e}, \quad (4.14)$$

where \mathcal{A}_t is the set of N resources in time slot t and \mathcal{E}_a is the vector of channel eigenvalues on resource a .

Given (3.22), (4.13) and (4.14), the optimization problem that minimizes the supply power consumption is of the form

$$\underset{\mathcal{U}_k, \forall k, P_{a,e}, \forall (a,e), D}{\text{minimize}} \quad P_{\text{supply}}(\mathbf{r}) = \frac{1}{T} \left(\sum_{t=1}^{T_{\text{Active}}} (P_{0,D} + \Delta_P P_{\text{Tx}}) + \sum_{t=1}^{T_{\text{Sleep}}} P_S \right) \quad (4.15a)$$

$$\text{subject to} \quad P_{\text{Tx}} \leq P_{\max}, \quad (4.15b)$$

$$T_{\text{Active}} + T_{\text{Sleep}} = T, \quad (4.15c)$$

$$R_k \leq \frac{w\tau}{\tau_{\text{frame}}} \sum_{a=1}^{|\mathcal{U}_k|} \sum_{e=1}^{|\mathcal{E}_{a,k}|} \log_2 \left(1 + \frac{P_{a,e} \mathcal{E}_{a,k}(e)}{P_N} \right) \quad (4.15d)$$

with the number of active transmission time slots T_{Active} , and DTX time slots T_{Sleep} . This is a set selection problem over the sets \mathcal{U}_k , and $\mathcal{E}_{a,k}$, as well as a minimization problem in $P_{a,e}$.

Complexity

Dynamic subcarrier allocation is known to be a complex problem for a single time slot in frequency-selective fading channels that can only be solved by suboptimal or computationally expensive algorithms [Wong *et al.*, 1999, Kivanc *et al.*, 2003, Jang & Lee, 2003]. In this study, two additional degrees of freedom are added by considering AA and DTX, increasing the complexity further. Consequently the problem is considered intractable and divided into two steps:

1. Real-valued estimates of the resource share per user, **DTX** duration, and number of active **RF** chains D , are derived based on simplified system assumptions.
2. The power-minimizing resource allocation over the integer set \mathcal{U}_k and power allocation are performed.

4.5.2 Step 1: **AA**, **DTX** and Resource Allocation

The first step to solving the global problem is based on a simplification of the system assumptions. This allows defining a convex subproblem with an optimal solution, which is later (sub-optimally) mapped to the solution of the global problem in step 2, described in Section 4.5.3.

Instead of time and frequency-selective fading it is assumed that channel gains on all resources are equal to the center resource block,

$$\mathbf{H}_k = \mathbf{H}_{n^c, t^c, k}, \quad (4.16)$$

where the superscript c signifies the center-most subcarrier and time slot. Step 1 thus assumes a block fading channel per user over $W = Nw$ and τ_{frame} .

The center resource block is selected due to the highest correlation with all other resources. Alternative methods to construct a representative channel state matrix are to take the mean or median of $\mathbf{H}_{n, t, k}$ over the **OFDMA** frame. However, application of the mean or median over a set of **MIMO** channels were found to result in a channel with lower capacity. See Section 4.5.4 for a comparison plot between different channel selection methods.

The link capacity is calculated using equal-power precoding and assuming uncorrelated antennas. In contrast to water-filling precoding, equal-power precoding provides a direct relationship between total transmit power and target rate. On block fading channels with real-valued resource sharing, **OFDMA** and **TDMA** are equivalent. Without loss of generality, resource allocation via **TDMA** is selected. These simplifications allow a convex optimization problem to be established that can be efficiently solved.

In a block fading multi-user downlink with equal power precoding, the average rate for user k is given by

$$\overline{R}_k = \mu_k W \sum_{e=1}^{|\mathcal{E}_k|} \log_2 \left(1 + \frac{P_k \mathcal{E}_k(e)}{D P_N} \right), \quad (4.17)$$

with the vector of channel eigenvalues per user \mathcal{E}_k , and transmission power on this link, P_k .

The transmission power is a function of the target rate, depending on the number of transmit and receive antennas. For the following configurations, (4.17) reduces to:

1x2 Single-Input Multiple-Output (SIMO),

$$P_k(\overline{R}_k) = \frac{P_N}{\epsilon_1} \left(2^{\left(\frac{\overline{R}_k}{W\mu_k}\right)} - 1 \right), \quad (4.18)$$

2x2 MIMO,

$$\overline{R}_k = \mu_k W \log_2 \left(1 + \frac{P_k}{2P_N} (\epsilon_1 + \epsilon_2) + \left(\frac{P_k}{2P_N} \right)^2 \epsilon_1 \epsilon_2 \right), \quad (4.19)$$

$$P_k(\overline{R}_k) = P_N \frac{-(\epsilon_1 + \epsilon_2) + \sqrt{(\epsilon_1 + \epsilon_2)^2 + 4\epsilon_1 \epsilon_2 (2^{\frac{\overline{R}_k}{W\mu_k}} - 1)}}{\epsilon_1 \epsilon_2}, \quad (4.20)$$

where $\mathcal{E}_k = (\epsilon_1, \epsilon_2)$. These equations can be extended in similar fashion to combinations with up to four transmit or receive antennas. Note that a higher number of antennas would require the general algebraic solution of polynomial equations with degree five or higher, which cannot be found in line with the Abel-Ruffini theorem [Rosen, 1995].

Like on the BS side, the number of RF chains used for reception at the mobile could be adapted for power saving. However, the power-saving benefit of receive AA is much smaller than in transmit AA, where a Power Amplifier (PA) is present in each RF chain. Moreover, multiple receive antennas boost the useful signal power and provide a diversity gain. Therefore, M_{Rx} is assumed to be fixed and set to $M_R = 2$ in the following.

Given the transmission power (4.18), (4.20), and the power model (3.21), the supply power consumption for TDMA is derived, similar to (4.12),

$$P_{\text{supply}}(\mathbf{r}) = \sum_{k=1}^K \mu_k (P_{0,D} + \Delta_P P_k(R_k)) + \nu P_S. \quad (4.21)$$

Consequently, the optimization problem is defined as:

$$\underset{(\mu_1, \dots, \mu_{K+1})}{\text{minimize}} \quad P_{\text{supply}}(\mathbf{r}) = \sum_{k=1}^K \mu_k (P_{0,D} + \Delta_P P_k(R_k)) + \mu_{K+1} P_S \quad (4.22a)$$

$$\text{subject to} \quad \sum_{k=1}^K \mu_k + \nu = 1 \quad (4.22b)$$

$$\nu \geq 0 \quad (4.22c)$$

$$\mu_k \geq 0 \quad \forall k \quad (4.22d)$$

$$0 \leq P_k(R_k) \leq P_{\max} \quad \forall k. \quad (4.22e)$$

The first constraint ensures that all resources are accounted for and upper bounds μ_k . The second and third constraint guarantee positive durations. The fourth

encompasses the transmit power budget of the BS and acts as a lower bound on μ_k . Note that due to the block fading assumption and TDMA, the transmission power per user, P_k , is equivalent to P_{Tx} in (3.22) at that point in time.

This problem is convex in its cost function and constraints (as proven in Appendix A.2). It can therefore be solved with available tools like the interior point method [Boyd & Vandenberghe, 2004]. As part of the RAPS algorithm, (4.22) is solved once for each possible number of transmit antennas. The number of transmit antennas is then selected according to which solution results in lowest supply power consumption.

The solution of this first step yields an estimate for the supply power consumption, the number of transmit antennas, D , the DTX time share, ν , and the resource share per user μ_k . If a solution for step 1 cannot be found, step 2 is not performed and outage occurs. Outage handling is left to a higher system layer mechanism which could, *e.g.* prioritize users and reiterate with reduced system load. If a solution to step 1 can be found, step 2 is performed as described in the following section.

4.5.3 Step 2: Subcarrier and Power Allocation

This section describes the second step of the RAPS algorithm. In step 2, the results of step 1 are mapped back to the global problem to find the resource allocation for each user, \mathcal{U}_k , the power level per resource and spatial channel, $P_{a,e}$, and the number of DTX slots, T_{Sleep} .

First, the real-valued resource share, μ_k , is mapped to the OFDMA resource count per user, $m_k \in \mathbb{N}$, such that

$$m_k = \lceil \mu_k NT \rceil \quad \forall k. \quad (4.23)$$

Possible rounding effects through the ceiling operation in (4.23) are compensated for by adjusting the number of DTX time slots, with

$$T_{\text{Sleep}} = \left\lfloor \frac{TN\mu_{K+1} - K}{N} \right\rfloor = \lfloor T\mu_{K+1} - K/N \rfloor. \quad (4.24)$$

The remaining time slots are available for transmission,

$$T_{\text{Active}} = T - T_{\text{Sleep}}. \quad (4.25)$$

The remaining unassigned resources,

$$m_{\text{rem}} = NT - \sum_{k=1}^K m_k - NT_{\text{Sleep}}, \quad (4.26)$$

are assigned to m_k in a round-robin fashion. After this allocation, it holds that $m_k = |\mathcal{U}_k|$.

Next, the number of assigned resource blocks per user, m_k , is equally subdivided into the number of resources per user and time slot, $m_{k,t}$, with

$$m_{k,t} = \left\lfloor \frac{m_k}{\sum_{l=1}^K m_l} N \right\rfloor. \quad (4.27)$$

The remaining unassigned resources per time slot,

$$m_{t,\text{rem}} = N - \sum_{k=1}^K m_{k,t}, \quad (4.28)$$

are allocated to different $m_{k,t}$ in a round-robin fashion.

Time slots considered for **DTX** are assigned statically, starting from the back of the frame. Note that the dynamic selection of **DTX** slots creates additional opportunities for capacity gains or power savings as they could be assigned to time slots with poor channel states, *e.g.* time slots experiencing deep fades. This opportunity is revisited in Chapter 5.

A corner case exists when $TN\mu_{K+1} < K$ and (4.24) becomes negative. This occurs when the **DTX** time share, ν , is very small and thus traffic load is high. Due to the high traffic load, it is possible that the target rates cannot be fulfilled within the transmit power constraint, leading to outage for at least one user. Accordingly, if $TN\mu_{K+1} < K$, $T_{\text{Active}} = T$ and the resource mapping strategy in (4.23) is adapted such that

$$m_k = \lfloor \mu_k NT \rfloor, \quad (4.29)$$

which guarantees that $m_k < NT$. The remaining resources are allocated to users as outlined above.

A subcarrier allocation algorithm from Kivanc *et al.* [Kivanc *et al.*, 2003] is adopted, which has been shown to work effectively with low complexity. The general idea of the algorithm is as follows: First assign each subcarrier to the user with the best channel. Then start trading subcarriers from users with too many subcarriers to users with too few subcarriers based on a nearest-neighbour evaluation of the channel state. The algorithm is outlined in Algorithm 1 and applied to each time slot t consecutively. The original algorithm from the literature is adapted as indicated in the caption.

At this stage, the **MIMO** configuration, the number of **DTX** time slots, and the subcarrier assignment are determined. Transmit powers are assigned in both spatial and time-frequency domains via an algorithm termed margin-adaptive power allocation [Yu *et al.*, 2002]. The notion of this algorithm is as follows: First, channels are sorted by quality and a ‘water-level’ is initialized on the best channel, such that the rate target is fulfilled. Then, in each iteration of the algorithm, the next best channel is added to the set of used channels, thus reducing the water-level in each step. The search is finished once the water-level is lower than the next channel metric to be added. Refer to Appendix A.3 for the derivation.

Algorithm 1 Adapted RCG algorithm performed on each time slot t . As compared to [Kivanc *et al.*, 2003] the cost parameter $h_{n,t,k}$ has been adapted and the absolute value has been added to the search of the nearest neighbour. $\mathcal{A}_{k,t}$ holds the set of subcarriers assigned to user k .

Ensure: $m_{k,t}$ is the target number of subcarriers allocated to each user k ,
 $h_{n,t,k} = |\overline{\mathbf{H}}_{n,t,k}|^2$ and $\mathcal{A}_{k,t} \leftarrow \{\}$ for $k = 1, \dots, K$.

- 1: **for all** subcarriers n **do**
- 2: $k^* \leftarrow \arg \max_{1 \leq k \leq K} h_{n,t,k}$
- 3: $\mathcal{A}_{k^*,t} \leftarrow \mathcal{A}_{k^*,t} \cup \{n\}$
- 4: **end for**
- 5: **for all** users k such that $|\mathcal{A}_{k,t}| > m_{k,t}$ **do**
- 6: **while** $|\mathcal{A}_{k,t}| > m_{k,t}$ **do**
- 7: $l^* \leftarrow \arg \min_{\{l: |\mathcal{A}_{l,t}| < m_{l,t}\}} \min_{1 \leq n \leq N} | -h_{n,t,k} + h_{n,t,l} |$
- 8: $n^* \leftarrow \arg \min_{1 \leq n \leq N} | -h_{n,t,k} + h_{n,t,l^*} |$
- 9: $\mathcal{A}_{k,t} \leftarrow \mathcal{A}_{k,t} / \{n^*\}, \mathcal{A}_{l^*,t} \leftarrow \mathcal{A}_{l^*,t} \cup \{n^*\}$
- 10: **end while**
- 11: **end for**

Let the number of bits to be transmitted to each user be

$$B_{\text{target},k} = R_k \tau_{\text{frame}}. \quad (4.30)$$

To fulfill $B_{\text{target},k}$, the following constraint must be met

$$B_{\text{target},k} - \sum_{a=1}^{|\mathcal{U}_k|} \sum_{e=1}^{|\mathcal{E}_{a,k}|} w \tau \log_2 \left(1 + \frac{P_{a,e} \mathcal{E}_{a,k}(e)}{P_N} \right) = 0, \quad (4.31)$$

which assesses the sum capacity according to (4.13).

The water-level v can be found via an iterative search over the set of channels that contribute a positive power, Ω_k , with

$$\log_2(v) = \frac{1}{|\Omega_k|} \left(\frac{B_{\text{target},k}}{w \tau} - \sum_{e=1}^{|\Omega_k|} \log_2 \left(\frac{\tau \mathcal{E}_{a,k}(e) w}{P_N \log(2)} \right) \right). \quad (4.32)$$

The water-level is largest on the first iteration and decreases on each iteration until it can no longer be decreased.

Using the Lagrangian method detailed in Appendix A.3, one arrives at a power-level per spatial channel of

$$P_{a,e} = \frac{v w \tau}{\log(2)} - \frac{P_N}{\mathcal{E}_{a,k}(e)}. \quad (4.33)$$

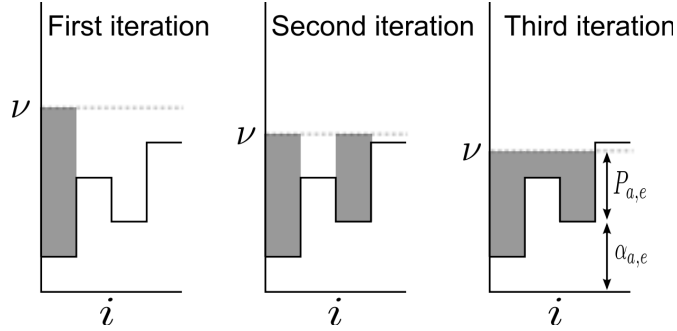


Figure 4.7: Illustration of margin-adaptive power allocation with three steps. The height of each patch i is given by $\alpha_{a,e} = P_N/\mathcal{E}_{a,k}(e)$. The water-level is denoted by ν . The height of the water above each patch is $P_{a,e}$. The first step sets the water-level such that the rate target is fulfilled on the best patch. The second and third step add a patch, thus reducing the water-level. After the third step, the water-level is below the fourth patch level, thus terminating the algorithm.

The margin-adaptive algorithm is illustrated for four channels in Fig. 4.7. The outcome of margin-adaptive power allocation as part of RAPS are the transmission power levels $P_{a,e}$ for each resource block. The supply power consumption after application of RAPS can be found by summation of transmission powers in each time slot and application of the affine power model. The entire RAPS algorithm is outlined in Fig. 4.8.

4.5.4 Results

In order to assess the performance of the RAPS algorithm Monte Carlo simulations are conducted. The simulations are configured as follows: mobiles are uniformly distributed around the BS on a circle with radius 250 m and a minimum distance of 40 m to the BS to avoid peak SNRs. Fading is computed according to the NLOS model described in 3GPP TR 25.814 [3GPP, 2010a] with 8 dB shadowing standard deviation, and the frequency-selective channel model B5 described in [IST-2003-507581 WINNER, 2005] with 3 m/s mobile velocity. All transmit and receive antennas are assumed to be mutually uncorrelated. Further system parameters are listed in Table 4.3.

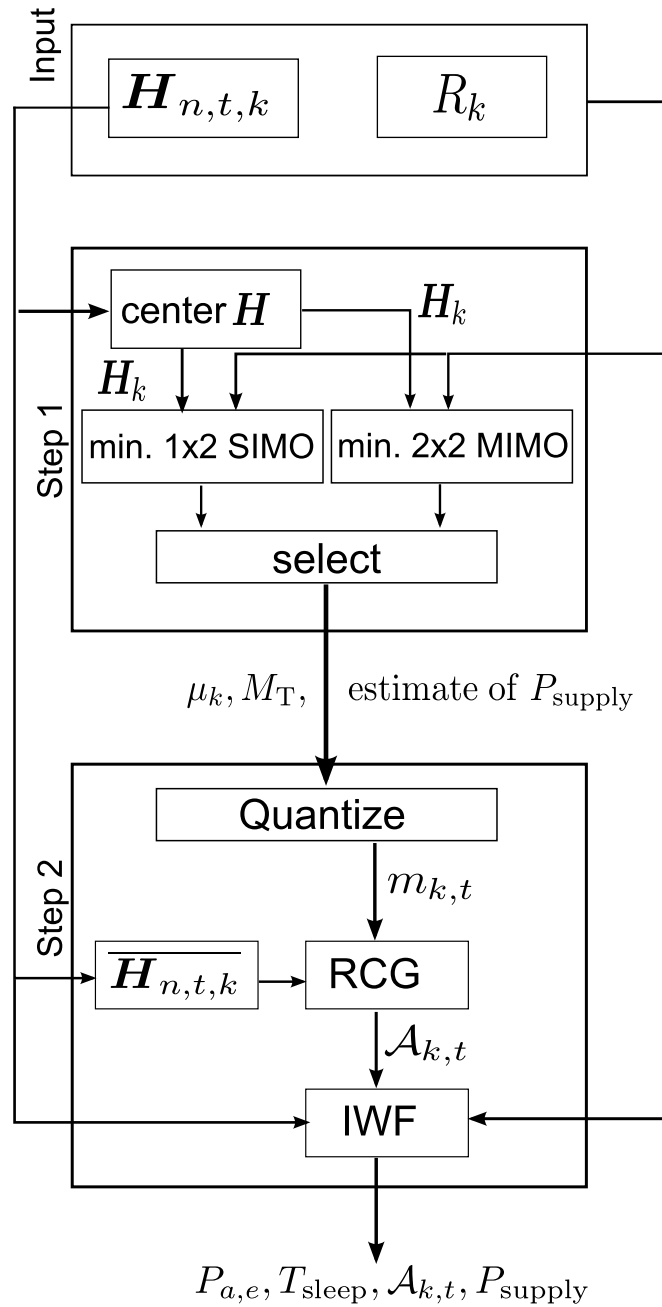


Figure 4.8: Outline of the RAPS algorithm.

Variable		Value
K	Number of users	10
N	Number of subcarriers	50
T	Number of time slots in an OFDMA frame	10
D	Number of transmit antennas	[1,2]
M_R	Number of receive antennas	2
P_{\max}	Maximum transmission power	46 dBm
τ_{frame}/τ	Duration of frame/time slot	10 ms/1 ms
W/w	System/subcarrier bandwidth	10 MHz/200 kHz
P_N	Thermal noise power per subcarrier	$4w \times 10^{-21}$ W

Table 4.3: System parameters

Benchmarks

The following transmission strategies are evaluated for comparison purposes:

- The theoretical limit of the **BS** power consumption is obtained by constant transmission at maximum power, P_1 .
- **BA**, which finds the minimum number of subcarriers that achieves the rate target. No sleep modes are utilized and all scheduled subcarriers transmit with a transmission power spectral density of P_{\max}/N . This benchmark represents the power consumption of **SotA BSs** which are neither capable of **DTX** nor **AA**.
- **DTX**, where the **BS** transmits with full power, P_1 , and switches to **DTX** once the rate requirements are fulfilled. This benchmark assesses the attainable savings when only **DTX** is applied.

Performance Analysis

The channel value selection in (4.16) serves as the channel gain for the block fading assumption of step 1. How the channel value selection of three possible alternatives (mean, median center) affects the supply power consumption is examined in Fig. 4.9. It can be seen that the selection of the mean channel gain results in the highest supply power consumption estimate after step 1. While the estimate can be improved in step 2, it is still inferior to the other alternatives. Use of the mean channel states causes step 1 to underestimate the channel quality. Consequently, too few time slots are selected for **DTX** in step 2. Choosing the median provides a better estimate than the mean and after step 2 the solution matches ‘step 2, center selection’. However, in center channel state selection the step 1 estimate and the step 2 solution have both the best match and the lowest supply power consumption. Therefore, as mentioned in Section 4.5.2, center channel state selection is chosen in the **RAPS** algorithm and all further analyses.

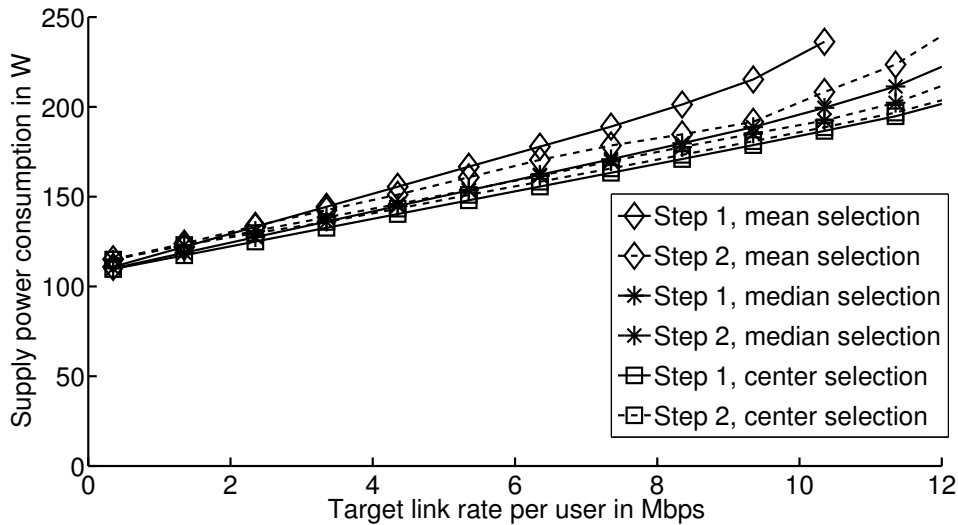


Figure 4.9: Performance comparison of different channel state selection alternatives.

Fig. 4.10 compares the outage probabilities of step 1 with that of the **BA** benchmark. Outage refers to the lack of a solution to step 1; when the user target data rates are too high for the given channel conditions, the convex subproblem has no solution, which causes the algorithm to fail. A reduction of user target data rates based on, *e.g.* priorities, latency or fairness, is specifically not covered by **RAPS**. One suggested alternative is to introduce admission control, in the way that some users are denied access, so that the remaining users achieve their target rates. Note that step 2 has no effect on the outage; if a solution exists after step 1, then step 2 can be completed. If a solution does not exist after step 1, then step 2 is not performed. Fig. 4.10 illustrates that **RAPS** selects two transmit antennas for target link rates above 14 Mbps with high probability, as target link rates cannot be achieved with a single transmit antenna. The **BA** benchmark and the step 1 **MIMO** solution have similar outage behavior.

Fig. 4.11 depicts the average number of **DTX** time slots over increasing target link rates. The effect of **AA** (*i.e.* switching between **SIMO** and **MIMO** transmission) can clearly be seen. For low target link rates, a large proportion of all time slots is selected for **DTX**. For higher target link rates, the number of **DTX** time slots must be reduced when operating in **SIMO** mode. For target link rates above 12 Mbps, which approach the **SIMO** capacity (as described in the previous paragraph), the system switches to **MIMO** transmission. The added **MIMO** capacity allows the **RAPS** scheduler to allocate more time slots to **DTX**. In the medium load region (around 15 Mbps) the standard deviation is highest, indicating that here the **RAPS** algorithm strongly varies the number of **DTX** time slots depending on channel conditions and whether **SIMO** or **MIMO** transmission is selected. These variations contribute strongly to the additional savings provided by **RAPS** over the benchmarks. Another observation from Fig. 4.11 is that it is

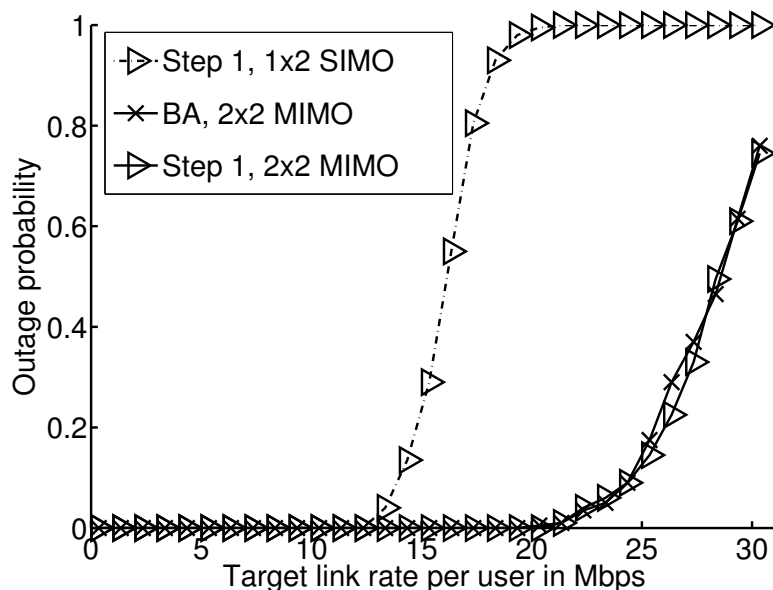


Figure 4.10: Outage probability in step 1 and the **BA** benchmark.

unlikely that more than two out of ten **DTX** time slots are scheduled at target link rates above 8 Mbps. This means that for a large range of target rates, no more than two **DTX** time slots are required to minimize power consumption. This is an important finding for applications of **RAPS** in established systems like **LTE**, where the number of **DTX** time slots may be limited due to constraints imposed by the standard.

A comparison of the supply power consumption estimates of step 1 and step 2 in Fig. 4.12 verifies that the estimate taken in step 1 as input for step 2 are sufficiently accurate. Although step 1 is greatly simplified with the assumption of block fading and its output parameters cannot be applied readily to an **OFDMA** system, it precisely estimates power consumption which is the optimization cost function. The slight difference between the step 1 estimate and power consumption after step 2 is caused by quantization loss and resource scheduling. Note that while step 1 supplies a good estimate of the power consumption, it is not a solution to the original **OFDMA** scheduling problem, since it does not consider the frequency-selectivity of the channel and does not yield the resource and power allocation.

The performance of **RAPS** in comparison to each benchmark is separately analyzed in Fig. 4.13. Here, a first observation is that even the supply power consumption of **BA** is significantly lower than the theoretical maximum for most target link rates. **BA** with a single transmit antenna always consumes less power than with two antennas, as long as the rate targets with one antenna can be met. **AA** is thus a valid power-saving mechanism for **BA**.

Second, the **DTX** power consumption is significantly lower than for **BA**,

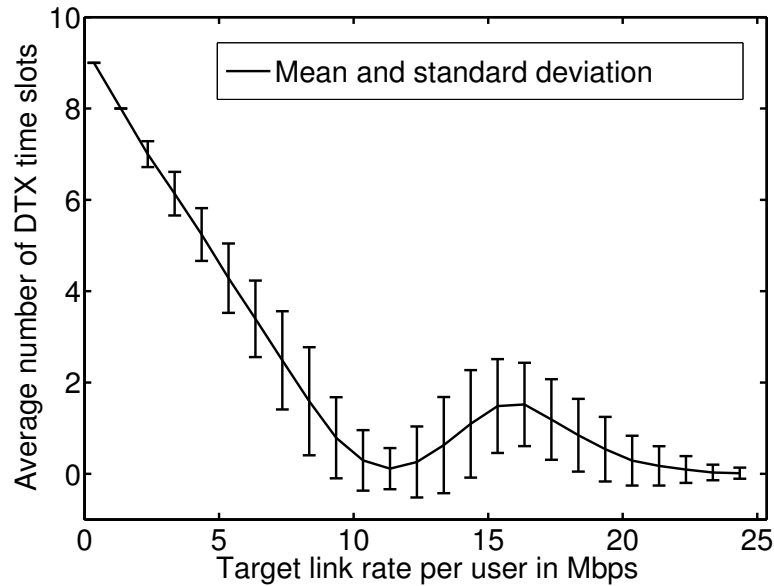


Figure 4.11: Average number of **DTX** time slots over increasing target link rates. Error bars portray the standard deviation. Total number of time slots $T = 10$.

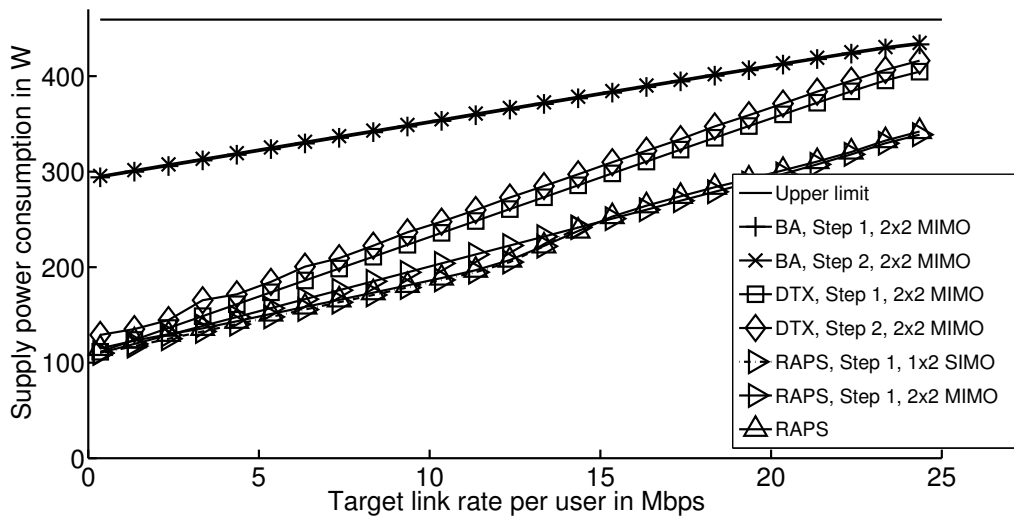


Figure 4.12: Supply power consumption for different **RRM** schemes on block fading and frequency-selective fading channels (comparison of step 1 and step 2) for ten users. Overlaps indicate the match between the step 1 estimate and the step 2 solution.

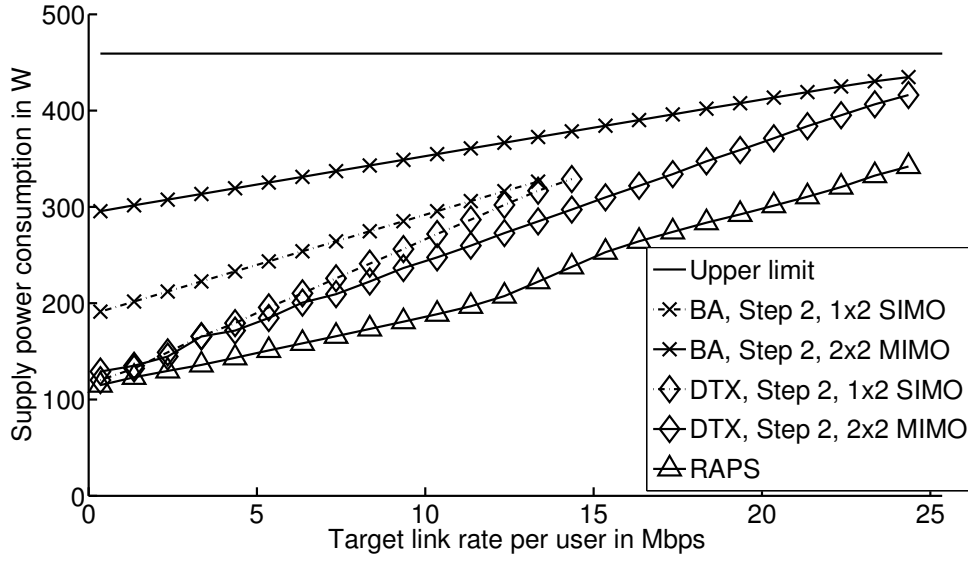


Figure 4.13: Supply power consumption on frequency-selective fading channels for different **RRM** schemes and **RAPS** for ten users. For a bandwidth-adapting **BS**, power consumption is always reduced by **AA**, while **AA** is never beneficial for a sleep mode capable **BS**. For **RAPS** energy consumption is reduced by **AA** at low rates. In general, **RAPS** achieves substantial power savings at all **BS** loads.

especially at low target rates, because lower target rates allow the **BS** to enter **DTX** for longer periods of time. As the **BS** load increases, the opportunities of the **DTX** benchmark to enter sleep mode are reduced, so that **DTX** power consumption approaches that of **BA**. Unlike in **BA**, it is never beneficial for a **BS** capable of **DTX** to switch operation to a single antenna, because transmitting for a longer time with a single antenna always consumes more power than a short two-antenna transmission, which allows for a longer **DTX** duration. (Note that this finding may not apply to other power models.)

Third, **RAPS** reduces power consumption further than **DTX** by employing **AA** at low rates and **PC** at high rates. Through **PC**, the slope of the supply power is kept low between 15 and 20 Mbps. At higher rates an upward trend becomes apparent, since link rates only grow logarithmically with the transmission power. In theory, when the **BS** is at full load, the supply power of all energy saving mechanism will approach maximum power consumption. However, when the **BS** load is very high, not all users may achieve their target rate and outage occurs (see Fig. 4.10). In other words, operating the **BS** with load margins controls outage and allows for large transmission power savings. Power savings of **RAPS** compared to the **SotA BA** range from 102.7 W (24.5%) to 136.9 W (41.4%) depending on the target link rate per user.

In addition to absolute consumption, the energy efficiency of **RAPS** is in-

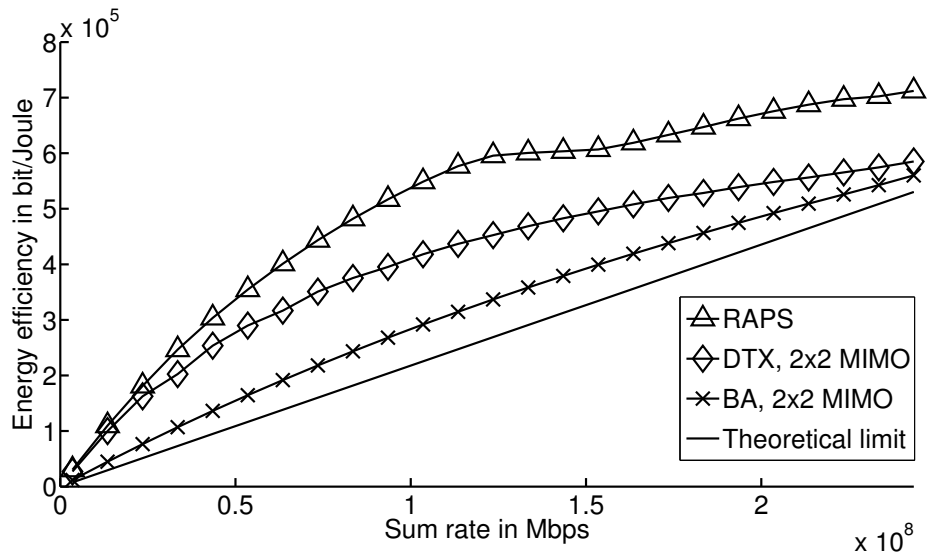


Figure 4.14: Energy efficiency as a function of sum rate. Energy efficiency can be increased by the **RAPS** algorithm. The **BS** remains most efficient at peak rate.

spected in Fig. 4.14. Energy efficiency is defined in bit/Joule as

$$E = P_{\text{supply}}^{-1} \sum_{k=1}^K R_k. \quad (4.34)$$

Observe that all data series are monotonically increasing. Therefore, **RAPS** does not change the paradigm that a **BS** is most efficiently operated at peak rates. However, **RAPS** will always offer the most efficient operation at any requested rate.

4.6 Summary

Starting with the Shannon limit, this chapter derived supply power optimal resource allocation in an **LTE** cell.

First, a literature review described the **SotA** of energy efficient **RRM** for cellular networks.

Next, the general interrelationships between bandwidth, power and time in transmissions were studied. As the **PA** consumption can be reduced by **PC**, a multi-user downlink **PC** allocation mechanism was proposed. Consideration of single links was found to be insufficient for power-saving, as a **BS** schedules multiple users on the same resources. It was shown that the power model, due to its affine mapping, does not affect the **PC** solution. Thus, it is also the solution to supply power minimization, when sleep modes are not considered.

As the power consumption reduction through **PC** is lower bounded by the idle power consumption of a transmitter, short sleep modes, *i.e.* **DTX**, have also

been taken into consideration. It was shown that the joint application of **PC** and **DTX** brings additional savings over the application of each individual scheme. Using convex optimization, a resource allocation mechanism called **PRAIS** was proposed. Using **PRAIS**, fundamental limits of power-saving resource allocation were identified on several power models. Power savings estimated on the basis of the affine model presented in Chapter 3 are in the range of 50%.

When adding the integer value constraint, which is present in practical systems where resources are only available in chunks and each has an individual channel state, the resource allocation problem becomes a mixed integer program. As this problem is highly complex, it was split into two steps. A convex subproblem was derived and solved in similar fashion as in the **PRAIS** algorithm. The solution to the subproblem yields an approximation of quantization, providing a configuration for the mixed integer problem. The overall algorithm is labelled **RAPS**. Application of the **RAPS** algorithm on this stricter constraint set achieved savings in the order of 25% to 40%.

The **RAPS** algorithm could be readily applied in current **LTE** systems. It adds complexity to scheduling, but offers significant power savings over all loads. Limitations lie in the fact that switching is not instantaneous in practice and **PAs** have limits on the **PC** range. If switching times are slower than the fraction of a time slot, power savings will not be as high as predicted. Due to linearity requirements, some **PAs** have a lower limit on transmission powers. Thus, **PC** may not be as effective as predicted in this chapter. Overall, these limitations only affect the achievable savings, not the functionality of the power-saving **RRM** algorithms presented in the chapter.

Chapter 5

Power Saving on the Network Level (Multi-cell)

5.1 Overview

Chapter 4 proposed how the power consumption of a Base Station (BS) could be minimized regardless of interference. This chapter expands the power-saving perspective to the network level, thus taking inter-cell interference into account. In particular, it studies how the Discontinuous Transmission (DTX) time slots scheduled by each BS in a network can be aligned constructively to avoid mutual interference. See Fig. 5.1 for an illustration of multiple cells, each choosing to transmit or schedule DTX in the available time slots.

In this chapter, the findings on channel allocation from literature are combined and adapted for power-saving. Four DTX alignment strategies for the cellular downlink are derived, one of which is an original contribution in which each BS independently and without coordination prioritizes time slots for transmission while maintaining system stability.

The remainder of the chapter is structured as follows. Section 5.3 formulates the system model and the problem at hand. In Section 5.4, three State-Of-The-Art (SotA) channel alignment solutions are described and the novel alignment method is introduced. Findings obtained from simulation are presented in Section 5.5. The chapter is summarized in Section 5.6.

The contents of this chapter have been previously accepted for publication in [Holtkamp & Haas, 2013] and submitted for publication in [Holtkamp *et al.*, 2013].

5.2 Channel Allocation in Literature

Generally, in channel allocation, the challenge is to assign frequency channels to different cells or links of a network such that mutual interference is avoided. Several centralized approaches to interference avoidance have been proposed [Li

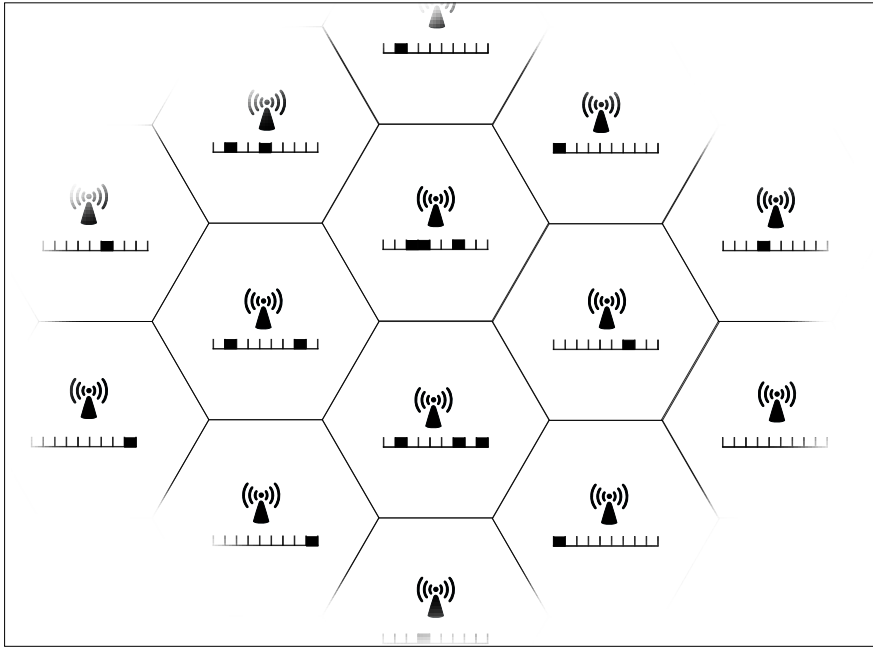


Figure 5.1: Each BS in a network select time slots for transmission (black) or DTX (blank).

& Liu, 2006, Uygungelen *et al.*, 2011, Rahman & Yanikomeroglu, 2010, Liang *et al.*, 2012]. However, to be applicable for future small-cell cellular networks, such channel allocation needs to be distributed, uncoordinated and dynamic. Distributed operation prevents the delay and backhaul requirements imposed by a central controller. If the allocation is also uncoordinated, it does not require message exchange through a backhaul of limited capacity. Furthermore, as networks, channels and traffic change rapidly, the allocation must be highly dynamic and updated often. Problems of this type are known to be NP-hard [Katzela & Naghshineh, 1996]. Therefore, different suboptimal approaches have been proposed. The simplest approach to distributing channels over a network is a fixed assignment in which it is predefined which links will use which channels, *e.g.* see [Proakis, 2000]. However, this is inflexible to changing or asymmetric traffic loads. For flexibility, dynamic channel allocation methods are required. A simple dynamic channel allocation method, Sequential Channel Search [Serizawa & Goodman, 1993], assigns channels with sufficient quality in a predefined order. This technique allows adjusting the number of channels flexibly, but is suboptimal due to its strong channel overlap between neighbors. Taking the channel quality into consideration by measurement is proposed in the Minimum Signal-to-Interference-and-Noise-Ratio (SINR) method [Serizawa & Goodman, 1993]. This technique offers increased spectral efficiency, but can lead to instabilities when allocations happen synchronously. Ellenbeck *et al.* [Ellenbeck *et al.*, 2008] introduce methods of game theory and respond to the instabilities by adding p-persistence to avoid simultaneous bad player decisions. However, the

proposed method only applies to single user systems and does not address target rates. Dynamic Channel Segregation [Akaiwa & Andoh, 1993] introduces the notion of memory of channel availability, allowing a transmitter to track which channels tend to be favorable for transmission. However, the algorithm only applies to sequential channel decisions based on an idle or busy state in circuit switched networks and cannot be applied to the concurrent alignment of channels as is required in Orthogonal Frequency Division Multiple Access (OFDMA) networks.

5.3 System Model and Problem Formulation

The network is considered as follows. BSs in a reuse-one OFDMA cellular network schedule a target rate, B_k , per OFDMA frame to be transmitted to each mobile $k = \{1, \dots, K\}$. All time slots are available for scheduling in all cells. Mobiles report perceived SINR from the previous OFDMA frame, $s_{n,t,k}$, on subcarrier $n = \{1, \dots, N\}$, time slot $t = \{1, \dots, T\}$ to their associated BS. BSs have a DTX mode available for each time slot during which transmission and reception are disabled and power consumption is significantly reduced to P_S compared to power consumption during transmission, which is a function of the power allocated to each resource block, ρ_{TX} . DTX is available fast enough to enable it within individual time slots of an OFDMA transmission such that transmission time slots are not required to be consecutive. A BS can schedule no transmission in one or more time slots and go to DTX mode instead. Scheduling a DTX time slot in one BS reduces the interference on that time slot to all other BSs. The OFDMA frames of all BSs are assumed to be aligned such that the interference over one time slot and subcarrier is flat and that all BSs can perform alignment operations in synchrony. The OFDMA frame consists of NT resource blocks. The channel is subject to block fading as described in Section 2.5.2. Interference is treated as noise.

To describe the resource allocation problem formally, the function

$$\begin{aligned} \Pi : \{1, \dots, T\} \times \{1, \dots, N\} &\rightarrow \{0, 1, \dots, K\} \\ (n, t) &\mapsto k \end{aligned} \tag{5.1}$$

is defined, which maps to each resource block a user k or 0, where 0 indicates that the resource block is not scheduled.

With $r_{n,t,k}$ the capacity of resource (n, t) if it is scheduled to k , the optimization

problem for the total BS power consumption, P_{total} , is as follows.

$$\underset{\Pi}{\text{minimize}} \quad P_{\text{total}} = P_S \frac{T_S}{T} + \rho_{\text{Tx}} N_{\text{Tx}} \left(\frac{T - T_S}{T} \right) \quad (5.2a)$$

subject to

$$N_{\text{Tx}} = \quad (5.2b)$$

$$|\{n \in \{1, \dots, N\} \mid (\Pi(n, t) \neq 0 \quad \forall t \in \{1, \dots, T\})\}|$$

$$T_S = \quad (5.2c)$$

$$|\{t \in \{1, \dots, T\} \mid (\Pi(n, t) = 0 \quad \forall n \in \{1, \dots, N\})\}|$$

$$B_k \leq \sum_{\{(n,t) \mid \Pi(n,t)=k\}} r_{n,t,k} \quad \forall k. \quad (5.2d)$$

With $|\cdot|$ the cardinality operator, T_S is the number of time slots in which for all n , no user is allocated and the BS can enable DTX and N_{Tx} is the number of resource blocks that are scheduled for transmission. The constraint (5.2d) provides the rate guarantee for each user.

The difficulty lies in finding the mapping Π . Under a brute force approach, there exist $(K + 1)^{NT}$ possible combinations. Due to the large number resource blocks present in typical OFDMA systems like Long Term Evolution (LTE), the computation of the solution is infeasible. Consequently, the next section resorts to heuristic methods.

Some of the methods compared in the following make use of a time slot ranking. In other works, *e.g.* [Akaiwa & Andoh, 1993], ranking is proposed to be based on SINR. However, in a multi-user OFDMA system each subcarrier and mobile terminal have a different SINR, thus generating a problem of comparability between time slots. Consequently, it is proposed to compare time slots by their hypothetical sum capacity, B_t , over all mobiles and subcarriers with

$$R_t = \sum_{k=1}^K \sum_{n=1}^N \log_2(1 + s_{n,t,k}). \quad (5.3)$$

5.4 DTX Alignment Strategies

In this section, four strategies to tackle the problem at hand are identified which differ in performance and complexity.

5.4.1 Sequential Alignment

In *sequential alignment*, the strategy is to always allocate as many time slots for transmission as required in sequential order as illustrated in Fig. 5.2 and set the remainder to DTX. This leads to strongest overlap and consequently highest



Figure 5.2: Illustration of sequential alignment of time slots for transmission (black) or **DTX** (blank) in six **BSs**.

interference on the first time slot and lowest overlap and possibly no transmissions at all on the last time slot. This strategy does not make use of the available channel quality information per subcarrier and provides valuable insights into questions of stability, reliability and convergence.

5.4.2 Random Alignment

Random alignment refers to a random selection of transmission time slots after every **OFDMA** frame and setting the remainder to **DTX**. This results in chaotic interference patterns. This strategy provides a reference for achievable gains, allows to assess the worst case effects of randomness and represents the **SotA** in today's unsynchronized, unaligned networks.

5.4.3 P-persistent Ranking

The synchronous alignment of uncoordinated **BSs** can lead to instabilities, when neighboring **BSs**—perceiving similar interference information—schedule the same time slots for transmission. This leads to oscillating scheduling which never reaches the desired system state [Ellenbeck *et al.*, 2008]. To address this problem, p-persistence is introduced to break the unwanted synchrony by only changing established **DTX** schedules with a probability $p = 0.3$. In initial tests, the value of p did not have a significant effect on the power consumption; exact tuning is presented in [Ellenbeck *et al.*, 2008]. P-persistent ranking first ranks time slots by their sum capacity as in (5.3), schedules time slots in that order, but only applies this new selection with probability p . Otherwise, the schedule from the last iteration remains active. After ranking, time slots are selected for transmission in order of B_t . The remainder of time slots is set to **DTX**.

5.4.4 Distributed DTX Alignment with Memory

To counter oscillation and achieve a convergent network state memory of past schedules is introduced into the alignment process. The notion of the *distributed DTX alignment with memory* algorithm is as follows. Taking into account current time slot capacities, R_t , past scores and slot allocations, each BS first updates the internal score of each time slot and then returns the priority of time slots by score. In case of equal scores, time slots are further sub-sorted by R_t . The score is updated in integers. All time slots which were used for transmission in the previous OFDMA frame receive a score increment of one. Furthermore, the time slot with highest R_t , Q_0 , receives an increment of one. Time slots which were not used for transmission in the previous OFDMA frame receive a decrement of one, except for Q_0 . Scores have an upper limit, ψ_{ul} , beyond which there is no increment and a lower limit, ψ_{ll} , below which there is no decrement. The difference between ψ_{ul} and ψ_{ll} can be interpreted as the depth of the memory buffer.

Algorithm 2 Distributed DTX alignment with memory

Ensure: ψ, Υ_u

```

1:  $Q \leftarrow \text{sort-desc-by-capacity}(\Upsilon)$ 
2: for all  $v$  in  $\Upsilon_u$  do
3:   if  $\psi(v) < \psi_{ul}$  then
4:      $\psi(v) \leftarrow \psi(v) + 1$ 
5:   end if
6: end for
7: for all  $v$  in  $\Upsilon_{uu} \setminus \{Q_0\}$  do
8:   if  $\psi(v) > \psi_{ll}$  then
9:      $\psi(v) \leftarrow \psi(v) - 1$ 
10:  end if
11: end for
12:  $\psi(Q_0) \leftarrow \psi(Q_0) + 1$ 
13:  $V \leftarrow \text{sort-desc-by-score}(Q, \psi, \Upsilon)$ 
14: return  $\psi, V, \Upsilon_u$ 

```

The algorithm is shown in Algorithm 2 with scoring map ψ , ranking tuple Q , and priority tuple V . The set of used time slots, Υ_u , and unused time slots, Υ_{uu} , make up the set of time slots, Υ , the cardinality of which is T . The function ‘sort-desc-by-capacity(Υ)’ returns a list of time slots ordered descending by R_t . The function ‘sort-desc-by-score(Q, ψ, Υ)’ returns a list of time slots ordered primarily by descending score and secondarily by descending R_t . After the execution of Algorithm 2, the first T_{Tx} time slots in V are scheduled for transmission.

In the following, the iterations over three OFDMA frames of Algorithm 2 for a system with three time slots are illustrated. In the example, the algorithm delays the change of Υ_u from c to b to buffer scheduling changes. The iteration begins with arbitrarily chosen $\Upsilon = \{a, b, c\}$, $\psi = \{a : 0, b : 2, c : 5\}$:

1. $\Upsilon_u = \{c\}$, $Q = (b, c, a)$
 $\rightarrow \psi = \{a : 0, b : 3, c : 5\}$, $V = (c, b, a)$
2. $\Upsilon_u = \{b, c\}$, $Q = (b, c, a)$
 $\rightarrow \psi = \{a : 0, b : 5, c : 5\}$, $V = (b, c, a)$
3. $\Upsilon_u = \{b\}$, $Q = (b, a, c)$
 $\rightarrow \psi = \{a : 0, b : 5, c : 4\}$, $V = (b, c, a)$

When applied, Algorithm 2 strongly benefits time slots which were used for transmission in the past (b, c in step 1 of the example). These time slots tend to repeatedly receive score increments until they all have maximum score ψ_{ul} (b, c in step 2 of the example). When the score is equal for some time slots (b, c in step 2 of the example), the ranking is based on R_t . A time slot which was used for transmission and has highest R_t , Q_0 , receives the highest increment (slot b in step 2 of the example). When a time slot has highest R_t , but was not selected for transmission in the previous OFDMA frame, it receives a score increment, but is not guaranteed to be used for transmission (slot b in step 1 of the example). When a time slot repeatedly has highest R_t , it reaches ψ_{ul} (b in the example). The algorithm thus buffers short term changes in the channel quality setting in favor of long term time slot selection.

5.5 Results

This section analyzes the four alignment strategies in simulation with regard to power consumption, convergence, reliability of delivered rates and algorithmic complexity after the introduction of the simulation environment and the resource block scheduling scheme.

Simulation Environment and Resource Block Scheduling

The four strategies were tested in a network simulation with 19-cell hexagonal arrangement with uniformly distributed mobiles and fixed target rates per mobile. Data was collected only from the center cell which is thus surrounded by two tiers of interfering cells. Power consumption of a cell is modelled by the affine model in (3.23). Table 5.1 lists additional parameters used which approximate an LTE system. The simulation is started with the assumption of full transmission power on all resources with a power consumption of 355 W per cell as a worst-case initial configuration.

In order to assess the performance of the four strategies, it is necessary to make assumptions about how the individual resource blocks are scheduled within a time slot. Resource block scheduling is itself challenging and can have a strong effect on power consumption. In order to avoid masking effects of the time slot scheduling algorithms under test, only a very simple sequential resource block allocation

Parameter	Value
Carrier frequency	2 GHz
Intersite distance	500 m
Pathloss model	3GPP UMa, NLOS, shadowing [3GPP, 2010a]
Shadowing standard deviation	8 dB
Bandwidth	10 MHz
Transmission power per resource block	0.8 W
Thermal noise temperature	290 K
Interference tiers	2 (19 cells)
Mobile target rate	1 Mbps to 3 Mbps
OFDMA subframes (time slots)	10
Subcarriers	50
Mobile terminals	10
ψ_{ul}	5
ψ_{ll}	0
Power model parameters, (3.23) (idle; load factor; DTX)	186 W; 4.2; 107 W
Subcarrier bandwidth	200 kHz

Table 5.1: Simulation parameters used.

is applied rather than sophisticated solutions from the literature. Sequential resource allocation is performed after the DTX alignment step is completed and allocates as many bits to an OFDMA resource as possible according to the Shannon capacity, followed in order by the next resource in the same time slot (sequentially), until the target rate has been scheduled to each mobile. Time slots are scheduled in the order provided by each of the four strategies. This sequential resource scheduler deliberately omits the benefits of multi-user diversity. This leads to underestimating achievable rates in simulation compared to a system which exploits multi-user diversity, in favor of allowing a fair comparison of the quality of different DTX alignment algorithms.

Power Consumption

To assess achievable power savings and the dynamic adaptivity over a large range of cell loads, the cell total power consumption is shown in Fig. 5.3. At low load very few resource blocks are required to deliver the target rate and more time slots can be scheduled for DTX than at high traffic loads, leading to monotonously rising power consumption over increasing target rates for all alignment methods.

Sequential alignment causes the highest power consumption over any target rate with an almost linear relationship between user target rates and power consumption. Sequential alignment consumes high power, as it schedules many resource blocks to achieve the target rate due to the high interference level present.

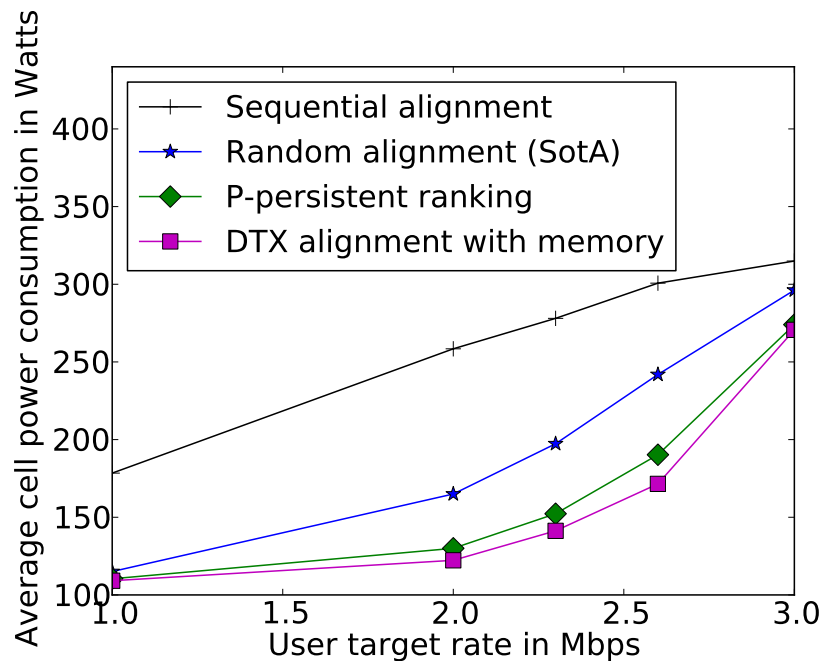


Figure 5.3: **BS** power consumption over different cell sum rates.

This power consumption is significantly lower for the **SotA**, random alignment. The randomness of time slot alignment creates a much lower average interference than with sequential alignment allowing more data to be transmitted in each resource block. As fewer resource blocks are required, less power is consumed.

P-persistent ranking and **DTX** with memory both achieve similarly low power consumption of up to 40% less than random alignment. The relationship between power consumption and target rate is noticeably non-linear, as it is flat at low target rates and grows more steeply at high target rates. This behavior is caused by the low interference level these strategies manage to create. Only at high rates, when the number of sleep time slots has to be significantly decreased, does the interference increase, leading to higher power consumption.

Also noteworthy is the fact that at 1 Mbps and 3 Mbps, random alignment performs nearly as good as p-persistent ranking. At these extreme points the network is almost unloaded and almost fully loaded, respectively. Consequently, either most time slots are scheduled for **DTX** or none, leaving very little room for optimization compared to randomness. The largest potential for time slot alignment for power saving is in networks which are medium loaded. Under medium load, the number of transmission and **DTX** time slots is similar, causing the effects of alignment to be most pronounced.

Convergence

Another relevant aspect is the convergence of the network to a stable state. As each **BS** makes iterative adjustments to its selection of time slots for transmission,

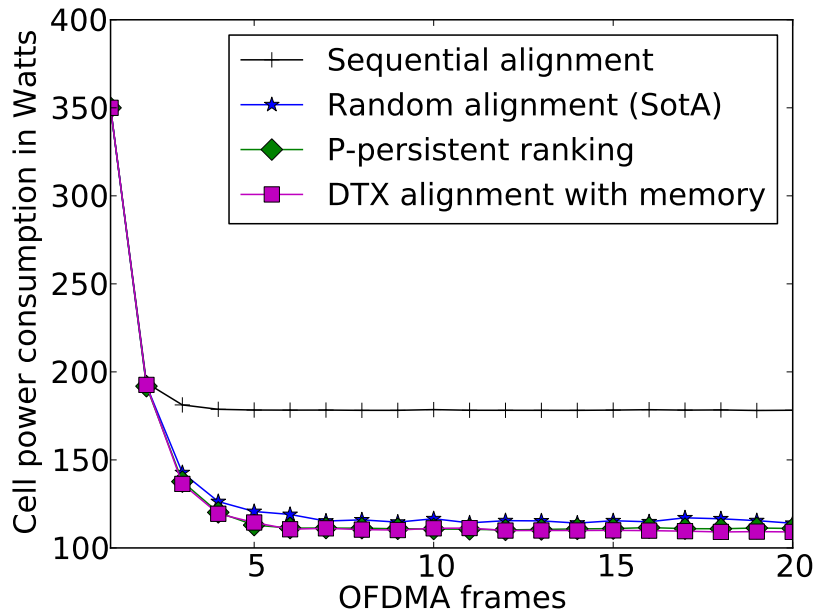


Figure 5.4: BS power consumption over OFDMA frames at 1 Mbps per mobile.

the speed of convergence as well as the convergence to a stable point of operation are relevant criteria. The effect of the iterative execution of the four strategies on the cell power consumption is illustrated in Fig. 5.4. Power consumption is found to converge to a stable value within within six OFDMA frames (alignment iterations). All strategies converge to the average power consumption values shown in Fig. 5.3. The simulation starts from a worst-case schedule of transmission on all resource blocks and then iteratively schedules time slots for transmission and DTX. In the case of 1 Mbps per user, one transmission time slot is sufficient to schedule the target rate. With transmissions only taking place during one time slot, there is very little difference between a random alignment and p-persistent ranking or DTX with memory.

At 2 Mbps per user, see Fig. 5.5, random alignment occasionally causes higher interference than p-persistent ranking or DTX with memory, leading to higher power consumption. Also, p-persistent ranking converges more slowly than DTX alignment with memory.

Reliability

An important aspect in dynamical systems with target rates is that scheduled target rates cannot always be fulfilled. As resource block scheduling is based on channel quality information which was collected in the previous OFDMA frame, the actual channel quality during transmission may differ, leading to lower than expected rates. Thus, although certain target rates are scheduled and although the system is not fully loaded, a BS may fail to deliver the targeted rate and require

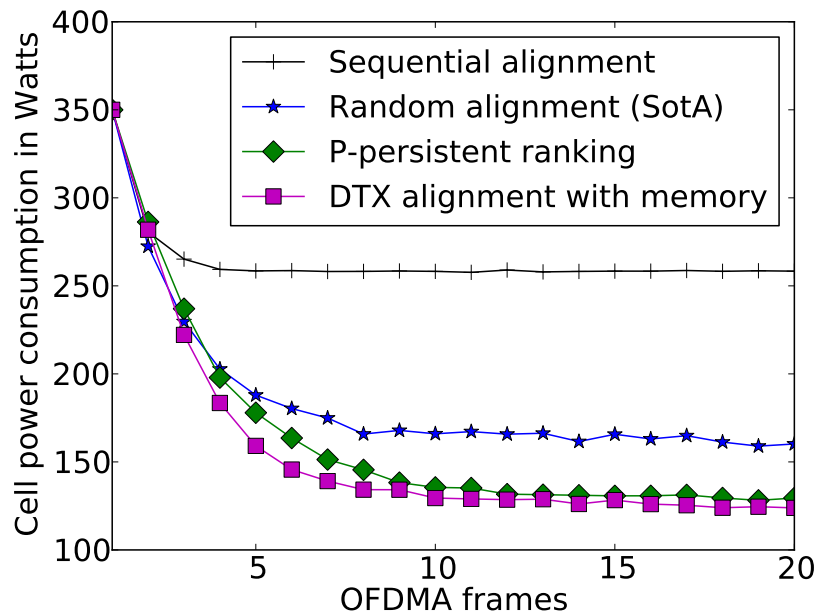


Figure 5.5: BS power consumption over OFDMA frames at 2 Mbps per mobile.

retransmission of some resource blocks. This metric is assessed by considering the retransmission probability for each strategy. The results are shown in Fig. 5.6 against a range of user target rates.

Easiest to interpret is sequential alignment which does not require retransmission for target rates up to 2.3 Mbps due to its determinism. The increase in the retransmission probability at high rates is not caused by a failure of the alignment, but by system overload. When high rates are combined with bad channel conditions, the system may be unable to deliver the target data rate, independent of the alignment strategy. This increase of the retransmission probability at high rates is present for all alignment strategies and constitutes outage.

The retransmission probability is highest for random alignment. This is caused by the strong fluctuation of interference under randomized scheduling. Channel quality measurements used for resource block scheduling are of very little reliability, as the interference changes quickly due to random time slot alignment.

P-persistent ranking performs slightly better than random alignment at 1 Mbps target rate. At 2 Mbps per user, where the alignment potential is highest, oscillation causes the highest retransmission probability.

DTX alignment with memory achieves a much lower retransmission probability in the range of 15% to 20%, due to the reduction in interference fluctuation introduced by the memory score.

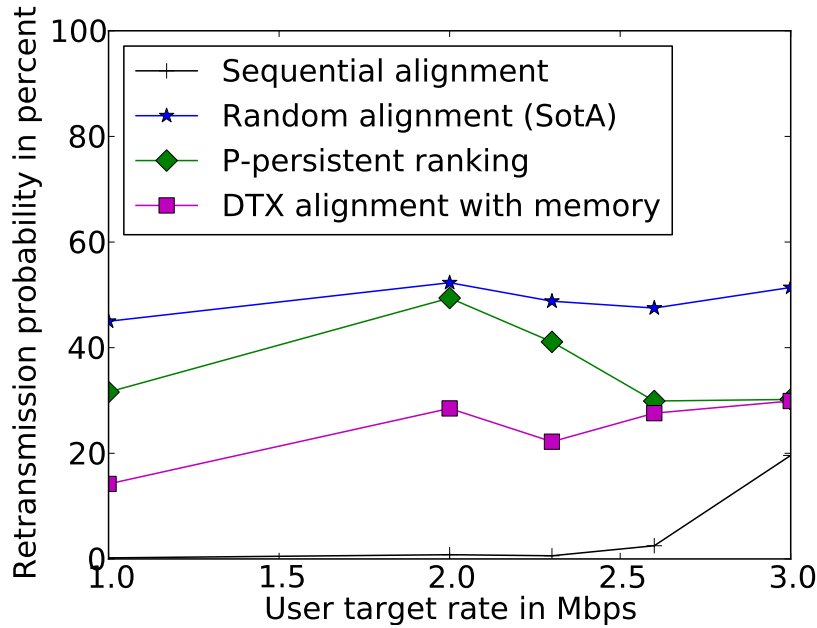


Figure 5.6: Retransmission probability over targeted rate.

Complexity

With regard to complexity, sequential and random alignment are of minimal complexity. These strategies involve no algorithmic decision-making on the set of transmission time slots. P-persistent ranking requires one ranking and time slot selection with probability p per iteration. The highest complexity is present in **DTX** with memory, which requires two executions of the time slot sort, one for the generation of the score and one for the output of the ranking. Although **DTX** with memory comprises the highest complexity in comparison, these operations pose a small burden on modern hardware as the number of time slots is typically small. For example, typical **LTE** systems are designed with 10 subframes (time slots).

Interpretation

DTX with memory was found to provide the best results. Under the present assumptions, it provides both a lower power consumption and lower retransmission probability than the **SotA** and p-persistent ranking. Future **DTX** capable networks can and should exploit this alignment potential.

5.6 Summary

In this chapter, the constructive uncoordinated and distributed alignment of **DTX** time slots between interfering **OFDMA BSs** for power-saving under rate

constraints was studied. The open problem was first formally established. Due to its complexity, it was approached with four alternative heuristic strategies: Sequential alignment, random alignment, p-persistent ranking and distributed **DTX** with memory. Distributed **DTX** with memory is an original contribution of this thesis. It addresses shortcomings of the other strategies by introducing memory to overcome short-term fluctuations and networks oscillations. The performance of the four strategies was tested in simulation. It was found that power consumption can be reduced significantly, especially at medium cell loads. All strategies converge within six **OFDMA** frames. **DTX** with memory reduces power consumption up to 40% compared to the **SotA**, combined with around 20% reduction in retransmission probability.

Chapter 6

Conclusions, Limitations and Future Work

6.1 Summary and Conclusions

In this thesis, the power consumption of Long Term Evolution (**LTE**) Base Station (**BS**) devices was studied and modelled. The findings from the model were applied to reduce power consumption through energy efficient Radio Resource Management (**RRM**) mechanisms while upholding user rate constraints. **RRM** mechanisms were applied to control links on the cell level and interference on the multi-cell level.

In Chapter 1, the importance of energy efficiency for current mobile networks was emphasized. As mobile traffic, the number of devices and the size of the infrastructure are constantly increasing, the CO₂ emission of mobile networks is expected to double between 2007 and 2020. Green Radio research efforts, such as this thesis, are directed to revert that trend.

Chapter 2 first inspected the power consumption life cycle of a mobile network. While the production of mobile equipment causes significant emissions of CO₂, the operation is power efficient. The situation was found to be almost the opposite for cellular **BSs** which cause the largest share of emissions during operation. This is caused by the significant number of stations in operation combined with their long life times. This situation motivated the reduction of operation power consumption of **BSs** as the topic of this thesis. Next, the State-Of-The-Art (**SotA**) of Green Radio was identified through a detailed literature survey. Finally, the chapter also discussed fundamental technical concepts in preparation for the original contributions in Chapters 3, 4, and 5.

Chapter 3 explored the sources of power consumption in an **LTE BS**. First, the difficulty of accurate power modeling and other existing power models were described. Next, the typical architecture of a **BS** was introduced. Each of its components was discussed and individually modelled. Components were found to be either load adaptive, like the Power Amplifier (**PA**) and Baseband (**BB**) unit,

have constant power consumption, like the Radio Frequency (RF) transceiver, or have a power consumption which scales with other components' consumption, like power conversion and cooling. The power consumptions of the subcomponents were combined to find the power consumption of the entire BS. Since the component model is too elaborate for many applications, a parameterized model was proposed which abstracts many parameters. The parameterized model only considers those parameters which are typically modified during operation such as bandwidth, transmission power, the number of transmission antennas, and sleep mode. Parameters were provided. The parameterized model was once more simplified into an affine model which can be applied in optimization. Overall, it was found that an increase of the energy efficiency in BSs must be based on reducing the PA power consumption through Power Control (PC) and setting the entire BS to a sleep mode. Hardware research should focus on enabling and amplifying these two mechanisms. Other manipulation such as the adaptation of coding, modulation or bandwidth are less promising. Simple models are found to capture the most relevant aspects sufficiently.

With the power model and saving techniques identified in the prior chapter, Chapter 4 explored three RRM mechanisms to reduce BS power consumption. The first technique is PC, through which power was adapted to match only the requested capacity per User Equipment (UE) instead of over-achieving. The second technique is Discontinuous Transmission (DTX), a very short sleep mode. Of the two, PC was found to provide strong savings in high load when transmission power is generally high, whereas DTX was most effective at low load when there is ample opportunity for sleep mode. It was shown that the joint application of PC and DTX achieves lower power consumption than either individual technique over all cell traffic loads in the Power and Resource Allocation Including Sleep (PRAIS) scheme. This joint problem was shown to be convex and thus efficiently solvable. This finding was combined with the third technique, Antenna Adaptation (AA), and applied by using it as the core of a power-saving Multiple-Input Multiple-Output (MIMO) Orthogonal Frequency Division Multiple Access (OFDMA) resource scheduler, called Resource allocation using Antenna adaptation, Power control and Sleep modes (RAPS). RAPS first solves a simplified convex real-valued subproblem. The solution of the subproblem is then quantized to the integer-valued OFDMA scheduling problem and joined with subcarrier allocation and power allocation. AA was found to provide little added value on top of the other two techniques. Application of RAPS was shown to reduce power consumption of LTE BSs by 25-40% in single-cell simulation. RAPS could be readily built into current LTE BSs.

Going beyond the cell level, Chapter 5 studied the exploration of intercell interference for power saving. It is beneficial to align the DTX mode of BSs constructively, to the effect that interference is reduced. Four alternative alignment techniques have been tested in simulation: sequential alignment, random alignment, p-persistent ranking, and distributed DTX with memory.

The latter is an original contribution by the author. Sequential alignment is a conservative technique which maximizes interference for the benefit of predictability. Random alignment is assumed was the **SotA**. P-persistent ranking is a popular technique for the suppression of oscillation. Distributed **DTX** with memory goes further and keeps track of past allocations and channel quality to enable convergence to a stable network state. The important finding was that—unlike for the single cell in Chapter 4—the power consumption could not be reduced through these mechanisms without affecting the Quality of Service (**QoS**). The interference dynamics cause occasional violations of the rate constraints, thus necessitating retransmissions. Random alignment caused regular rate constraint violations at medium power consumption. P-persistent ranking was slightly more reliable with lower retransmission probability at low power consumption. However, distributed **DTX** with memory provided a much lower retransmission probability than p-persistent ranking at lower power consumption. It thus provided the best best retransmission probability and power saving. The power saving of distributed **DTX** with memory over the **SotA** was found to be up to 40%, depending on the cell loads.

In conclusion, this thesis provides three readily applicable supply power models for **LTE BSs**, including the model derivations. From these models, **DTX** and **PC** were identified as most effective and applied to reduce **BS** operating power consumption. **PC** and **DTX** were optimized jointly and integrated into a comprehensive **MIMO OFDMA** scheduler. The inherent **DTX** time slots of such a scheduler were then aligned constructively between neighbouring **BSs**. Reducing **BS** power consumption by 50% through software is thus well within reach.

6.2 Limitations and Future Work

The most important limitation to the techniques proposed in this thesis lies in the restrictions imposed on the scheduler by a transmission standard like **LTE**. In this research, it was assumed that a scheduler can select any resource block for transmission or sleep. In practice, however, this selection will be limited as the standard reserves some resources for signaling, channel sounding, or pilot transmission. Since the scheduler will be less potent due to this limited selection, power consumption is expected to be higher under these constraints.

Next, the power model in Chapter 3 as well as all later chapters assume that a **BS** can be switched on and off in an instant. Yet, although switching times are assumed to be in the order of tens of microseconds [Frenger *et al.*, 2011], they are not fully instantaneous. This has to be considered in **DTX** and wake-up scheduling. If sleep modes are deeper, switching times will become longer. Following this line of argument, there may actually be more than one sleep mode available; for example, an OFF state with zero power consumption, a deep sleep with very low consumption, and a light sleep for **DTX**. In that case, a scheduler would have to consider the wake-up times in its selection of sleep modes.

Finally, the validity of the results presented over the coming years is strongly dependent on the assumptions made in the power model. Drastic changes in the architecture of BS, for example through the proliferation of massive MIMO [Larsson *et al.*, 2013], may change the way BSs consume power. In such a case, the effectiveness of different saving techniques will have to be re-evaluated.

For future research, the most immediate goal is to combine the RAPS scheduler with distributed DTX with memory and assess the joint power savings. As the RAPS scheduler makes no assumptions about the time slots allocated for DTX, it can provide instructions for the DTX alignment scheme. A further planned extension to the DTX alignment scheme is an decrease of the retransmission probability. It is expected that a rate margin imposed on the rate constraint, *i.e.* requesting a higher rate target, will be beneficial.

Another important addition is the consideration of standards limitations. The strength of the impact of standards limitations has to be assessed. If the standard in its current form severely caps power savings, future standards could be designed to be more open to power saving.

The power-saving RRM mechanisms established herein can also be applied to BSs which are smaller than macro. In smaller BS types, the load dependence is smaller. Thus, PC is less effective compared to DTX. Consideration of smaller BS types is also related to the field of HetNets [Hu *et al.*, 2011]. Since coverage is generally assumed to overlap in HetNets, new options for longer sleep modes arise as UEs will have guaranteed coverage even when some BSs are asleep.

All analyses in this work assumed a uniform distribution of BSs. However, with the advance of HetNets, it may also be relevant to explore distributions such as Poisson Point Processes [Haenggi *et al.*, 2009]. This will have an effect particularly on the multi-cell DTX alignment work.

Appendix A

Appendix

A.1 Proof of Convexity for Problem (4.12)

This proof shows that (4.12) is convex.

Proof. For $P_S = 0$, the first derivative of the cost function for link k is

$$f'_{0,k} = \frac{\partial P_{\text{supply}}(\bar{R}_k)}{\partial \mu_k} = P_0 + \Delta_p \frac{P_N}{G_k} \left[-1 + 2^{\frac{\bar{R}_k}{W\mu_k}} \left(1 - \frac{\bar{R}_k}{W\mu_k} \ln(2) \right) \right]. \quad (\text{A.1})$$

The second derivative of $f_{0,k}$ is given by

$$f''_{0,k} = \frac{\partial^2 P_{\text{supply}}(\bar{R}_k)}{\partial^2 \mu_k} = \Delta_p \frac{P_N}{G_k} \left(\frac{\bar{R}_k}{W} \right)^2 \ln^2(2) \frac{2^{\frac{\bar{R}_k}{W\mu_k}}}{\mu_k^3}. \quad (\text{A.2})$$

All variables in the second derivative are positive, thus $f''_{0,k} \geq 0$ within the parameter bounds. Therefore, each $f_{0,k}$ is convex within the bounds.

The non-negative sum preserves convexity. Thus, f_0 is convex. \square

A.2 Proof of Convexity for Problem (4.15)

This proof shows that (4.15) is convex.

Proof. The partial second derivative of the MIMO cost function in (4.15) with respect to μ_k is

$$\frac{\partial^2 P_{\text{supply},k}(\mathbf{r})}{\partial^2 \mu_k} = \Delta_p \log^2(2) \frac{R_k}{W} \frac{2^{\frac{R_k}{W\mu_k}} \left((\epsilon_1 + \epsilon_2)^2 + 2\epsilon_1\epsilon_2 \left(2^{\frac{R_k}{W\mu_k}} - 2 \right) \right)}{\mu_k^3 \left((\epsilon_1 + \epsilon_2)^2 + 4\epsilon_1\epsilon_2 \left(2^{\frac{R_k}{W\mu_k}} - 1 \right) \right)^{\frac{3}{2}}}, \quad (\text{A.3})$$

which is non-negative since

$$2\epsilon_1\epsilon_2 2^{\frac{R_k}{W\mu_k}} \geq 2\epsilon_1\epsilon_2 \quad (\text{A.4})$$

within the parameter bounds. Thus the cost function is convex in μ_k within the bounds. \square

Convexity of the Single-Input Multiple-Output (SIMO) cost function and the constraint function can be shown similarly and is omitted here for brevity.

A.3 Margin-adaptive Resource Allocation

Margin-adaptive power allocation over a set of resource blocks, \mathcal{U}_k , and a vector of channel eigenvalues, $\mathcal{E}_{a,k}$, minimizes power consumption while fulfilling a target rate [Yu *et al.*, 2002].

Assuming block-diagonalization precoding, the problem is to

$$\underset{P_{a,e}}{\text{minimize}} \quad \sum_{a=1}^{|\mathcal{U}_k|} \sum_{e=1}^{|\mathcal{E}_{a,k}|} P_{a,e} \quad (\text{A.5a})$$

$$\text{subject to} \quad B_{\text{target},k} = \sum_{a=1}^{|\mathcal{U}_k|} \sum_{e=1}^{|\mathcal{E}_{a,k}|} w\tau \log_2 \left(1 + \frac{P_{a,e}\mathcal{E}_{a,k}(e)}{P_N} \right), \quad (\text{A.5b})$$

$$P_{a,e} \geq 0 \quad \forall a, e, \quad (\text{A.5c})$$

$$\sum_{a=1}^{|\mathcal{U}_k|} \sum_{e=1}^{|\mathcal{E}_{a,k}|} P_{a,e} \leq P_{\max}. \quad (\text{A.5d})$$

With Lagrange multipliers λ, β, ν , the Karush-Kuhn-Tucker optimality conditions for (A.5) are

$$-P_{a,e} \leq 0 \quad \forall a, e \quad (\text{A.6a})$$

$$\sum_{a=1}^{|\mathcal{U}_k|} \sum_{e=1}^{|\mathcal{E}_{a,k}|} P_{a,e} - P_{\max} \leq 0 \quad (\text{A.6b})$$

$$B_{\text{target},k} - \sum_{a=1}^{|\mathcal{U}_k|} \sum_{e=1}^{|\mathcal{E}_{a,k}|} w\tau \log_2 \left(1 + \frac{P_{a,e}\mathcal{E}_{a,k}(e)}{P_N} \right) = 0 \quad (\text{A.6c})$$

$$\lambda_{a,e}^* \geq 0 \quad \forall a, e, \quad \beta \geq 0 \quad (\text{A.6d})$$

$$\lambda_{a,e}^* (-P_{a,e}^*) = 0 \quad \forall a, e \quad (\text{A.6e})$$

$$\beta \left(\sum_{a=1}^{|\mathcal{U}_k|} \sum_{e=1}^{|\mathcal{E}_{a,k}|} P_{a,e} - P_{\max} \right) = 0 \quad (\text{A.6f})$$

$$\frac{\partial \mathcal{L}}{\partial P_{a,e}} = 0, \quad (\text{A.6g})$$

where (A.6a), (A.6b), (A.6c) ensure the primal feasibility, (A.6d) the dual feasibility and (A.6e), (A.6f) the complementary slackness.

The derivative of the Lagrangian at the minimum is

$$\frac{\partial \mathcal{L}}{\partial P_{a,e}} = 1 - \lambda + \beta - \frac{v w \tau \mathcal{E}_{a,k}(e)}{\log(2) (P_N + \mathcal{E}_{a,k}(e) P_{a,e})} = 0, \quad (\text{A.7})$$

with λ the multiplier for the first inequality constraint, β for the second (power-limit) constraint and v the equality constraint multiplier. When reducing the conditions to $P_{a,e} > 0$, $\lambda = 0$. When considering that the power constraint is always loosely bound with $\left(\sum_{a=1}^{|\Omega_k|} \sum_{e=1}^{|\mathcal{E}_{a,k}|} P_{a,e} - P_{\max} \right) < 0$, then by (A.6f), $\beta = 0$.

Solving the remainder for $P_{a,e}$,

$$P_{a,e} = \frac{v w \tau}{\log(2)} - \frac{P_N}{\mathcal{E}_{a,k}(e)}, \quad (\text{A.8})$$

which can be inserted into the equality constraint of (A.5) to yield the water-level, v , by

$$\log_2(v) = \frac{1}{|\Omega_k|} \left(\frac{B_{\text{target},k}}{w \tau} - \sum_{e=1}^{|\Omega_k|} \log_2 \left(\frac{\tau \mathcal{E}_{a,k}(e) w}{P_N \log(2)} \right) \right). \quad (\text{A.9})$$

The water-level can be found via an iterative search over the vector Ω_k of channels that contribute a positive power. Since the sum power is reduced on each iteration, the power constraint (accounted for by the multiplier β) only needs to be tested after the search is finished.

Appendix B

List of Publications

This chapter contains a list of publications related to this thesis ordered by academic publication status (published, accepted, submitted) and other type (project reports and book contributions).

B.1 Published

- Gunther Auer and István Gódor and László Hévizi and Muhammad Ali Imran and Jens Malmodin and Péter Fasekas and Gergely Biczók and **Hauke Holtkamp** and Dietrich Zeller and Oliver Blume and Rahim Tafazolli, “Enablers for Energy Efficient Wireless Networks”, *Proceedings of the IEEE Vehicular Technology Conference (VTC) Fall-2010*, 2010 [[Auer et al., 2010](#)]
- **Hauke Holtkamp** and Gunther Auer, “Fundamental Limits of Energy-Efficient Resource Sharing, Power Control and Discontinuous Transmission”, *Proceedings of the Future Network & Mobile Summit 2011*, 2011 [[Holtkamp & Auer, 2011](#)]
- **Hauke Holtkamp** and Gunther Auer and Harald Haas, “Minimal Average Consumption Downlink Base Station Power Control Strategy”, *Proceedings of the 2011 IEEE 22nd International Symposium on Personal Indoor and Mobile Radio Communications (PIMRC)*, 2011 [[Holtkamp et al., 2011b](#)]
- **Hauke Holtkamp** and Gunther Auer and Harald Haas, “On Minimizing Base Station Power Consumption”, *Proceedings of the Vehicular Technology Conference (VTC) Fall-2011*, 2011 [[Holtkamp et al., 2011a](#)]
- Claude Desset and Björn Debaillie and Vito Giannini and Albrecht Fehske and Gunther Auer and **Hauke Holtkamp** and Wieslawa Wajda and Dario Sabella and Fred Richter and Manuel Gonzalez and Henrik Klessig and István Gódor and Per Skillermark and Magnus Olsson and Muhammad Ali Imran and Anton Ambrosy and Oliver Blume, “Flexible Power Modeling of

LTE Base Stations”, *Proceedings of the 2012 IEEE Wireless Communications and Networking Conference*., 2012 [[Desset et al., 2012](#)]

- **Hauke Holtkamp** and Gunther Auer and Samer Bazzi and Harald Haas, “Minimizing Base Station Power Consumption”, *IEEE Journal on Selected Areas in Communications*, 2014 [[Holtkamp et al., 2013a](#)]

B.2 Accepted

- **Hauke Holtkamp** and Gunther Auer and Vito Giannini and Harald Haas, “A Parameterized Base Station Power Model”, *IEEE Communications Letters*, 2013 [[Holtkamp et al., 2013b](#)]
- **Hauke Holtkamp** and Harald Haas, “OFDMA Base Station Power-saving Via Joint Power Control and DTX in Cellular Systems”, *Proceedings of the Vehicular Technology Conference (VTC) Fall-2013*, 2013 [[Holtkamp & Haas, 2013](#)]

B.3 Submitted

- **Hauke Holtkamp** and Guido Dietl and Harald Haas, “Distributed DTX Alignment with Memory”, *Proceedings of the 2014 IEEE International Conference on Communications (ICC)*, 2014 [[Holtkamp et al., 2013](#)]

B.4 Project Reports

- EARTH Project Work Package 2, “Deliverable D2.2: Reference Systems and Scenarios”, 2012
- EARTH Project Work Package 3, “Deliverable D3.3: Green Network Technologies”, 2012 [[EARTH Project Work Package 3, 2012](#)]

B.5 Contributions

- Jinsong Wu and Sundeep Rangan and Honggang Zhang, “Green Communications: Theoretical Fundamentals, Algorithms and Applications”, *Taylor & Francis Group*, 2012 [[Wu et al., 2012a](#)]

Appendix C

Attached Publications

This chapter contains all work either published or submitted for publication to academic conferences or journals. For brevity, Energy Aware Radio and neTwork tecHnologies (**EARTH**) project deliverables [[EARTH Project Work Package 3, 2012](#)] and a book chapter [[Wu *et al.*, 2012a](#)] are not listed here.

Literature References

- [01, a] (a). <http://www.python.org>. Retrieved 17 June 2013.
- [01a, a] (a). <http://www.mathworks.com/products/matlab>. Retrieved 17 June 2013.
- [01b, a] (a). <http://www.ict-earth.eu>. Retrieved 17 June 2013.
- [3GPP, 2010a] 3GPP (2010a). www.3gpp.org/ftp/Specs/. Retrieved 15 January 2013.
- [3GPP, 2010b] 3GPP (2010b). 3GPP TS 36.321 V 9.2.0 (2010-03).
- [Abdallah *et al.*, 2012] Abdallah, K., Cerutti, I., & Castoldi, P. (2012). In: *Communications (ICC), 2012 IEEE International Conference on* pp. 5238 – 5242,.
- [Abgrall *et al.*, 2010] Abgrall, C., Strinati, E. C., & Belfiore, J.-C. (2010). In: *Proc. of the 21st IEEE International Symposium on Personal, Indoor and Mobile Radio Communications (PIMRC)* pp. 1118–1122, Istanbul, Turkey:.
- [Akaiwa & Andoh, 1993] Akaiwa, Y. & Andoh, H. (1993). *Selected Areas in Communications, IEEE Journal on*, **11** (6), 949 –954.
- [Al-Shatri & Weber, 2010] Al-Shatri, H. & Weber, T. (2010). In: *Proceedings of the International ITG Workshop on Smart Antennas 2010* pp. 350–354,.
- [Alekklett *et al.*, 2010] Alekklett, K., Höök, M., Jakobsson, K., Lardelli, M., Snowden, S., & Söderbergh, B. (2010). *Energy Policy*, **38** (3), 1398 – 1414.
- [Ambrosy *et al.*, 2012] Ambrosy, A., Wilhelm, M., Blume, O., & Wajda, W. (2012). In: *Proceedings of Globecom 2012* pp. 3502–3507,.
- [Andrews *et al.*, 2001] Andrews, M., Kumaran, K., Ramanan, K., Stolyar, A., Whiting, P., & Vijayakumar, R. (2001). *Communications Magazine, IEEE*, **39** (2), 150–154.
- [Arnold *et al.*, 2010] Arnold, O., Richter, F., Fettweis, G., & Blume, O. (2010). In: *Future Network and Mobile Summit, 2010* pp. 1 –8,.

- [Ashraf *et al.*, 2011] Ashraf, I., Boccardi, F., & Ho, L. (2011). *Communications Magazine, IEEE*, **49** (8), 72–79.
- [Auer *et al.*, 2011a] Auer, G., Giannini, V., Gódor, I., Skillermark, P., Olsson, M., Imran, M., Sabella, D., Gonzalez, M. J., & Desset, C. (2011a). In: *Proceedings of the VTC 2011-Spring* ,.
- [Auer *et al.*, 2011b] Auer, G., Giannini, V., Gódor, I., Skillermark, P., Olsson, M., Imran, M. A., Gonzalez, M. J., Desset, C., Blume, O., & Fehske, A. (2011b). *IEEE Wireless Communications*, **18** (5), 40–49.
- [Auer *et al.*, 2010] Auer, G., Gódor, I., Hévizsi, L., Imran, M. A., Malmudin, J., Fasekas, P., Biczók, G., Holtkamp, H., Zeller, D., Blume, O., & Tafazolli, R. (2010). In: *Proc. of the Vehicular Technology Conference (VTC)* ,.
- [Badic *et al.*, 2009] Badic, B., O’Farrell, T., Loskot, P., & He, J. (2009). In: *Proc. of the 70th Vehicular Technology Conference (VTC)* pp. 1–5, Anchorage, USA:.
- [Bhatia & Kodialam, 2004] Bhatia, R. & Kodialam, M. (2004). In: *INFOCOM 2004. Twenty-third Annual Joint Conference of the IEEE Computer and Communications Societies* volume 2 pp. 1457–1466, IEEE.
- [Bi *et al.*, 2001] Bi, Q., Zysman, G., & Menkes, H. (2001). *Communications Magazine, IEEE*, **39** (1), 110–116.
- [Biglieri *et al.*, 2007] Biglieri, E., Calderbank, A. R., Constantinides, A. G., Goldsmith, A., & Paulraj, A. (2007). *MIMO Wireless Communications*. Cambridge University Press.
- [Blume *et al.*, 2010] Blume, O., Zeller, D., & Barth, U. (2010). In: *4th International Symposium on Communications, Control and Signal Processing (ISCCSP)* pp. 1–5,.
- [Bories *et al.*, 2011] Bories, S., Dussopt, L., Giry, A., & Delaveaud, C. (2011). In: *Wireless Conference 2011 - Sustainable Wireless Technologies (European Wireless), 11th European* pp. 1–3,.
- [Boyd & Vandenberghe, 2004] Boyd, S. & Vandenberghe, L. (2004). *Convex Optimization*. Cambridge University Press.
- [Brazell *et al.*, 2005] Brazell, J., Donoho, L., Dexheimer, J., Robert Hannenman, P., & Langdon, G. (2005). *M2M: The Wireless Revolution*. Texas State Technical College Publishing.
- [Capozzi *et al.*, 2012] Capozzi, F., Piro, G., Grieco, L., Boggia, G., & Camarda, P. (2012). *Communications Surveys Tutorials, IEEE*, **PP** (99), 1–23.

- [Chong & Jorswieck, 2012] Chong, Z. & Jorswieck, E. (2012). In: *Mobile Lightweight Wireless Systems* pp. 18–29. Springer.
- [Cisco, 2013] Cisco (2013). <http://www.cisco.com/>. Retrieved 18 April 2013.
- [Condor Team, 2013] Condor Team (2013). <http://research.cs.wisc.edu/htcondor/>. Retrieved 17 June 2013.
- [Cui *et al.*, 2004] Cui, S., Goldsmith, A. J., & Bahai, A. (2004). *IEEE Journal on Selected Areas in Communications*, **22**, 1089–1098.
- [Cui *et al.*, 2005] Cui, S., Goldsmith, A. J., & Bahai, A. (2005). *IEEE Transactions on Wireless Communications*, **4**, 2349–2360.
- [Dahlman *et al.*, 2011] Dahlman, E., Parkvall, S., & Sköld, J. (2011). *4G LTE/LTE-Advanced for Mobile Broadband*. Academic Press, 1 edition.
- [de Domenico, 2012] de Domenico, A. (2012). *Energy Efficient Mechanisms for Heterogeneous Cellular Networks*. PhD thesis Université de Grenoble.
- [Deruyck *et al.*, 2012] Deruyck, M., Joseph, W., & Martens, L. (2012). *Transactions on Emerging Telecommunications Technologies*, .
- [Desset *et al.*, 2012] Desset, C., Debaillie, B., Giannini, V., Fehske, A., Auer, G., Holtkamp, H., Wajda, W., Sabella, D., Richter, F., Gonzalez, M., Klessig, H., Gódor, I., Skillermark, P., Olsson, M., Imran, M. A., Ambrosy, A., & Blume, O. (2012). In: *2012 IEEE Wireless Communications and Networking Conference: Mobile and Wireless Networks (IEEE WCNC 2012 Track 3 Mobile & Wireless)*, ..
- [EARTH Project Work Package 2, 2010] EARTH Project Work Package 2 (2010). <https://www.ict-earth.eu/publications/deliverables/deliverables.html>. Retrieved April 18, 2013.
- [EARTH Project Work Package 3, 2012] EARTH Project Work Package 3 (2012). <https://www.ict-earth.eu/publications/deliverables/deliverables.html>. Retrieved 18 April 2013.
- [EARTH Project Work Package 4, 2012] EARTH Project Work Package 4 (2012). <https://www.ict-earth.eu/publications/deliverables/deliverables.html>. Retrieved April 18, 2013.
- [Ellenbeck *et al.*, 2008] Ellenbeck, J., Hartmann, C., & Berlemann, L. (2008). In: *Proc. of the 14th European Wireless Conference (EW)* pp. 1–7, Prague, Czech Republic.
- [Ephremides, 2002] Ephremides, A. (2002). *Wireless Communications, IEEE*, **9** (4), 48–59.

- [Ericsson AB, 2012] Ericsson AB (2012). Technical report Ericsson AB.
- [Fehske *et al.*, 2010] Fehske, A., Malmodin, J., Biczók, G., & Fettweis, G. (2010). *IEEE Communications Magazine*, **49**, 55–62.
- [Ferling *et al.*, 2010] Ferling, D., Bohn, T., Zeller, D., Frenger, P., Gódor, I., Jading, Y., & Tomaselli, W. (2010). In: *Future Network & Mobile Summit 2010* pp. 1–9,.
- [Fettweis & Zimmermann, 2008] Fettweis, G. & Zimmermann, E. (2008). In: *Proceedings of the 11th International Symposium on Wireless Personal Multimedia Communications (WPMC 2008)* ,.
- [Frenger *et al.*, 2011] Frenger, P., Moberg, P., Malmodin, J., Jading, Y., & Gódor, I. (2011). In: *Proceedings of the IEEE VTC 2011-Spring* pp. 1–5,.
- [Garg, 2010] Garg, V. (2010). *Wireless Communications & Networking*. The Morgan Kaufmann Series in Networking. Elsevier Science.
- [Glover & Grant, 1998] Glover, I. A. & Grant, P. M. (1998). *Digital Communications*. Prentice Hall.
- [Goldsmith *et al.*, 2003] Goldsmith, A., Jafar, S., Jindal, N., & Vishwanath, S. (2003). *IEEE Journal on Selected Areas in Communication*, **21** (5), 684–702.
- [Gonzalez *et al.*, 2011] Gonzalez, M., Ferling, D., Wajda, W., Erdem, A., & Maugars, P. (2011). In: *Future Network Mobile Summit (FutureNetw), 2011* pp. 1–8,.
- [Gruber *et al.*, 2009] Gruber, M., Blume, O., Ferling, D., Zeller, D., Imran, M., & Strinati, E. (2009). In: *Personal, Indoor and Mobile Radio Communications, 2009 IEEE 20th International Symposium on* pp. 1–5,.
- [GSA Secretariat, 2013] GSA Secretariat (2013). Technical report Global mobile Suppliers Association.
- [Gupta & Strinati, 2011] Gupta, R. & Strinati, E. (2011). In: *Personal Indoor and Mobile Radio Communications (PIMRC), 2011 IEEE 22nd International Symposium on* pp. 2424–2429,.
- [Haenggi *et al.*, 2009] Haenggi, M., Andrews, J. G., Baccelli, F., Dousse, O., & Franceschetti, M. (2009). *Selected Areas in Communications, IEEE Journal on*, **27** (7), 1029–1046.
- [Hammi *et al.*, 2010] Hammi, O., Kwan, A., Helaoui, M., & Ghannouchi, F. M. (2010). In: *Vehicular Technology Conference Fall (VTC 2010-Fall), 2010 IEEE 72nd* pp. 1–5, IEEE.

- [Han *et al.*, 2011a] Han, C., Harrold, T., Armour, S., Krikidis, I., Videv, S., Grant, P. M., Haas, H., Thompson, J. S., Ku, I., Wang, C.-X., *et al.* (2011a). *Communications Magazine, IEEE*, **49** (6), 46–54.
- [Han *et al.*, 2011b] Han, S., Yang, C., Wang, G., & Lei, M. (2011b). In: *Personal Indoor and Mobile Radio Communications (PIMRC), 2011 IEEE 22nd International Symposium on* pp. 1536–1540, IEEE.
- [Han & Ansari, 2012] Han, T. & Ansari, N. (2012). *Communications Letters, IEEE*, **16** (6), 866–869.
- [Hedayati *et al.*, 2012] Hedayati, M., Amirijoo, M., Frenger, P., & Moe, J. (2012). In: *Proceedings of the IEEE VTC 2012-Spring* pp. 1–5,.
- [Hevizi & Gódor, 2011] Hevizi, L. G. & Gódor, I. (2011). In: *Personal Indoor and Mobile Radio Communications (PIMRC), 2011 IEEE 22nd International Symposium on* pp. 2415–2417, IEEE.
- [Holtkamp & Auer, 2011] Holtkamp, H. & Auer, G. (2011). In: *Proceedings of the Future Network & Mobile Summit 2011* ,.
- [Holtkamp *et al.*, 2013a] Holtkamp, H., Auer, G., Bazzi, S., & Haas, H. (2013a). *Selected Areas in Communications, IEEE Journal on*, **PP** (99).
- [Holtkamp *et al.*, 2013b] Holtkamp, H., Auer, G., & Giannini, V. (2013b). *IEE Communications Letters*, . submitted on April 19, 2013.
- [Holtkamp *et al.*, 2011a] Holtkamp, H., Auer, G., & Haas, H. (2011a). In: *Proceedings of the IEEE VTC 2011-Fall* ,.
- [Holtkamp *et al.*, 2011b] Holtkamp, H., Auer, G., & Haas, H. (2011b). In: *Personal Indoor and Mobile Radio Communications (PIMRC), 2011 IEEE 22nd International Symposium on* pp. 2430 –2434,.
- [Holtkamp *et al.*, 2013] Holtkamp, H., Dietl, G., & Haas, H. (2013). In: *2013 IEEE 22nd International Symposium on Personal, Indoor and Mobile Radio Communications: Fundamentals and PHY Track (PIMRC'13 - Fundamentals and PHY Track)* , London, United Kingdom:. submitted on April 15, 2013.
- [Holtkamp & Haas, 2013] Holtkamp, H. & Haas, H. (2013). In: *Proceedings of the IEEE VTC 2013-Fall* ,. submitted on March 31, 2013.
- [Hoydis *et al.*, 2011] Hoydis, J., Kobayashi, M., & Debbah, M. (2011). *Vehicular Technology Magazine, IEEE*, **6** (1), 37–43.
- [Hu *et al.*, 2011] Hu, R. Q., Qian, Y., Kota, S., & Giambene, G. (2011). *Wireless Communications, IEEE*, **18** (3), 8–9.

- [IST-2003-507581 WINNER, 2005] IST-2003-507581 WINNER (2005). <https://www.ist-winner.org/DeliverableDocuments/>. Retrieved 15 April 2007.
- [IST-4-027756 WINNER II, 2006] IST-4-027756 WINNER II (2006). <https://www.ist-winner.org/WINNER2-Deliverables/>. Retrieved 5 February 2008.
- [Jang & Lee, 2003] Jang, J. & Lee, K. B. (2003). *IEEE Journal on Selected Areas in Communications*, **21** (2), 171–178.
- [Katzela & Naghshineh, 1996] Katzela, I. & Naghshineh, M. (Jun 1996). *Personal Communications, IEEE*, **3** (3), 10–31.
- [Khirallah & Thompson, 2012] Khirallah, C. & Thompson, J. S. (2012). *Journal of Signal Processing Systems*, **69** (1), 105–113.
- [Kim *et al.*, 2009] Kim, H., Chae, C.-B., de Veciana, G., & Heath, R. W. (2009). *IEEE Transactions on Wireless Communications*, **8** (8), 4264–4275.
- [Kivanc *et al.*, 2003] Kivanc, D., Li, G., & Liu, H. (2003). *IEEE Transactions on Wireless Communications*, **2** (6), 1150–1158.
- [Klessig *et al.*, 2011] Klessig, H., Fehske, A., & Fettweis, G. (2011). In: *Sarnoff Symposium, 2011 34th IEEE* pp. 1–6,.
- [Kühn, 2006] Kühn, V. (2006). *Wireless Communications over MIMO Channels*. John Wiley & Sons Ltd.
- [Larsson *et al.*, 2013] Larsson, E. G., Tufvesson, F., Edfors, O., & Marzetta, T. L. (2013). *arXiv preprint arXiv:1304.6690*, .
- [Li & Liu, 2006] Li, G. & Liu, H. (2006). *IEEE Transactions on Wireless Communications*, **5** (12), 3451–3459.
- [Liang *et al.*, 2012] Liang, Y.-S., Chung, W.-H., Yu, C.-M., Zhang, H., Chung, C.-H., Ho, C.-H., & Kuo, S.-Y. (2012). In: *Vehicular Technology Conference (VTC Fall), 2012 IEEE* pp. 1–5,.
- [López-Pérez *et al.*, 2011] López-Pérez, D., Chu, X., Vasilakos, A. V., & Claussen, H. (2011). In: *Proceedings of the ACM SIGCOMM 2011 Conference SIGCOMM '11* pp. 410–411, New York, NY, USA: ACM.
- [Louhi & Scheck, 2008] Louhi, J. & Scheck, H. (2008). In: *Proc. Int. Symp. Wireless Personal Multimedia Communications (WPMC), Lapland, Finland*, .
- [Malmodin *et al.*, 2010] Malmodin, J., Moberg, A., Lundén, D., Finnveden, G., & Lövehagen, N. (2010). *Journal of Industrial Ecology*, **14** (5), 770–790.

- [Malmodin *et al.*, 2001] Malmodin, J., Oliv, L., & Bergmark, P. (2001). In: *Environmentally Conscious Design and Inverse Manufacturing, 2001. Proceedings EcoDesign 2001: Second International Symposium on* pp. 328–334,.
- [Meshkati *et al.*, 2007] Meshkati, F., Poor, V., & Schwartz, S. (May 2007). *IEEE Signal Processing Magazine: Special Issue on Resource-Constrained Signal Processing, Communications and Networking*, .
- [Miao *et al.*, 2008a] Miao, G., Himayat, N., & Li, G. (2008a). *Global Telecommunications Conference, 2008. IEEE GLOBECOM 2008*, **58**, 545–554.
- [Miao *et al.*, 2008b] Miao, G., Himayat, N., Li, Y., & Bormann, D. (2008b). In: *IEEE International Conference on Communications* pp. 3307 –3312,.
- [Mobile VCE, a] Mobile VCE (a). <http://www.mobilevce.com/green-radio>. Retrieved 12 June, 2013.
- [Nema *et al.*, 2010] Nema, P., Nema, R., & Rangnekar, S. (2010). *Renewable and Sustainable Energy Reviews*, **14** (6), 1635–1639.
- [Niu *et al.*, 2010] Niu, Z., Wu, Y., Gong, J., & Yang, Z. (2010). *Communications Magazine, IEEE*, **48** (11), 74–79.
- [NTT DOCOMO Technical Journal Editorial Office, 2012] NTT DOCOMO Technical Journal Editorial Office (2012). *NTT DOCOMO Technical Journal*, **13** (4), 96–106.
- [Oh & Krishnamachari, 2010] Oh, E. & Krishnamachari, B. (2010). In: *Global Telecommunications Conference (GLOBECOM 2010), 2010 IEEE* pp. 1–5, IEEE.
- [Palomar & Eldar, 2010] Palomar, D. P. & Eldar, Y. C. (2010). *Convex Optimization in Signal Processing and Communications*. Cambridge University Press New York.
- [Pike, 1998] Pike, S. (1998). In: *Personal Communications in the 21st Century (I) (Ref. No. 1998/214), IEE Colloquium on* pp. 1–725, London:.
- [Proakis, 2000] Proakis, J. G. (2000). *Digital Communications*. McGraw-Hill Series in Electrical and Computer Engineering. McGraw-Hill Higher Education, 4 edition.
- [Rahman & Yanikomeroglu, 2010] Rahman, M. & Yanikomeroglu, H. (2010). *Wireless Communications, IEEE Transactions on*, **9** (4), 1414–1425.
- [Ran, 2011] Ran, Y. (2011). *Communications Magazine, IEEE*, **49** (1), 44–47.
- [Richter *et al.*, 2009] Richter, F., Fehske, A., & Fettweis, G. (2009). In: *Vehicular Technology Conference Fall (VTC 2009-Fall), 2009 IEEE 70th* pp. 1–5,.

- [Rosen, 1995] Rosen, M. (1995). *The American Mathematical Monthly*, **102** (6), 495–505.
- [Saker *et al.*, 2010] Saker, L., Elayoubi, S.-E., & Chahed, T. (2010). In: *Wireless Communications and Networking Conference (WCNC), 2010 IEEE* pp. 1–6,.
- [Sandvine, 2010] Sandvine (2010). <http://www.sandvine.com/downloads/documents/2010%20Global%20Internet%20Phenomena%20Report.pdf>. Retrieved 17 June 2013.
- [Scalia *et al.*, 2011] Scalia, L., Biermann, T., Choi, C., Kozu, K., & Kellerer, W. (2011). In: *Computer Communications Workshops (INFOCOM WKSHPS), 2011 IEEE Conference on* pp. 253–258,.
- [Serizawa & Goodman, 1993] Serizawa, M. & Goodman, D. (1993). In: *Vehicular Technology Conference, 1993., 43rd IEEE* pp. 528 –531,.
- [Sesia *et al.*, 2009] Sesia, S., Toufik, I., & Baker, M. (2009). *LTE - The UMTS Long Term Evolution: From Theory to Practice*. Wiley, 1 edition.
- [Shannon, 1948] Shannon, C. (1948). *Bell System Technical Journal*, **27**, 379–423 & 623–656.
- [Sinanović *et al.*, 2007] Sinanović, S., Serafimovski, N., Haas, H., & Auer, G. (2007). In: *Proc. of the 50th IEEE Global Telecommunications Conference (GLOBECOM)* pp. 3684–3688, IEEE Washington, USA:.
- [Skillermark & Frenger, 2012] Skillermark, P. & Frenger, P. (2012). In: *Vehicular Technology Conference (VTC Spring), 2012 IEEE 75th* pp. 1–5,.
- [Stavridis *et al.*, 2012] Stavridis, A., Sinanovic, S., Di Renzo, M., Haas, H., & Grant, P. (2012). In: *Computer Aided Modeling and Design of Communication Links and Networks (CAMAD), 2012 IEEE 17th International Workshop on* pp. 231–235, IEEE.
- [Strinati *et al.*, 2011] Strinati, E., De Domenico, A., & Duda, A. (2011). In: *Wireless Communications and Networking Conference (WCNC), 2011 IEEE* pp. 108–113,.
- [Sugiyama, 2012] Sugiyama, Y. (2012). In: *Design for Innovative Value Towards a Sustainable Society*, (Matsumoto, M., Umeda, Y., Masui, K., & Fukushige, S., eds) pp. 739–742. Springer Netherlands.
- [Ternon *et al.*, 2013] Ternon, E., Bharucha, Z., & Taoka, H. (2013). In: *International ITG Conference on Systems, Communications and Coding* ,.
- [Uyungelen *et al.*, 2011] Uyungelen, S., Auer, G., & Bharucha, Z. (2011). In: *Proc. of the 73rd IEEE Vehicular Technology Conference (VTC)* , Budapest, Hungary:.

- [Vereecken *et al.*, 2012] Vereecken, W., Deruyck, M., Colle, D., Joseph, W., Pickavet, M., Martens, L., & Demeester, P. (2012). *EURASIP Journal on Wireless Communications and Networking*, **2012** (1), 1–14.
- [Videv & Haas, 2011] Videv, S. & Haas, H. (2011). In: *International Conference on Communications* pp. 1–5,.
- [Wächter & Laird, a] Wächter, A. & Laird, K. (a). retrieved May 2, 2013.
- [Wang *et al.*, 2012] Wang, X., Vasilakos, A. V., Chen, M., Liu, Y., & Kwon, T. T. (2012). *Mobile Networks and Applications*, **17** (1), 4–20.
- [Weidman & Lundberg, 2000] Weidman, E. & Lundberg, S. (2000). In: *Electronics and the Environment, 2000. ISEE 2000. Proceedings of the 2000 IEEE International Symposium on* pp. 136–142,.
- [Wireless Week, 2010] Wireless Week (2010). <http://www.wirelessweek.com/news/2010/03/cisco-1-trillion-connected-devices-2013>. Retrieved 14 April 2013.
- [Wong *et al.*, 1999] Wong, C. Y., Cheng, R. S., Lataief, K. B., & Murch, R. D. (1999). *IEEE Journal on Selected Areas in Communications*, **17** (10), 1747–1758.
- [Wu *et al.*, 2011] Wu, G., Talwar, S., Johnsson, K., Himayat, N., & Johnson, K. (2011). *Communications Magazine, IEEE*, **49** (4), 36–43.
- [Wu *et al.*, 2012a] Wu, J., Rangan, S., & Zhang, H. (2012a). *Green Communications: Theoretical Fundamentals, Algorithms and Applications*. Taylor & Francis Group.
- [Wu *et al.*, 2012b] Wu, X., Sinanovic, S., Di Renzo, M., & Haas, H. (2012b). In: *Computer Aided Modeling and Design of Communication Links and Networks (CAMAD), 2012 IEEE 17th International Workshop on* pp. 261–265,.
- [Xiang *et al.*, 2011] Xiang, L., Pantisano, F., Verdone, R., Ge, X., & Chen, M. (2011). In: *Personal Indoor and Mobile Radio Communications (PIMRC), 2011 IEEE 22nd International Symposium on* pp. 41–45, IEEE.
- [Xu *et al.*, 2011] Xu, Z., Yang, C., Li, G. Y., Zhang, S., Chen, Y., & Xu, S. (2011). In: *Proceedings of the VTC Fall 2011* pp. 1–5,.
- [Ye *et al.*, 2002] Ye, W., Heidemann, J., & Estrin, D. (2002). *INFOCOM 2002. Twenty-First Annual Joint Conference of the IEEE Computer and Communications Societies. Proceedings. IEEE*, **3**, 1567–1576.
- [Yu *et al.*, 2002] Yu, W., Ginis, G., & Cioffi, J. M. (2002). *Selected Areas in Communications, IEEE Journal on*, **20** (5), 1105–1115.